

SURFACE MODIFICATION OF TITANIUM DIOXIDE (TiO₂) THIN FILMS AND THEIR APPLICATIONS

A thesis submitted in fulfilment of the requirements for the degree of

DOCTOR OF PHILOSOPHY

IN

PHYSICS AND MATERIALS SCIENCE

By

BANDNA BHARTI

Under the Supervision of

Dr. RAJESH KUMAR



DEPARTMENT OF PHYSICS AND MATERIALS SCIENCE

**JAYPEE UNIVERSITY OF INFORMATION TECHNOLOGY WAKNAGHAT,
DISTRICT SOLAN, H.P., INDIA**

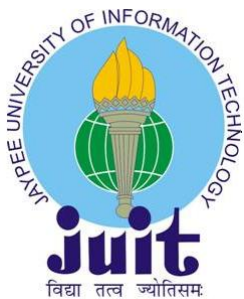
MONTH DECEMBER, YEAR 2017

@ Copyright JAYPEE UNIVERSITY OF INFORMATION TECHNOLOGY

WAKNAGHAT

MONTH DECEMBER, YEAR 2017

ALL RIGHTS RESERVED



JAYPEE UNIVERSITY OF INFORMATION TECHNOLOGY

(Established by H.P. State Legislative vide Act No. 14 of 2002)
Waknaghat, P.O. Dumehar Bani, Kandaghat, Distt. Solan – 173234
(H.P.) INDIA

Website: www.juit.ac.in

Phone No. (91) 07192-257999 (30 Lines)

Fax: (91) 01792 245362

DECLARATION

I hereby declare that the work reported in the PhD thesis entitled **“Surface Modification of Titanium Dioxide (TiO₂) Thin Films and Their Applications”** submitted at **Jaypee University of Information Technology, Waknaghat, India**, is an authentic record of my work carried out under the supervision of **Dr. Rajesh Kumar**. I have not submitted this work elsewhere for any other degree or diploma. I am fully responsible for the contents of my Ph.D. Thesis.

BANDNA BHARTI

Department of Physics and Materials Science
Jaypee University of Information Technology,
Waknaghat, India

Date:



JAYPEE UNIVERSITY OF INFORMATION TECHNOLOGY

(Established by H.P. State Legislative vide Act No. 14 of 2002)
Waknaghat, P.O. Dumehar Bani, Kandaghat, Distt. Solan – 173234 (H.P.) INDIA

Website: www.juit.ac.in

Phone No. (91) 07192-257999 (30 Lines)

Fax: (91) 01792 245362

CERTIFICATE

This is to certify that the work reported in the Ph.D. thesis entitled **“Surface Modification of Titanium Dioxide (TiO₂) Thin Films and Their Applications”**, submitted by **Bandna Bharti** at **Jaypee University of Information Technology, Waknaghat, India**, is a bonafide record of her original work carried out under my supervision. This work has not been submitted elsewhere for any other degree or diploma.

Dr. Rajesh Kumar

Supervisor

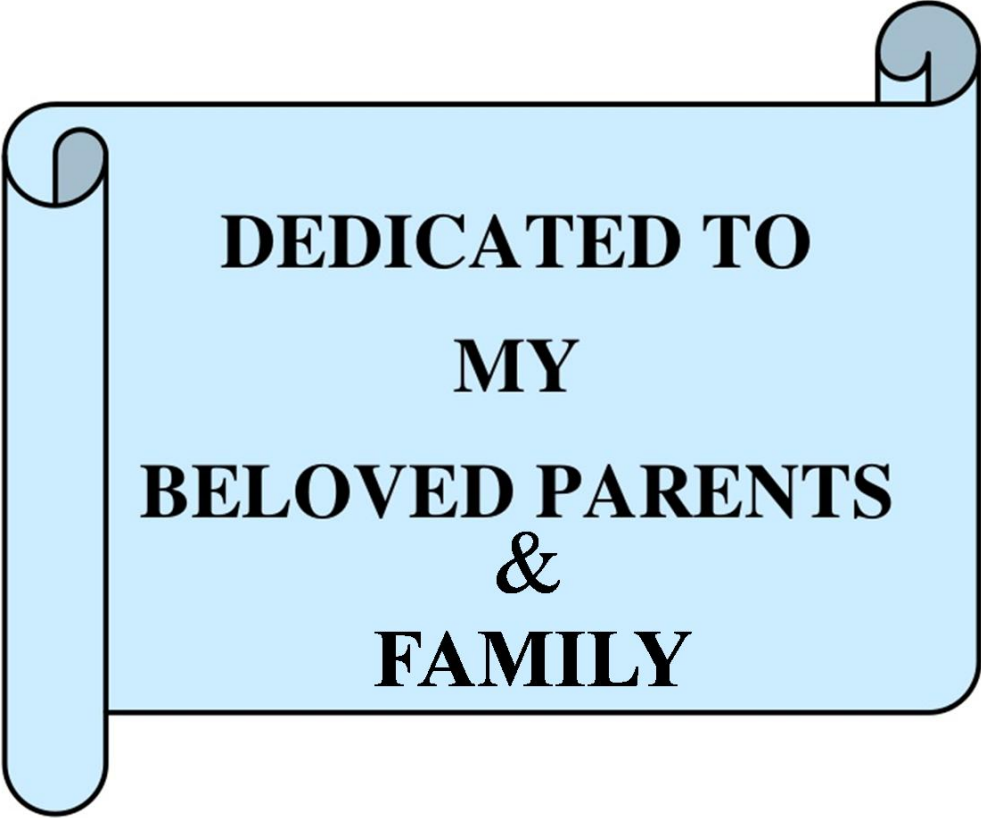
Assistant Professor

Department of Physics and Materials Science

Jaypee University of Information Technology

Waknaghat, Solan, H.P. India-173234

Date:



**DEDICATED TO
MY
BELOVED PARENTS
&
FAMILY**

ACKNOWLEDGEMENT

GOD is my ultimate strength and power who bring best out of me

I deem it my privilege and honors to consign my appreciation and thanks to the following without whose supervision, support and apprehension I would not have been able to complete my Ph. D thesis.

*I feel fortunate to convey my deep sense of reverence and gratitude to my revered mentor, **Dr. Rajesh Kumar**, for his support, immaculate guidance, constructive criticism, constant encouragement and providing requisite facilities to persist my research which otherwise would have remained incomplete. His nurturing and gentle concern has been a stimulus which I will always cherish. I also appreciate his untiring efforts during the entire tenure of my research work and patience during writing of this thesis. I have no words to express my gratitude for everything he has contributed in my Ph.D. and without his blessings it was surely impossible for me to finish my work. I thank him from bottom of my heart.*

*I emphatically express my loyal and venerable thanks to **Prof. (Dr.) Vinod Kumar** (Vice Chancellor, JUIT), **Brig. (Retd.) K.K Marwah** (Registrar and Dean of Student Welfare JUIT), and **Prof. (Dr.) Samir Dev Gupta** (Dean, Academic & Research, JUIT) for giving a opportunity to pursue Doctorate Degree and teaching assistantship.*

*I gratefully acknowledge the help rendered by **Prof. P. B. Barman** (HOD, Department of Physics and Materials Science) for his encouragement, timely help and cooperation throughout my research work. It gives me immense pleasure to express my gratitude to him for his positive disposition coming to my rescue in solving my problems and suggestions which helped me in maintaining my confidence.*

*This document would have remained an infant had it not received its necessary 'diet' in the form of comments, suggestions etc. by **Professor Sunil Bhooshan, Prof. Sunil Kumar Khah, Dr. Vineet Sharma, Dr. Pankaj Sharma, Dr. Dheeraj Sharma, Dr. Ragini Raj Sing, Dr. Surajit Kumar Hazra and Dr. Sanjiv Kumar Tiwari** and my former guide **Dr. Sunil Kumar** (Department of Chemistry, SSU), **Dr. Susheel Kalia** (Associate Professor & Head Dept. of Chemistry, ACC Wing (Academic Block) Indian Military Academy Dehradun). I am short of words in expressing my thanks to them, for their innovative ideas that shaped this document.*

*I appreciatively acknowledge the help rendered by **Prof. Heong-No Lee** (Dean of INFONET Laboratory at Gwangju Institute of Science and Technology, Republic of Korea), **Dr. Santosh Kumar** (School of Materials Science and Engineering, Gwangju Institute of Science and*

Technology (GIST), 123 Cheomdangwagi-ro Buk-gu, Gwangju, 61005, South Korea) and **Dr. Manoj Kumar**(Centre for Nanotechnology, Bharat Heavy Electricals Ltd., Hyderabad(A.P.),India)for theirstimulating suggestions and huge help throughout my whole research work.

I am also grateful to all the members of technical and non-technical staff of the department**Engg.Kamlesh Kumar Mishra,Mr. Ravender Tiwari, Mr. Deepak Singhand Ranvijay Singh** for their help and preciousassistance.

I am fortunate to have seniors and friends who have always stood beside me. I extend my heartfelt thanks to my bestfriends**Charu, Priyanka Chauhan,Dr. Hitanshu Minhas and Dr. Rajinder** who have always been listened my insane thoughts and ideas in spite of not understanding a bit of it. I am also grateful to my Seniors **Dr. Shweta Thakur, Dr. Sapna Thakur,Dr. Abhishek, Dr. Pawan, Jai Vardhan, Dr. Richa khokhra, Dr. Dikshita Gupta, Dr. Sarita Kangoo and Rajender Singh**for being there to make me sail through all the twists and turns of this journey. It is my pleasure to express my gratitude to **Rohit, Prashant, Jonny, Sampan, Krishnahari Sharma, Subhash, Neha and Asha**, research scholars of the Department of Physics and Materials Science for keeping me blessed with best wishes.I would like to thank my roommates **Nupur and Kavita**. The time spent with them willbe cherished throughout my life. The intention of this acknowledgement will be imperfect if I fail to appreciate the moral support and encouragement rendered by the most important person of my life i.e. my **parent's, brotherand family**who has always been my inspiration and never let me felt abandoned. It was their blessings and love which constantly motivated me and helped in the successful completion of my research work. I would like to express my heartfelt gratitude to all those who have contributed directly or indirectly towards obtaining my doctorate degree and apologize if have missed out anyone.

BANDNA BHARTI

ABSTRACT

A low temperature and economical method i.e. sol-gel method has been adopted to prepare TiO₂ sol. After the formation of TiO₂ sol, thin films of TiO₂ were prepared on the glass substrate by dip coating method. These films were formed both undoped and doped forms. The films were exposed in air plasma for varying time intervals to alter their surface properties. We observed a remarkable variation in the hydrophilic, optical and Photocatalytic properties of undoped and doped TiO₂ films after plasma treatment. The films coated on the surface of glass substrate when exposed to air plasma exhibited significant change in contact angle, which is basically a representative of wetting property. We found that the contact angle for deionized water and ethylene glycol reduced to considerable limits 3.02° and 1.85° from its initial value 54.40° and 48.82°, respectively. The variation in the hydrophilic property of films depends upon the dangling bonds and nanometer scale surface roughness created after plasma treatment. The variation in the surface roughness was estimated with the help of atomic force microscopy (AFM), which occurred from 4.6nm to 19.8nm with the plasma exposure time. Further, the variation in the values of contact angle and surface roughness with increasing plasma exposure time reveal that not only the surface roughness but the dangling bonds also contribute to the hydrophilic property of surface modified TiO₂ film. Based upon nanometer scale surface roughness and dangling bonds, a variation in the surface energy of TiO₂ film was estimated which was found to increase from 49.38 to 88.92mJ/m². In order to investigate the variation in the surface chemistry, X-ray photoelectron spectroscopy (XPS) studies were carried out. These results show that there was an increase in the intensity of Ti2p and O1s, and a decrease in the intensity of C1s. These surface modified films were examined for their antifogging properties by exposing then in water steam, which resulted as a good antifogging material on the surface of glass substrate.

In case of variation in the optical properties, we observed that a controlled, post-fabrication tuning of optical band gap of TiO₂ thin film is possible by plasma treatment. The controlled tuning of optical band gap is achieved by adjusting the time of plasma treatment. Again when studied by XPS, we observed that an alteration in the states of surface species viz. Ti³⁺, Ti⁴⁺, O²⁻, oxygen vacancies and OH group do occur by plasma treatment. In this case both the undoped (pure TiO₂) and doped (Fe and Co) TiO₂ were investigated. It is observed that widening or

narrowing of the optical band gap after plasma depends upon the type of impurity doping. We found that the plasma widened the band gap of Co doped TiO₂ film from 3.24 to 3.57eV, whereas it narrowed the band gap of Fe doped TiO₂ films from 3.36 to 3.10eV. The variation in surface states/chemistry and band gap was analyzed by X-ray photon spectroscopy (XPS) and UV-Vis spectroscopy, respectively. In this case too, the resultant band gap depends upon the plasma treatment time, higher the treatment time is more the band gap variation is; therefore, band gap can be precisely tuned just by adjusting treatment time. This approach facilitates band gap manipulation any number of times till the required/precise value is obtained, and liberates from in-situ band gap manipulation condition as in the traditional approaches. This approach mitigates band gap tuning, and is suitable for many optoelectronic applications. In the third experiment, the undoped and doped (Fe and Co) TiO₂ films were investigated for their Photocatalytic properties in sun light. The Photocatalytic activity of dip coated undoped, Fe and Co doped TiO₂ films was checked the degradation of Methylene blue (MB) dye. The Fe doped TiO₂ films show 50% degradation of Methylene blue due to the reduction in the band gap, formation of oxygen vacancies, Fe³⁺, and Fe²⁺ states. In case of Co doped TiO₂films, 30% degradation of MB dye in observed. Since we found that the Co doped TiO₂ films exhibited widen band gap which indicated that other factors; mainly formation of oxygen vacancies, then band gap is responsible for degradation of MB dye in sun light. Therefore, the generation of oxygen vacancies by air plasma can enhance the Photocatalytic activity of doped TiO₂ films. Thus we conclude that exposure to air plasma alters the surface states of TiO₂ films significantly and makes them applicable for many applications, such as photo electrochemical cells, antibacterial coating, self-cleaning materials, water splitting, solar cell, water purification etc.

TABLE OF CONTENTS		
INNER FIRST PAGE		i
ABSTRACT		xi-xii
ACKNOWLEDGMENT		ix-x
LIST OF FIGURES		xvi-xix
LIST OF TABLES		xx
LIST OF PUBLICATIONS		xxi-xxii
CHAPTER 1		1-27
	Introduction	
	1.1 Introduction	
	1.2 TiO ₂	
	1.2.1 Rutile	
	1.2.2 Anatase	
	1.2.3 Phase Transition	
	1.3 Applications of TiO ₂ nanostructures	
	1.4 Surface modification of TiO ₂ thin films	
	1.5 Synthesis methods for TiO ₂ thin films	
	1.6 Objectives of the thesis	
	1.7 Thesis Outline	
CHAPTER 2		28-40
	Synthesis and Characterization Techniques	
	2.1 Synthesis of TiO ₂ thin films	
	2.1.1 Materials	
	2.1.2 Preparation of TiO ₂ sol	
	2.1.3 Role of stabilizing agent	
	2.2 Thin film preparation	
	2.2.1 Substrate	
	2.3 Formation of TiO ₂ thin film by sol-gel dip coating method	
	2.3.1 Synthesis of Fe and Co doped TiO ₂ thin films	
	2.3.2 Surface modification of TiO ₂ , Fe-TiO ₂ and Co- TiO ₂ thin	

	films 2.4 Contact angle measurements and surface energy estimation 2.5 Characterization techniques 2.5.1 X-ray Diffractometer (XRD) 2.5.2 Scanning Electron Microscopy (SEM) 2.5.3 Energy Dispersive X-ray Spectroscopy (EDX) 2.5.4 Optical Characterizations (UV-Visible spectroscopy) 2.5.5 X-ray Photoelectron Spectroscopy (XPS) 2.5.6 Atomic Force Microscopy (AFM)	
CHAPTER 3		41-63
	<p style="text-align: center;">Super hydrophilic TiO₂ Thin Film by Nanometer Scale Surface Roughness and Dangling Bonds</p> 3.1 Introduction 3.2 Experimental method 3.2.1 Fabrication of TiO ₂ thin films 3.2.2 Surface modification of thin films by plasma exposure 3.3 Results and discussions 3.3.1 Structural analysis 3.3.2 Wetting State: experimental data and its interpretation 3.3.3 Atomic force microscopy observation 3.3.4 Explanation for the wetting properties 3.3.5 XPS analysis 3.4 Antifogging experiment 3.5 Summary	
CHAPTER 4		64-90
	<p style="text-align: center;">Enhancement of Optical Properties of TiO₂ Thin Films as a Result of Oxygen Vacancies and Ti³⁺ States by Air Plasma Treatment</p>	

	4.1 Introduction 4.2 Experimental methods 4.3 Materials characterization 4.4 Results and discussion 4.4.1 Structural and morphological studies 4.4.2 Optical studies 4.4.3 Surface characterization 4.4.3.1 X-ray Photoelectron microscopy (XPS) study 4.5 Summary	
CHAPTER 5		91-104
	Photocatalytic Activity of Fe and Co Doped TiO₂ Thin Films	
	5.1 Introduction 5.2. Experimental Section 5.2.1 Photocatalytic activity experiment 5.2.3 Sample characterization 5.3 Results and discussion 5.3.1 XRD Analysis 5.3.2 Morphological analysis 5.3.3 XPS analysis of pure and doped TiO ₂ films 5.4. Photocatalytic performance of undoped and doped TiO ₂ films 5.5 Summary	
CHAPTER 6		105-109
	Summary and Future Scope	
	References	110-133

LIST OF FIGURES

Figure Number	Caption	Page Number
Fig.1.1:	Different application encompasses by nanotechnology.	4
Fig.1.2:	Bulk structure of rutile and anatase.	7
Fig.1.3:	Phase diagram of the TiO ₂ system.	9
Fig.1.4:	Schematic diagram for the different application of TiO ₂ .	11
Fig.1.5:	Photo activation of a semiconductor and primary reactions occurring on its surface.	13
Fig.1.6:	Schematic diagram of different wetting angle: (a) Young's angle, (b) Wenzel angle and (c) Cassie angle.	14
Fig.1.7:	Different wetting states taking place on rough surfaces: (a) Cassie air trapping state, (b) Wenzel state, (c) Cassie impregnating wetting state and (d) mixed wetting state.	16
Fig.1.8:	Schematic diagram for the different fabrication methods of thin film.	22
Fig.2.1:	A flow chart for the formation of TiO ₂ sol.	31
Fig.2.2:	A schematic representation for TiO ₂ sol formation.	33
Fig.3.1:	XRD pattern of (a) unexposed TiO ₂ thin film and (b) exposed TiO ₂ thin film.	48
Fig.3.2:	EDX spectra of unexposed (a) and plasma exposed (b) TiO ₂ thin films, (c, d) SEM images of unexposed and plasma exposed TiO ₂ thin films	48
Fig.3.3:	Test liquids behaviour and contact angles of H ₂ O (left) and C ₂ H ₆ O ₂ (right).	49
Fig. 3.4:	AFM images of unexposed and exposed TiO ₂ film with glow discharge plasma for (a) 0 sec, (b) 10 sec, (c) 30 sec, (d) 120 sec, and (e) 180 sec.	54
Fig. 3.5:	RMS values of the plasma exposed TiO ₂ thin films as a function of exposure time.	55

Fig.3.6:	Difference in contact angle (a) surface energy and its ' γ_{LV}^P ', ' γ_{LV}^D ' component (b) with plasma treatment time.	58
Fig.3.7:	XPS survey spectra of TiO ₂ thin films (a) 0 sec, (b) 10 sec, (c) 30 sec, and (d) 120 sec.	59
Fig.3.8:	XPS spectra of Ti2p (a,b) and O1s (c,d) core level for TiO ₂ thin films.	60
Fig.3.9:	Comparison of antifogging properties of uncoated and TiO ₂ coated glass and plasma exposed samples for (a) 30 sec, (b) 60 sec and (c) 120 sec.	62
Fig.4.1:	SEM images of TiO ₂ , Fe doped TiO ₂ and Co doped TiO ₂ thin films (a) pure TiO ₂ film, (b) pure/treated TiO ₂ film; plasma treatment time 60 seconds, (c) Fe doped/untreated TiO ₂ film, (d) Fe doped/treated TiO ₂ film; plasma treatment time 60 seconds (e) Co doped/untreated TiO ₂ film, (f) Co doped/treated TiO ₂ film; plasma treatment time 60 seconds.	71
Fig.4.2:	EDX spectrum of thin film of (a) pure TiO ₂ , (b) Fe doped TiO ₂ , and (c) Co doped TiO ₂ .	72
Fig.4.3:	X-ray diffraction spectra of (a) Fe doped/untreated TiO ₂ film; plasma treatment time 0 second, (b) Fe doped/treated TiO ₂ film, plasma treatment time 60 second, (c) Co doped/untreated TiO ₂ film, plasma treatment time 0 second and (d) Co doped/treated TiO ₂ film; plasma treatment time 60 second.	73
Fig.4.4:	X-ray diffraction spectra of thin films for 30 seconds of plasma treatment (a) pure TiO ₂ , (b) Fe doped TiO ₂ , and (c) Co doped TiO ₂ film.	74
Fig.4.5:	Optical absorption spectra and Tauc plot ($(\alpha h\nu)^{1/2}$ versus $h\nu$ plots) in the inset for (a) Fe doped/untreated TiO ₂ film; plasma treatment time 0 second, (b) Fe doped/treated TiO ₂ film; plasma treatment time 10 second (c) Fe doped/treated TiO ₂ film; plasma treatment time 30 second and (d) Fe doped/treated TiO ₂ film; plasma treatment time 60 second.	77
Fig.4.6:	Optical absorption spectra and Tauc plot ($(\alpha h\nu)^{1/2}$ versus $h\nu$ plot) in the inset for (a) Co doped/untreated TiO ₂ film; plasma treatment time 0 second, (b) Co doped/treated TiO ₂ film; plasma treatment time 10 second, (c) Co doped/treated TiO ₂	78

	film; plasma treatment time 30 second and (d) Co doped/treated TiO ₂ film; plasma treatment time 60 second.	
Fig.4.7:	Plots for variation of optical band gap of Fe and Co doped TiO ₂ thin film with plasma treatment time.	79
Fig.4.8:	XPS survey spectra in a(i) pure TiO ₂ film indicating all the peaks of elements present in the sample, here the appeared carbon peak is instrumental impurity, a(ii) Fe doped/untreated TiO ₂ film; plasma treatment time 0 seconds, a(iii) Fe doped/treated TiO ₂ ; plasma treatment time 60 seconds, b(i) pure TiO ₂ film which is similar to a(i), and b(ii) Co doped/untreated TiO ₂ film; plasma treatment time 0 seconds, b(iii) Co doped/treated TiO ₂ film; plasma treatment time 60 seconds.	80
Fig.4.9:	High resolution XPS spectra of Ti2p and O1s in (a) pure/untreated TiO ₂ film, (b) Fe doped/untreated TiO ₂ film; plasma treatment time 0 second, (c) Fe doped/treated TiO ₂ film; plasma treatment time 60 seconds, (d) O1s for pure/untreated TiO ₂ film, (e) O1s for Fe doped/untreated TiO ₂ film; plasma treatment time 0 second, and (f) O1s for Fe doped/treated TiO ₂ film; plasma treatment time 60 seconds.	82
Fig.4.10:	High resolution XPS spectra of Fe2p in (a) Fe doped/untreated TiO ₂ film; plasma treatment time 0 second, (b) Fe doped/treated TiO ₂ film; plasma treatment time 60 seconds, (c) and (d) are Gaussian fit of (a) and (b).	84
Fig.4.11:	High resolution XPS spectra of Ti2p and O1s in (a) pure/untreated TiO ₂ film, (b) Co doped/untreated TiO ₂ film; plasma treatment time 0 second, (c) Co doped/treated TiO ₂ film; plasma treatment time 60 seconds, (d) O1s for pure/untreated TiO ₂ film, (e) O1s for Co doped/untreated TiO ₂ film; plasma treatment time 0 second, and (f) O1s for Co doped/treated TiO ₂ film; plasma treatment time 60 seconds.	86
Fig.4.12:	High resolution XPS spectra of Co2p in (a) Co doped/untreated TiO ₂ film; plasma treatment time 0 second, (b) Co doped/treated TiO ₂ film; plasma treatment time 60 seconds, (c) and (d) are Gaussian fit of (a) and (b).	88
Fig.4.13:	Schematic diagram of the energy levels of (a) pure/untreated TiO ₂ films, (b) Fe doped/untreated TiO ₂ film, (c) Fe doped/treated TiO ₂ ; for 60 seconds of treatment time, (d) Co doped/untreated TiO ₂ film, (e) Co doped/treated TiO ₂ film; for 10, 30 and 60 seconds of treatment time, indicating Burstein	90

	Moss effect (O_v represents oxygen vacancies).	
Fig.5.1:	Schematic diagram of the preparation of undoped, Fe and Co doped TiO_2 films (left) and cleaning of the glass substrate (right).	96
Fig.5.2:	XRD pattern of (a) pure TiO_2 , (b) Fe doped TiO_2 and (c) Co doped TiO_2 films.	97
Fig.5.3:	SEM micrograph of pure TiO_2 , Fe doped TiO_2 and Co doped TiO_2 thin films.	98
Fig.5.4:	XPS survey spectra of (a) Fe doped TiO_2 and (b) Co doped TiO_2 film.	99
Fig.5.5:	Sunlight degradation of Methylene Blue (a) undoped TiO_2 , (b) Fe doped TiO_2 and (c) Co doped TiO_2 films.	100
Fig.5.6:	Photocatalytic activity of undoped, Fe and Co doped TiO_2 films under sunlight irradiation.	101
Fig.5.7:	Representation of degradation mechanism by undoped, Fe doped and Co doped TiO_2 films in the sunlight.	103

LIST OF TABLES

Table Number	Caption	Page Number
Table 1.1	Physical and structural properties of TiO ₂ .	8
Table 2.1	Surface tension components of the testing liquids.	35
Table 3.1	Known surface tension of test liquids.	47
Table 3.2	Effect of plasma exposure time on the contact angle and corresponding surface energy of TiO ₂ films.	50
Table 4.1	Variation in absorption edge and band gap of Fe and Co doped TiO ₂ thin films with plasma treatment time.	75
Table 4.2	XPS data of different chemical states of O, Ti, Fe and Co elements on the surface of untreated TiO ₂ , Fe doped/treated TiO ₂ and Co doped/treated TiO ₂ where O _L represents lattice oxygen, O _s represents sub oxide and O _{NL} non lattice oxygen/oxygen vacancies.	81

LIST OF PUBLICATIONS

PAPERS IN INTERNATIONAL REFEREED JOURNALS:

1. **Bandna Bharti**, Santosh Kumar, Heung-No Lee & Rajesh Kumar “Formation of oxygen vacancies and Ti^{3+} state in TiO_2 thin film and enhanced optical properties by air plasma treatment” **Scientific Reports** 6:32355.
2. **Bandna Bharti**, Santosh Kumar & Rajesh Kumar “Superhydrophilic TiO_2 thin film by nanometer scale surface roughness and dangling bonds” **Applied Surface Science** (Vol 364, Pages 51–60, 2016).

Other

3. Richa khokhra, **Bandna Bharti**, Heung-No Lee & Rajesh Kumar “Visible and photodetector in ZnO nanostructured thin films via simple tuning of solution method” **Scientific reports** 7 (2017).

PUBLICATIONS IN PROCEEDINGS:

1. **Bandna Bharti** and Rajesh Kumar (2016). Formation of surface groups to enhance the wettability of titanium dioxide (TiO_2) thin films, International Conference on Advances in Nanomaterials and Nanotechnology (ICANN-2016) from 4-5 November 2016, organized by center for Nanoscience and Nanotechnology, JamiaMilliaIslamia, New Delhi, India.
2. **Bandna Bharti**, Partha, Bir Barman, Rajesh Kumar (2015). XRD analysis of Titanium Dioxide (TiO_2) and Fe doped TiO_2 nanoparticles by Williamson Hall Method, 4th National conference on advanced materials and radiation physics. *AIP Proceedings of the AMRP2015* [Sangroor, Punjab, India: March 13-14, 2015].

MANUSCRIPT COMMUNICATED:

1. Cobalt doped TiO₂ Nano thin films: Plasma treatment, Phase Structure, Surface, and Magnetic Properties”
2. Photocatalytic activity of Fe and Co doped TiO₂ thin films-Effect of plasma treatment.

PRESENTATIONS IN NATIONAL AND INTERNATIONAL CONFERENCES:

1. International Conference on Advances in Nanomaterials and Nanotechnology (ICANN-2016) from 4-5 November 2016, organized by center for Nanoscience and Nanotechnology, Jamia Millia Islamia, New Delhi, India.
2. International Conference on Science: Emerging Scenario & Future Challenges (SESFC 2016) 11 - 12 June 2016, Dharamshala (H.P.) **(Best Poster Presentation)**.
3. International conference Nano SciTech 2014 held in Punjab University, Chandigarh from 18-20 March 2016.
4. National Conference on Advanced Materials and Radiation Physics (AMRP-2015) (March 13-14, 2015)[SLIET, Longowal (Punjab) India].
5. National Conference on Multifunctional Advanced Materials, at Shoolini University, Solan, India, June 11-12, 2014.
6. National Seminar on “Recent Trends in Materials, Energy and Environment” (NSRTMEE-2014) held in Sri Sai University Palampur, (H.P) 18th January 2014.
7. One-week Workshop on “Nanotechnology (Fabrication and Characterization)” December 11, 2013 at JUIT Warknaghat.



CHAPTER I

Introduction

1.1. Introduction

The term “*Nano*” is arguably the most inspirational thing to take place in science and technology since the space race. Nanotechnology is moderately new, while the essence of operative devices and structures of nanometer range is not innovative because they exist on the earth as long as life itself. Nanotechnology is a growth industry in the field of research, over four billion dollars per years growing at an annual rate of about 20% [1] running by worldwide government funded research. Application and production of chemical, physical and biological system encircle by nanotechnology differ from discrete atom or molecule to submicron extent. Nanotechnology spread much area which is shown in Fig.1.1. In the early 21st century, there is great impact of nanotechnology on our society and economy as compared to cellular & microbiology, informational & semiconductor technology. Thus, science and technology investigation in nanotechnology penetrate in areas such as manufacturing and materials, nanoelectronics, healthcare energy and medicine, biotechnology and national security. There are many benefits to research and exploration of nanotechnology. The scientific possibilities are endless and we have only just begun to breach the frontier of nanoscience. Hence, nanotechnology associated with fabrication and/or manipulation, and characterization of structure devices or materials that have at least one dimensional that is approximately 1-100nm in length. In fact, public view regarding the general application of nanotechnology has varied from neutral to slightly positive [2-5]. At the nanometer scale, materials are the essence of technology, because the atomic group and the arrangement not only describe the properties of the materials but also the purpose of the devices at the nanotechnologies scale. Basically, nanotechnology controlled the atomic/molecular placements, arrangements and promotes the technologies into distinctive materials, structures and devices. This new type of formation requires advanced methodology, to understand the development of materials on the nanoscale. Mentioned nanomaterials involved all the nano-object like nano-plates, nano-fiber (rods, tubes), and nano-thin films which can be expressed by distinctive materials to form aggregate [6-8]. Thus with the wide spread industrialization of nanotechnology, nanomaterials applications in the area of materials

modification, degradation of environment pollutants, area of medical diagnostics, and biotechnology are rapidly increasing [9].

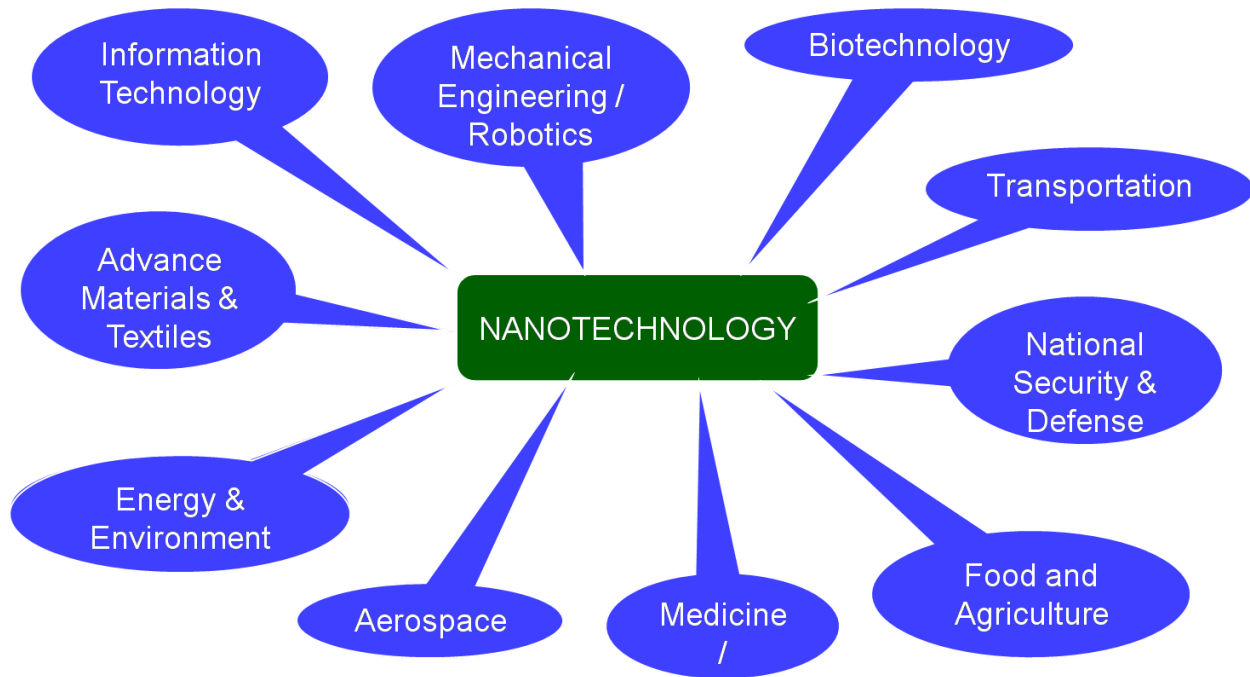


Fig.1.1: Different application encompasses by nanotechnology.

Nanomaterials are well known to possess excellent optical, catalytic, electrical, thermal and strong mechanical strength which offers great opportunity to construct nanomaterials based sensors and other devices [10]. When the size of the material particle is reduced, and it comes to the range of less than 100nm its physical and chemical properties are altered. The resultant properties are also depending upon the shape of the nanostructures, for example the same material in different forms such as nano-dot, nanowires, nanocones etc. shows different properties. There are many resorts on the properties and fabrication procedures of the nanomaterial [11]. When the size of the material is reduced to nanometer scale, it affects the motion of the electrons and holes in the structure and thus resulting in changed properties [12-15]. Also, with the reduction of the size, the surface area of structure increases, creating new surface, and thus the free bonds on it that also affects many physical and chemical properties [16].

In fact, the research in this field desiresto discover some unique structures properties and synthesis mechanisms so that the nanostructures can be produced commercially.To understand the fundamental phenomenon in the nano range it is quite reasonable to know the synthesis processes as well as the structure of materials at the atomic level for the effective growth of nanostructures for the commercial purpose.

Metal oxides are tremendously studied in the areas of physics, chemistry, materials science, biology and medical science [17, 18]. The chemical and electronic properties of metal oxide made them a stimulating candidate for technological and scientific applications. These oxides are frequently used for fabricating rust proof coatings of surfaces [19], catalysts [20], sensors [21], energy cells [22], microelectronic circuits [23] and optoelectronic devices [24]. Due to the difference in electronic structure, the metal oxide exhibits semiconducting, metallic or insulating behavior. Oxides comprise an extensive variety of electrical properties from wide band gap insulators to extremely conducting metals and even that of superconducting materials. The wide band gap semiconducting oxides, such as MoO_3 , SnO_2 , TiO_2 , ZnO , Al_2O_3 etc., are useful for many applications, including gas sensors, transparent conducting oxides and optical components. Among various materials, Titanium Dioxide (TiO_2) is better oxide materials investigated in today literature due to its optoelectronics properties for a variety of applications due to its strong oxidizing power, long term stabilization against photo/chemical corrosion, biological inertness and its inoffensively behavior [25]. Its particles films possessing large surface areas are more important as they provide enhance properties in many applications such as adsorption of dye to absorb photons in solar cell and photocatalyticactivity. In the present work, we have adopted sol-gel dip coating method for the fabrication of thin films. These prepared TiO_2 thin films were used for environmental, optical and opto-electronics application.

1.2. TiO_2

TiO_2 correspond to the group of transition metal oxides. TiO_2 exists in both crystalline and amorphous forms. Titanium is the most important element in the earth's crust comprising an estimated 0.62% of the earth crust [26]. The naturally occurring ores of TiO_2 is ilmenite (FeTiO_3), mineral rutile and brookite [27]. At atmospheric pressure, TiO_2 is only the natural

occurring oxide of titanium, found to exhibit three different polymorphs: Rutile, Anatase and Brookite [28]. Anatase and Brookite are the metastable phases whereas Rutile is the most stable phase of TiO_2 . Srilankite, cubic fluorite, pyrite, monoclinic baddeleyite and cotunnite are the phases of TiO_2 occurring at high pressure. Durability of these phases discussed by several authors [29]; however, they are of minor significance for the application point of view. Though, only anatase and rutile play role in most of the application of TiO_2 . In both the structure the basic units are TiO_6 octahedron and the structures of TiO_2 depends upon their configuration.

1.2.1. Rutile

Rutile phase of TiO_2 is most stable; it shows stability at all the temperatures and pressure up to 60 kbar. The rutile phase shows small free energy as compared with anatase and brookite phase. Rutile TiO_2 has a tetragonal structure; each Ti is bonded to six O atoms (Fig. 1.2) with the equatorial Ti-O bond length of 1.946\AA . The lattice parameters for rutile phase are $a=b=4.583\text{\AA}$, $c=2.958\text{\AA}$. The TiO_6 octahedron is slightly distorted. Two phases' i.e. anatase and brookite transforms to the rutile phase depending upon the particle size, which is more stable phase if the particle size is more than 14 nm [30]. The activity of the rutile phase as a photocatalyst is generally very poor. Depending on its preparation conditions, the activity (active or inactive) of the rutile phase can suggest [31].

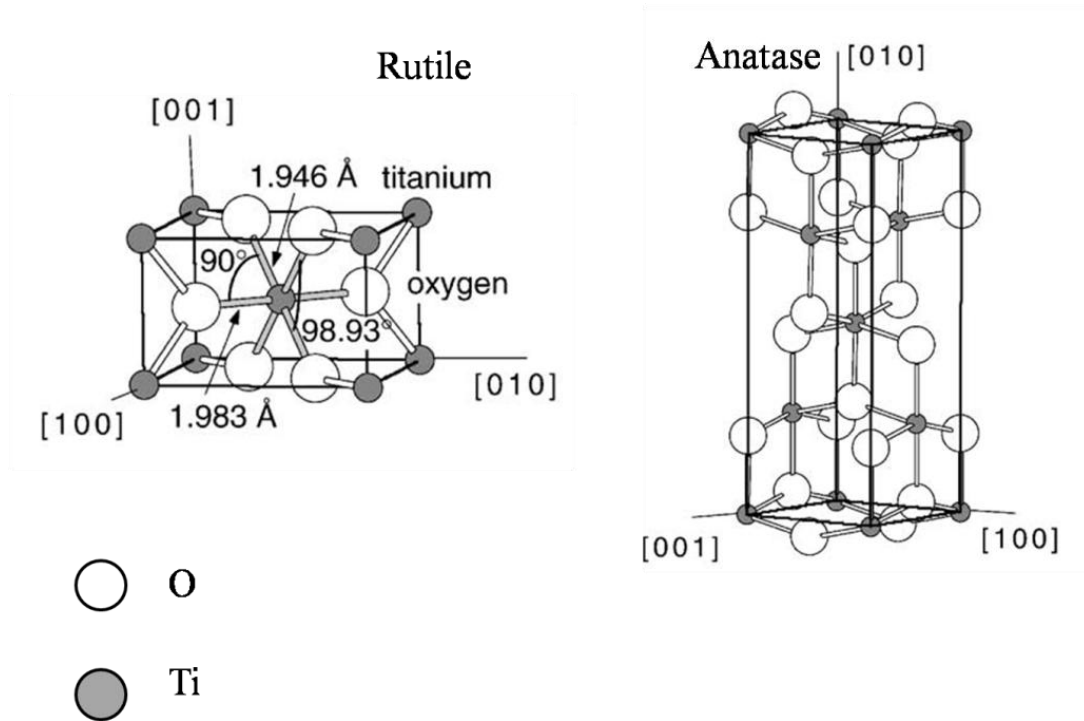


Fig.1.2: Bulk structure of rutile and anatase.

1.2.2. Anatase

The anatase phase of TiO_2 has a tetragonal crystalline structure same as the rutile, but it shows slightly more distortion of TiO_6 octahedron as shown in Fig. 1.2. The energy difference between anatase and rutile phase is very small (2 to 10 kJ/mol), however, the stability at 0K of anatase phase is more than the rutile phase. The lattice parameter for anatase TiO_2 are $a=b=3.784\text{\AA}$, $c=9.502\text{\AA}$ with equatorial and apical bond length of 1.934\AA and 1.980\AA , respectively. Anatase shows slightly higher fermi level position, which increase in the photo reactivity, smaller capability to absorb oxygen and higher degree of hydroxylation [32]. The anatase structure is preferred over other phases as it shows higher value of the conduction band edge, and small recombination rates of the electrons and holes. Some of the physical and structural properties of TiO_2 phase were shown in the Table 1.1[33]

Table 1.1 Physical and structural properties of TiO₂.

Property	Anatase	Rutile
Molecular Weight(g/mol)	79.88	79.88
Melting Point (°C)	1825	1825
Boiling point (°C)	2500-3000	2500-3000
Specific Gravity	3.9	4.0
Light Absorption (nm)	$\lambda \leq 385$ nm	$\lambda \leq 415$ nm
Mohr's Hardness	5.5	6.5 to 7
Refractive Index	2.55	2.75
Dielectric Constant	31	114
Crystal Structure	Tetragonal	Tetragonal
Lattice Constant	a=3.784, c=9.502	a=4.593, c=2.958
Density (g/cm ³)	3.79	4.13
Solubility in Water	Insoluble	Insoluble
Solubility in HF	Soluble	Insoluble

1.2.3. Phase transition

The transformation from anatase to rutile phase at higher temperature can be easily explained by the phase diagram. With a variety of crystal structure, the Ti-O phase diagram is very affluent with many stable phases. When the titanium dioxide stoichiometry is varied from 0 to 2, Ti, Ti₂O, TiO, Ti₂O₃, Ti₃O₅, Ti_nO_{2n-1}, and TiO₂ are encountered as shown in Fig.1.3. Rutile and anatase structures are compatible with stoichiometry higher than 1.95 only. Above 700°C rutile phase occurs, as titanium dioxide becomes liquid, whereas after 500°C anatase phase of TiO₂ were formed.

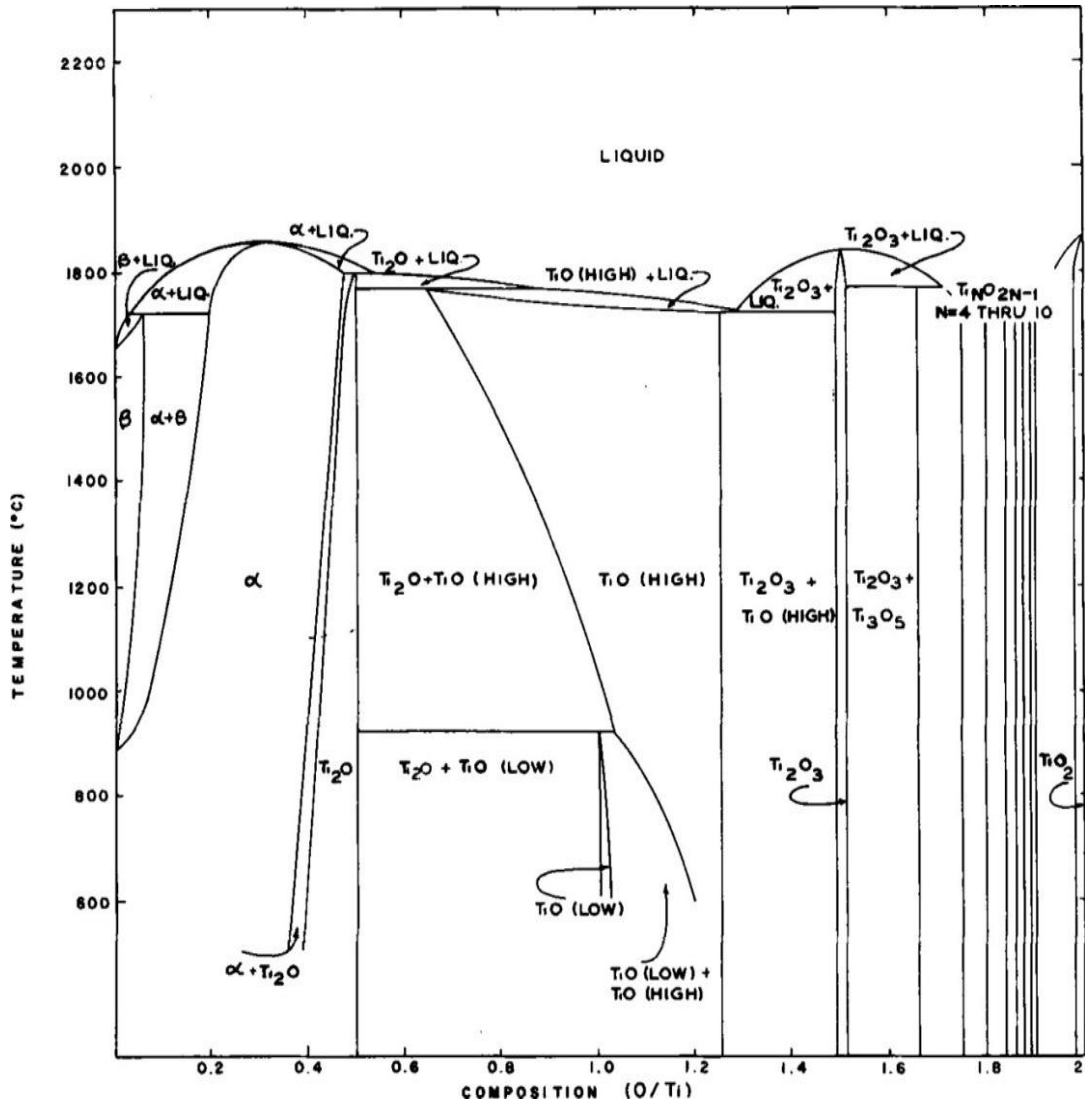


Fig.1.3: Phase diagram of the Ti-O system [34].

Thus size, shapes, organization and surface properties altered the chemical and physical properties of TiO_2 .

1.3. Applications of TiO₂ nanostructures

Owing to a huge commercial market of TiO₂-based products, large numbers of work has been reported since last two decades. The viable and auspicious applications of TiO₂ nanomaterials include toothpaste, paint, photovoltaics, photocatalysis, UV protection, sensing and photochromic as well as electrochromic. TiO₂nanomaterials have high absorption in the UV region because the electronic band gap of TiO₂ normally larger than 3.0eV. Optical and biologically amiable properties of TiO₂ allow them to be suitable candidate for UV protection applications [35-38].As summary of applications, TiO₂is used in a broad range of research areas shown in Fig.1.4 [39].

In sensing applications, TiO₂films have been used due to their optical or electrical properties which were change upon adsorption. Grimes *et al.* [40, 41] organized a sequence of admirable studies on sensing using TiO₂ nanotubes. They observed that TiO₂ nanotubes were act as a brilliant hydrogen sensor not only with a high sensitivity but in additions they have the ability of self-cleaning andphoto activity. Besides these TiO₂nanomaterials shows potential for CO, methanol and ethanol sensing. In display applications such as electrochromic displays and windows [42] nanostructures ofTiO₂ have been investigated mostly owing to their significant properties of titania electrode i.e. broad surface area, high surface affinity toward certain ligand, visible light transparency, and electronic conductivity [43, 44]. For example, *Choi et al.* [45] fabricated thin film electrodes represented by meso-nc-TiO₂-V (2+) for the electrochromic application. They also observed that well-organized meso-nc-TiO₂-V (2+)electrode display similar reversibilityandcolor switching speedas nanocrystallinetitaniabut with enhanced performance in terms of color dissimilarity.Similarly, the dye-sensitized TiO₂ is used in chromic smart windows by Pichot*et al.* [46]. A typical transmittance of 75% of visible light is observed initially, and when the device was exposed to visible light the transmittance reduced to 30%. Upon removal of the light source the window returned to its initial state of without illumination. In this mechanism, the window ideally behaved like a capacitor. In energy production applications such as solar cells the TiO₂nanocrystalline electrodes have been used [47].

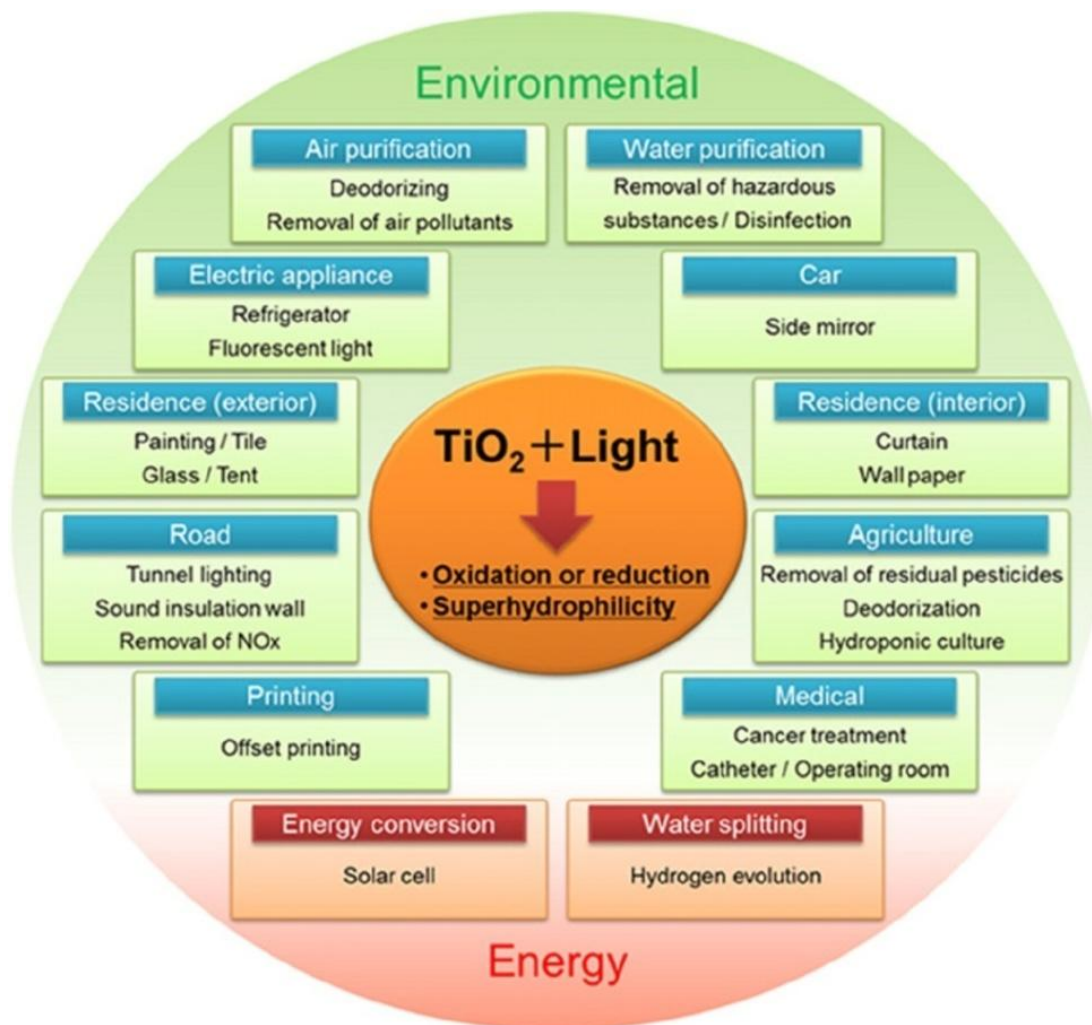


Fig.1.4: Schematic diagram for the different application of TiO_2 .

Although, TiO_2 has wide band gap and can absorb UV radiation of the spectrum, but when the band gap is tuned it can absorb visible spectrum of the light. In some of the solar related applications it is used with photo-sensitizers such as dye [48]. For example, in the dye sensitized solar cell, when TiO_2 is used with dye, the dye molecules absorb visible radiations and the photo-generated electrons are entered to the TiO_2 used as sensitizer, making absorption of visible light. The generated photo-voltage is determined by the chemical potential [49]. In this process,

separation of the charge takes place at the surface of dye and TiO_2 , and the factors causing this separation are driven from the enthalpy and entropy forces. In these applications, the porosity is an important factor because a high porous surface can absorb larger amount of the dye [50]. In the clean energy applications, this material is used for efficient production of the electricity and/or hydrogen.

Again, for the production of energy, taking the advantage of suitable electronic band structure of TiO_2 which gives redox potential of water; studies have been done for the water splitting and hydrogen origination [51]. In these processes, there is a generation of holes/electrons in their respective valence and conduction band when TiO_2 absorbs light. This charge carrier was responsible for the redox reaction. H_2 are formed when H_2O molecules reduced by the electrons and oxidized by the holes to form oxygen molecule which give the overall water splitting [52]. The potential of TiO_2 is just rely on the potential of H_2 and O_2 which are thermodynamically required. The highest level of valence band must be more positive than the oxidation potential of $\text{O}_2/\text{H}_2\text{O}$ (1.23 V) while the lowest level of the conduction band has to be more negative than the reduction potential of H^+/H_2 (0 V vs NHE). TiO_2 is considered as the most experienced and environmentally approachable photocatalyst, and it has been broadly used for photo-degradation of different pollutants [53-55].

In environmental/photocatalytic applications, TiO_2 photocatalyst has been accomplished with *E. coli* suspensions to kill bacteria [56] and it can be used for the cancer treatment to kill the tumor cells due to the strong oxidizing power of TiO_2 [57]. The mechanism for the photocatalytic reaction is straightforward. Electron/hole pairs are formed when light is absorbed by the photons with energy greater than their band gap.

The produced charge carrier moves around the surface, and reacts with the adsorbed chemicals on the surface to decompose them. Intermediate species such as H_2O_2 , $\cdot\text{OH}$, O_2 or O^{2-} resulted from the photodecomposition process which were very essential for the photocatalytic reaction mechanisms (as shown in Fig. 1.5). The factors affecting the photocatalytic activity are basically absorption properties of the material, rates of oxidation and reduction by photo-generated electron and hole, and their electron/holes recombination rates.

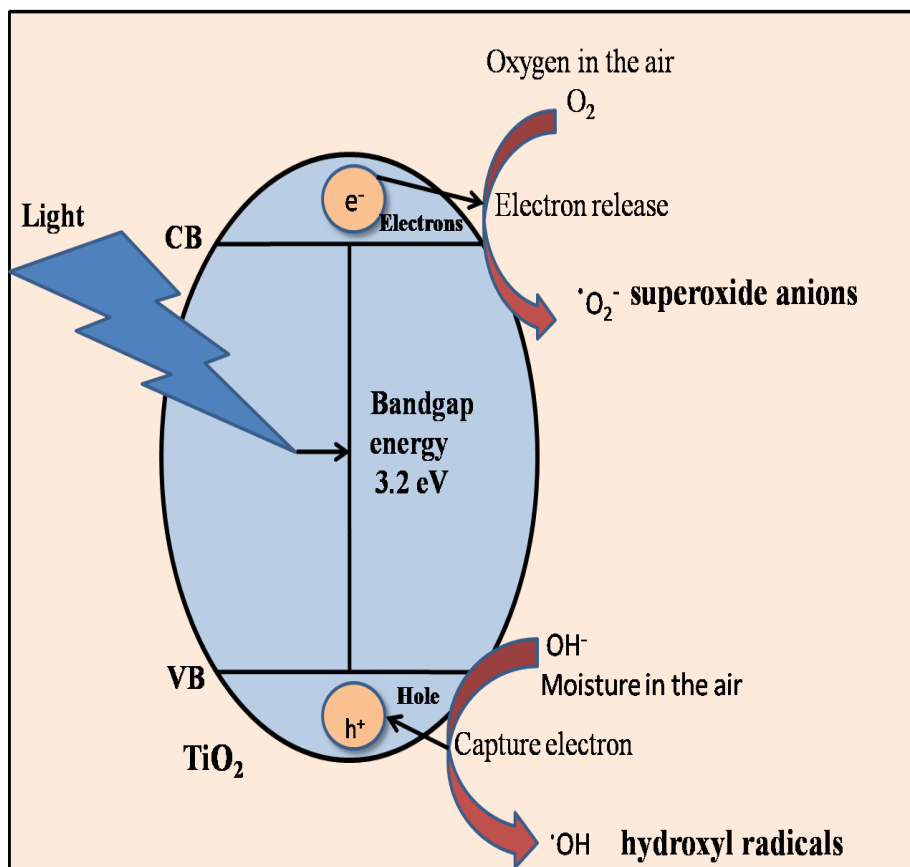


Fig.1.5: Photo-activation of a semiconductor and primary reactions occurring on its surface.

By virtue of its property as a semiconductor, when ultraviolet light applied to TiO₂ it gives rise to electron/hole pairs which are applicable for many applications. While as a superior photocatalyst, TiO₂ works only in the UV region (<380nm) owing to its wide band gap which confines its uses. Thus, it would be important if the visible portion of the light could be used for making photocatalysts based upon the TiO₂ material. However, in certain applications such as photocatalysts and optical absorbing material for photovoltaic cells the band gap of TiO₂ needs to be modified to bring its optical band gap into the visible light range, and to generate electron/hole pairs essential for such functionalities.

Similarly, in wetting applications TiO₂ nanomaterial shows antifogging behavior on diverse glasses product, i.e., eyeglasses & mirrors, having super hydrophobic or Superhydrophilic surfaces.

[58]. Feng *et al.* [59] found that when the TiO₂nanorods films were subjected to UV light, surface oxygen vacancies were created by the reaction of lattice oxygen with photo generated hole. Due to the creation of oxygen vacancies on the surface of the TiO₂, the water spreads and enters to the groves on the surface showing a contact angle near to 0 degree, which is the state of super hydrophilicity.

Wetting is crucial occurrence in different natural and technical processes together with the wetting of soils, painting, printing, textile impregnation, etc. During the earlier period, the wetting of rough surfaces has paying much attention[60]. When a water droplet is positioned or falls onto a solid surface, there is an appearance of sessile drop as the shape of a sphere. There is an isolated and substantial contact angle between the water droplet sphere and the surface at the spherical solid/liquid/vapor three phase contact line. In 1804 *Thomas Young* recommended that every solid/liquid pair has an “appropriate angle of contact” [61] in “An Essay on the Cohesion of Fluids.” For smooth surfaces, the wetting is designated by the equilibrium or Young angle, given by the widely known Young equation:

$$\cos\theta = \frac{\gamma_{SA} - \gamma_{SL}}{\gamma} \quad (1.1)$$

where the symbols γ , γ_{SA} and γ_{SL} correspond to the surface tensions at the liquid/air, solid/air interfaces and solid/liquid, respectively. *Young* equation affords a single value of the contact angle for the certain combinations of solid, liquid and gaseous phases. Schematic representation of *Young*, *Wenzel* and *Cassie* angle is shown in Fig. 1.6.

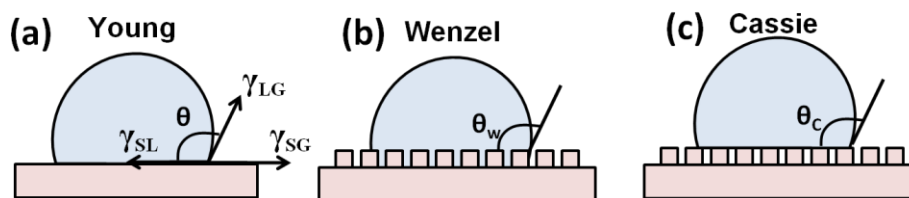


Fig.1.6: Schematic of different wetting angle: (a) Young’s angle, (b) Wenzel angle and (c) Cassie angle.

Unfortunately, due to some complicated experimental situation on flat surfaces, a uniformity of

contact angles is observed by its extended range interaction between molecules forming the three-phase contact line of the droplet. Further some experimental and theoretical perception must be highlighted on the wetting of liquids on the rough surfaces which is not clear since most of the natural and artificial solid surfaces are rough to some extent. *Cassie and Wenzel* 50 years ago developed the main theoretical routes to the wetting properties [62]. According to the *Cassie* model [63], when a drop is fall on the surface air can remain trapped in the pores under the drop, creating “air pockets” as shown in Fig.1.7(a). *Wenzel* [64] developed a model for the wetting of rough chemically homogeneous surfaces. According to this model, surface roughness r_f is defined as the ratio of the real surface in contact with liquid to its projection onto the horizontal plane which always magnifies the causal wetting properties (Fig.1.7(b)). The relation between surface roughness and apparent *Wenzel* contact angle is given by

$$\cos\theta^* = r_f \cos\theta \quad (1.2)$$

In fact, pure *Cassie* and *Wenzel* wetting were hardly occurring so after *Cassie* and *Wenzel* Marmur [65] suggested a merged wetting state. In this state, when a drop is placed on the surface it partially wets the surface and partially settle down on the air pockets, as depicted in Fig.1.7(d). Therefore, apparent contact angle (APCA) in this case is as follows:

$$\cos\theta^* = r_f f \cos\theta + f - 1 \quad (1.3)$$

Where the symbol f represents the fraction of the projected area which is soaked by the liquid. When $f = 1$, equation (1.3) turns into the *Wenzel* equation (1.2). *Bico et al.* [66] introduced one more wetting state that is *Cassie* penetrating state described in Fig.1.7(c).

$$\cos\theta^* = 1 - f_s + f_s \cos\theta \quad (1.4)$$

From the above discussion, it is obvious that most of the applications involve surface properties of TiO_2 nanostructures. Most of the applications utilize thin film of TiO_2 , indicating that the thin film structure of TiO_2 are comparatively important in many technological applications. From the above discussion, we also conclude that for the efficient utilization of TiO_2 in environmental and optical applications its surface as well as optical properties needs to be improved. In the following section, we give a brief literature related to the need of surface modification and its methods.

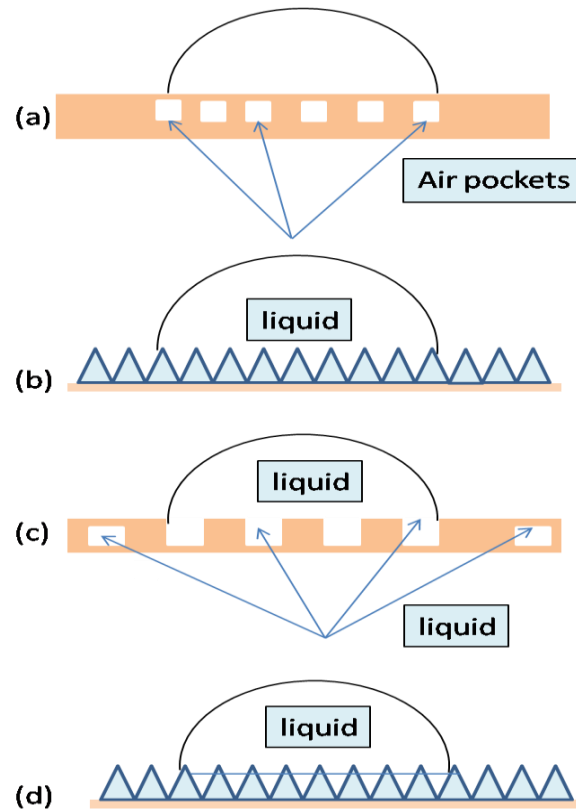


Fig.1.7: Different wetting states taking place on rough surfaces: (a) Cassie air-trapping state, (b) Wenzel state, (c) Cassie impregnating wetting state and (d) mixed wetting state.

1.4. Surfacedmodification of TiO_2 thin films: need and methods

Surface modification not only influence the charge separation, optical properties (absorption edge, optical band gap), and recombination processes but also have significant impact on their interfacial energy. There are many ways to modify the surface of a material to improve its functionality [67, 68]. Numerous experiments have been done to modify TiO_2 to respond to the visible light. Some of the metal and nonmetal element have been employed to tune electronics and photocatalytic activity of TiO_2 by chemical or physical methods. They

include: doping and deposition of TiO₂ using noble metals such as platinum [69], silver [70], gold [71] etc., inclusion of transition elements such as Cr, Fe, Co, W, Cu, V [72-77], and doping of non-metals such as S, P, F, N, C [78-82] etc. To enhance the absorption in the visible region, transition metals doping in TiO₂ (V, Cr, Mn, Fe, Co, and Ni) is mainly recognized as one of the finest routes to narrow the band gap. However, these transition metal ions reduced the photo-generated charge carrier life time. Therefore, with the reduction in the life time of charge carrier and increase in their recombination rate results in a decreased photo catalytic activity of doped TiO₂. So to minimize the recombination processes by introducing trap state for electron/hole, when a small concentration of transition metals (around 1-2 at. %) were inserted into the TiO₂ matrix. Choi *et al.* [83, 84] reported a consistent research on TiO₂ through the addition of 21 metal ions. They considered that between varieties of transition metal ions, Fe³⁺ was declared advantageous due to their stable half-filled configuration. With proper concentration of Fe³⁺ ions, it has been found that Fe³⁺ ions are not only narrow the band of TiO₂ but also support the electron/hole pairs separation. Wu *et al.* [85] conducted a succession of vanadium-TiO₂ photocatalyst synthesized by 2 modified sol-gel methods. As synthesized vanadium-TiO₂ exhibit a red-shift in the UV-vis spectrum and shows higher activity in the dye degradation under visible light as compared to pure TiO₂. Similarly, Ali *et al.* [86] fabricated V doped TiO₂ thin films by RF sputtering. They found the increased photocatalytic properties when V is substituted in the Ti⁴⁺ state resulted in the additional bands in the photoluminescence of TiO₂. Sathasivam *et al.* [87] have used CVD method for the fabrication of photo catalytically active, electrically conductive and transparent, thin films of W-TiO₂ films. The optical transparency in the visible region makes them appropriate candidates for the photovoltaic devices (as electrodes). Moreover, in the removal of supportive redox dye when irradiated by UVA radiation the W doped films revealed the superior photocatalytic activity as compared to the undoped TiO₂. Xin *et al.* [88] reported that with appropriate content of Cu (about 0.06 mol %) the Cu-TiO₂ photocatalyst acquire abundant electronic trap, which efficiently inhibits the recombination of photo induced charge carriers, ameliorate the photocatalytic activity of TiO₂. Similarly, Tian *et al.* [89] concluded that the band gap of Co doped TiO₂ thin films vary between 3.10 and 3.26 eV. With increasing the concentration of Co, the band gap first increase and then

decreases. The reason for the increase in the band gap is related to the compressive stress and reduced grain size, whereas due to the presence of defect and impurity the band gap decreased. In another study, Peng *et al.* [90] synthesized Cr-doped TiO₂ nanocrystalline film by a sol-gel method. These films have been systematically investigated to see the effect of Cr content and annealing temperature on the photocatalytic activity of TiO₂. The crystalline phases of undoped TiO₂ thin films convert from pure anatase to rutile structure between 600 and 700°C. Cr-doping not only conclusively reduced the grain size but also decrease the phase transition temperature of anatase to rutile phase of TiO₂. With Cr doping there was the formation of oxygen vacancy which improved the photocatalytic activity of Cr-TiO₂ films. Several reports of Cr doping have been shown by different authors who revealed the decrease photocatalytic activity of TiO₂ under UV light irradiation [91, 92]. The decrease in the photocatalytic activity was attributed to either reduced redox power or the formation of recombination centers. After numerous failed efforts with cationic doping, anionic nitrogen doping has become progressively more popular. Many anionic dopants have consequently been studied; due to the easy adaption of nitrogen in TiO₂ lattice it has become the ideal dopant as compared to other elements. However, the disadvantages of cationic doping are that their localized d-levels were positioned deep in the band gap of TiO₂, acting as trapping centers for charge carriers, but the detrapping process is often slow and serve as recombination center for photoengraved charge carriers [93].

In 1986, non-metal doped TiO₂ was elucidated by Sato *et al.* [94]. By calcination of commercial titanium hydroxide, they formed N-TiO₂ powders and presented high photocatalytic activity by the oxidation of C₂H₆ and CO. But at that time, these finding did not attract much consideration. Asahi *et al.* [95] reported that with nitrogen doping into the substitutional sites of TiO₂ (TiO_{2-x}N_x) enhanced the hydrophilic and photocatalytic properties.

Hattori *et al.* [96] synthesized F⁻ doped TiO₂ thin films/powder. They concluded that with the addition of F⁻ ions, a significant enhancement in the photocatalytic activity of TiO₂ attributed to the increase in the anatase crystallinity. Also, Sotelo-Vazquez *et al.* [97] addressed Pdoped TiO₂ films with both P⁵⁺ and P³⁻ states which are fabricated by APCVD. This deposition technique controls the impurities oxidation state which presents a novel approach to attain films with both self-cleaning and transparent conducting oxide properties. For a wide range of applications, these

innovative P-doped TiO₂ films are a breakthrough in the progress of multifunctional advanced materials with their tuned properties. Renet *et al.* [98] have synthesized C doped TiO₂ nanostructures by using glucose as carbon precursor. As compared to pure titanium dioxide, C doped TiO₂ presented a red shift in the band gap. They also formulated the increased photocatalytic activity with carbon doping for the degradation of rhodamine B (RhB). This method can be simply used for the degradation of various pollutants on industrial scale by the formulation of visible light active photocatalyst due to its convenience and energy saving properties. Park *et al.* [99] investigated that when sulfur is introduced in the matrix of mesoporous TiO₂ thin films there is an increase in the stability of the structure by the retardation of new phase formation and simultaneously their resistivity is decreased with the reduction in their band gap. It should be noted that heavy doping of metal and non-metal has resulted in the opposite effect despite the increased visible light absorption. As technically pointed out by the several authors, with low doping concentrations there is only a little change in the band gap because high concentration should be essential to expand efficient light activity. The mechanism of observed photo response of doped or modified TiO₂ is still unclear; however, a generally accepted concern is that the photo absorption of a material is explained better by the introduction of defects in the lattice of TiO₂, for example Ti³⁺ and oxygen vacancies creating trap centers, rather than the recombination centers.

Besides the above methods, there are other approaches which narrow the band gap of TiO₂ thin film and enhance their photocatalytic activity in visible region. The methods of surface modification generally include surface hydrogenation, vacuum activation and plasma treatment. Recently Chen *et al.* [100] fabricated a new approach to generate disordered phase of TiO₂ by incorporating hydrogen into TiO₂ through the hydrogenation of TiO₂ nanocrystal. Hydrogenation of commercial P25 TiO₂ was done at hydrogen atmosphere with enhanced photocatalytic activity by Haiqian *et al.* [101]. They also studied that after 15 days the hydrogen treated sample were black in color which enhanced the photocatalytic activity in visible region. But the hydrogenation method requires high temperature during the process of incorporation of hydrogen in TiO₂ matrix, making the films unable for many optoelectronic applications such as transparent electrode in the optoelectronic devices. Alexander *et al.* [102] showed that hydrogen plasma

treated TiO₂ thin films which improved the absorption in the visible region due to the surface reduction. Plasma treatment methods create highly stable Ti³⁺ and oxygen vacancies. In the plasma treatment methods, generally gases such as H₂, Ar, O₂, N₂ and mixture of gases such as H₂&O₂, N₂&O₂ etc. were used. The partial reduction of anataseTiO₂ by Arand H₂plasma treatment were used to investigate the differences in catalyst characteristics in the visible-light region reported by Chae *et al.* [103]. Oxygen defects were the major factors for the broader; red shifted absorption bands in the visible-light region and showed confirmationfor visible-light absorption.

Huang *et al.* [104] fabricated TiO₂powders by thermal N₂plasma treatment at RF power of 400W. During the N₂plasma,the treatment time greatly impact the visible light absorption, IPA adsorption, photocatalytic activity and BET surface of the prepared TiO₂samples. They also studied that the oxygen vacancies were produced which is confirmed by XPS results, attributed to increase in the visible absorbance and the improvement of photocatalyticactivity.Kim *et al.* [105] utilized PECVD method for the H₂ plasma treatment of nanostructured TiO₂.The efficiency of DSSCs was appreciablyrelay on the plasma power. They also reported the power efficiency of 6.94% in case of plasma treated TiO₂ which were much higher than the untreated TiO₂ samples.

Han *et al.* [106] studied the effect of plasma treatment (O₂, N₂ and Ar) on the contact angle of TiO₂thin films prepared by reactive sputtering technique. By the drop shape analysis, the water contact angles on the surface of TiO₂ films were measured, which is remarkably decreased with plasma treatment time. Enhancement in the hydrophilic property of TiO₂ thin film is due to the surface oxidation, surface etching, ultraviolet radiation, and of plasma treatment. Recently, the hydrophilicity stability of radio frequency co-sputtered Ti_xSi_{1-x}O₂ thin films in dark were reported by Mirshekari *et al.* [107]. Plasmas contain radicals, ions, electrons and, neutral molecules that connected with surfaces, proceeding in physical and chemical modifications of the surfaces. Jung *et al.* [108] observed good hydrophilicity when irradiated TiO₂ thin films with microwave and rf plasmas of 50-200 W for 5 min under 25 Pa. However, the mechanism for the hydrophilicity induced by various plasma treatments was still unclear. Wang *et al.* [109] reported the mechanism of hydrophilicity, when the TiO₂ thin films were irradiated with 115 W rf oxygen

plasma for 30 min. With oxygen plasma lattice oxygen form oxygen molecules because of the oxidation of lattice oxygen which disappear the oxygen vacancies on the lattice oxygen atoms to form oxygen molecules.

In this work, we utilized low cost air plasma for the surface modification of TiO₂ thin films. The air plasma also avoids utilization of harmful gases unlike the other reports.

1.5. Synthesis methods for TiO₂ thin films

This section describes different approaches utilized for TiO₂ thin film formation. There are many approaches mentioned in the literature but here we confined ourselves to the method of thin film formation only. A concise and short depiction of few of the chemical and physical methods for nanostructures synthesis is as follows and illustrated in Fig.1.8.

Chemical vapor deposition (CVD) is an extensively used for materials-processing technology. In this process one or more volatile precursors were exposed to the substrate, which react and/or dissolve on the surface of the substrate to create a non-volatile solid deposit or thin film. Mostly this method was used for the formation of solid thin-film coatings to surfaces. Different chemical reactions were involved in CVD method due to its versatile nature.

Yang *et al.*[110] used PECVD deposition for the formation of amorphous TiO₂ films, by taking mixtures of titanium tetraisopropoxide and oxygen. It was observed that, deposition rate decreased with plasma power and increased with equivalence ratio. Capacitance–voltage measurements were used for the metal-insulator-silicon devices. The dielectric constant of TiO₂ increased as the thickness of the films increase. Kolouchet *al.*[111] fabricated TiO₂ thin films by Plasma Enhanced Chemical Vapor Deposition. Oxygen with Titanium (IV) isopropoxide was used as the working gas. Glass and silicon substrates were used for the deposition of the films. Based upon the experimental conditions photo induced hydrophilicity and photocatalytic activity of the films were studied. Ion bombardment and deposition temperature strongly influenced the photocatalytic properties of the films.

Iancuet *al.* [112] fabricated TiO₂ thin films by atomic layer deposition (ALD) using proper post processing anneals in various ambient environments to control their electrical properties. With ALD, hole mobilities larger than 400 cm²/(V·s) are approachable which replace the use of

extrinsic doping, which usually produces orders of magnitude smaller values. This behavior is due to the presence of excess oxygen in the films. This finding enables completely new categories of TiO₂ devices and applications, and unlocks the prospective to improve existing ones. Naam *et al.* [113] synthesized TiO₂ thin films by metal organic chemical vapor deposition (MOCVD) at deposition temperature in the range of 300–750°C for the application of dye-sensitized solar cells. Si(100) substrate were used for the deposition of crack-free, highly oriented TiO₂ polycrystalline thin films with anatase phase at temperature as low as 450°C. Below 500°C, XRD data showed that the TiO₂ thin films were dominantly grow-up in the [211] direction on Si(100), the core film growth direction was corrected to [200] with the increase in the deposition temperature to 700°C. Rutile phase TiO₂ thin films have only been obtained above 700°C.

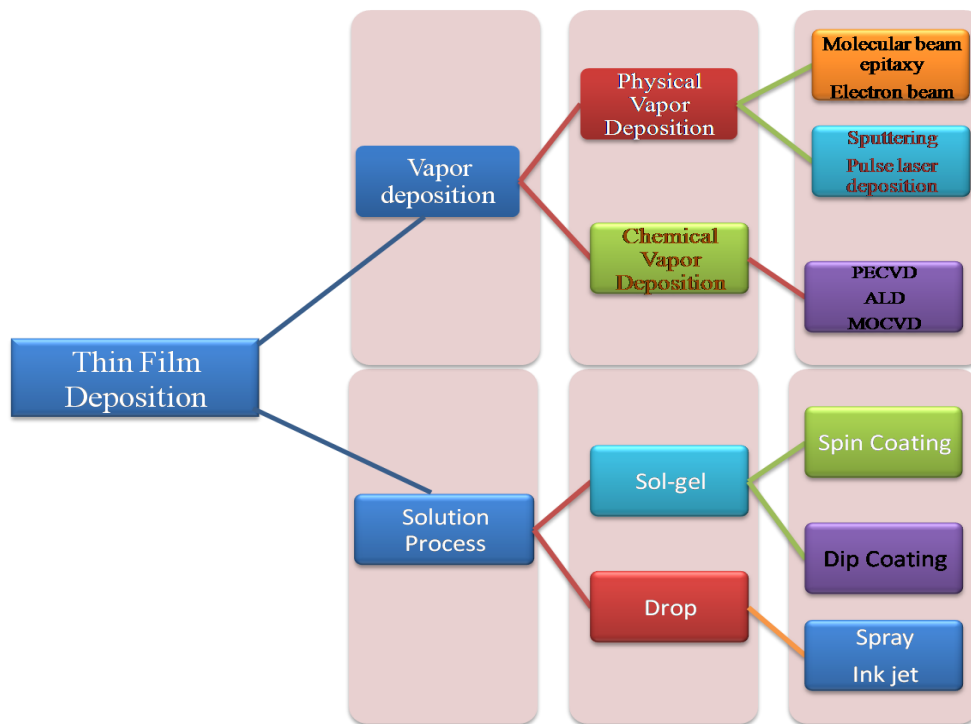


Fig.1.8: Schematic diagram for the different fabrication methods of thin film.

Dongale *et al.* [114] reported the hydrothermal method for the fabrication of memristor device (Ag/TiO₂/Al) with TiO₂ active layer. The deposited TiO₂ films show the optical reflectance of 15–22% in the visible region.

Pulsed laser deposition (PLD) is a high energy process which also provides [115] surfaces with high specific surface area, to get effective thin film with good mechanical rigidity. Inert and reactive gases were also deposited by PLD in a wide range of operating temperature and pressure. Kishore *et al.* [116] fabricated TiO₂ thin films on Si (111) substrate by using (PLD) ArF excimer laser (operating with wavelength 193 nm). Alterations in the resistances of samples; sensor detects the different concentrations of CO gas. The temperature varies from room temperature to 230°C. AFM and XRD were applied to characterize the surface morphology and structure of the deposited TiO₂/Si films.

Zhao *et al.* [117] synthesized N-doped titanium dioxide (TiO_{2-x}N_x) thin films using PLD deposition on quartz glass substrates by maintaining the nitrogen atmosphere to evaporate the titanium dioxide target. Two characteristic deep levels located at 1.0 and 2.5 eV below the conduction band which were revealed by UV–vis spectroscopy measurements. O vacancy state was available at 1.0 eV level whereas the 2.5 eV level is introduced by N doping, which contributes to the reduction in the bandgap by mixing with the O 2p valence band.

Molecular beam epitaxy (MBE) is an ultrahigh-vacuum epitaxial-growth technology. In MBE, ultrahigh vacuum environment was required. Molecular beams of specific materials impinge upon an appropriately prepared wafer. Because of this reaction, there is a growth of thin epitaxial film on the wafer's surface. This process can be controlled by manipulating the temperature of the wafer surface and arrival rates of the beams so that layers of specified materials are grown.

Callon *et al.* [118] prepared TiO₂ thin films onto Au(100) single crystals by MBE. TiO₂ film expands epitaxial on the substrate at 300°C illustrating the rutile (100) surface. XPS results revealed that there was the formation of Ti³⁺ state with the reduction of Ti⁴⁺ at the Au(100) interface. At higher substrate temperature, a stoichiometric and crystalline oxide was formed.

Lyandres *et al.* [119] examined the effect of reactive gas partial pressure and substrate radio frequency (RF) bias on the photo reactivity and structure of TiO₂ films fabricated by reactive DC magnetron sputtering. Both the film texture and reactivity were influenced by the change in the

RF bias. When RF bias optimized to 50 volts, prepared films exhibit biaxial texture with maximum crystallinity and degree of orientation.

Sol-gel method is one of the established and significant techniques for making optical coatings about 50 years ago and in the last decade paying much attention due to the demanding growth of sol-gel technology. This method has been broadly adopted to synthesize different type of materials in bulk, powder, fibers, nanosheet, and thin films etc. for different advanced technological applications. In this method, low temperature is required for the mixing of precursors which give superior control to different components at atomic level. Thus, the sol-gel route is more appropriate for the synthesis of crystalline and glassy/amorphous materials than conventional methods.

Sol-gel method associated with the formation of a sol, which is consequently dehydrated by evaporation or solvent extraction, resulting in a gel. This method modifies certain preferred structural characteristic such as grain size, particle morphology, porosity, and compositional homogeneity. In a typical sol-gel method, two steps are main important for the formation of sol i.e. hydrolysis and the polymerization reaction of precursors which are usually metal oxide or inorganic metal salt.

Wang *et al.* [120] deposited thin-films of TiO₂ on Si wafers by dip coating techniques. The change in crystal structure with different temperature and the in homogeneity of TiO₂ thin film bring up by dip coating were revealed to be significant variables in this system. Refractive index of pore water was measure using ellipsometry under proscribed humidity. Unexpectedly, with increasing ionic strength the refractive index of pore water decreases, which is the opposite case of bulk water as measured by the ellipsometry. To obtain the capacitance of TiO₂ thin film, electrochemical charge-discharge measurements were performed using TiO₂ thin films coated on platinized Ti coupons.

Hashizume *et al.* [121] established anew approach for the formation of self-supporting ultrathin films of titania by spin-coating process. They observed that these self-supporting thin film were microscopely consistent only when the films thickness varies between 10-20nm. The embossed Nano pore should be important for the growth of permselective ceramic membranes. They readily organize the self-supporting titania films with 10nm thickness and 10 cm² size.

Among the above discussed approaches for thin film formation, sol-gel process has advantages than other methods for film deposition as discussed above. These advantages are: (i) it provides high optical and quality films, (ii) it is an economical method, (iii) it can produce thick coating to provide the corrosion protection performance (iv) capable of making small thickness films, (v) low temperature is required and (vi) coating of large surface is very easy.

Hafizuddin *et al.*[122] prepared TiO₂ thin films onto SiO₂ via sol-gel technique. They studied gas sensing properties and microstructures of TiO₂ thin films. TiO₂ thin film exhibits a reasonable response towards C₂H₅OH and CH₃OH vapor. However, the potential to select varied type of gases remain the main problem as the detection pattern for both gases are similar where XRD investigation shows that thin films were amorphous. In the present work, we have used simple and low cost sol-gel method for thin film formation on the surface of glass substrates. The obtained films were annealed and exposed in the air plasma for their surface modification. These, plasma treated and untreated films were characterized using the following characterization tools.

1.6. Synthesized TiO₂ nanostructures were characterized using the following techniques:

(i) X-ray Diffraction (XRD): X-ray diffraction provides a convenient and a practical means for the qualitative structural identification of compounds because of the uniqueness of the pattern for each compound.

(ii) Field Emission Scanning Electron Microscopy (FE-SEM) installed with Energy Dispersive X-rays (EDAX): Using FE-SEM, we have observed the surface morphology. From EDX the information corresponding to the different elements present in the nanostructures have been obtained.

(iii) UV-Vis Spectroscopy: UV-Vis spectroscopy is used to study the optical properties of compounds. It is characteristically used in analytical chemistry for the quantitative determination of different analysis, such as highly conjugated organic compounds, biological macromolecules and transition metal ions.

(iv) Atomic Force Microscopy (AFM): To observe three-dimensional geometry of the nanostructures above the surface of substrate AFM is a powerful tool.

(v) X-ray Photoelectron Microscopy (XPS): XPS is used to identify the chemical state of the all elements that are present on the surface.

1.7. Thesis Outline

Here we outline thesis chapters:

Chapter 1 initiates with the basic introduction of the nanotechnology. A brief explanation of the different synthesis methods is explained. Different applications of nanostructures have been discussed successively and the reason of selecting the present work has been discussed in the last of this chapter.

Chapter 2 describes the detailed information about the synthesis and characterization techniques that were employed to the preparation of all TiO₂ thin film. In this chapter, we explain sol-gel dip coating method for the fabrication of TiO₂, Fe doped TiO₂ and Co doped TiO₂ thin films. Structural, morphological, optical, and surface properties of the fabricated TiO₂ thin films were

studied by X-ray Diffraction (XRD), Scanning Electron Microscope (SEM), UV-Vis Absorption Spectroscopy (UV-Vis), Atomic Force Microscopy (AFM) and X-ray Photoelectron Spectroscopy (XPS). In the experimental work, all the arrangements employed have been described in this chapter.

Chapter 3 started with a brief introduction of TiO₂ thin films and their applications. The second section of this chapter involves the formation mechanism of TiO₂ thin films and their modification by plasma treatment. In the next section, details description of structure of TiO₂ thin films and their analysis is presented. The antifogging performances of the thus prepared TiO₂ thin films have been discussed in the succeeding section. The recognized antifogging behaviors are the directly consequences of the development of the Superhydrophilic thin films discussed in the last.

Chapter 4 starts with the introduction of transition metal doped TiO₂ thin films, and then the experimental method for doped TiO₂ films method is given. In the next section, detailed analysis of the results for optical, morphological and electronic properties is discussed. And finally, the chapter ends with a summary.

Chapter 5 starts with a brief introduction of the different photocatalyst and their performances in different radiation conditions. In the next section, preparation of doped photo catalyst films of TiO₂ by air plasma is presented. Performance of thus produced photocatalyst in the visible light is presented in the next section. In last of this chapter, a summary describing the effect of air plasma treatment on the doped films for visible light photocatalytic mechanism is given.

Chapter 6 states summary and important suggestion towards the future work.



CHAPTER II

Synthesis and Characterization Techniques

This chapter presents the detailed information about synthesis and characterization techniques that were employed to the prepared TiO_2 films. Explanation to measure the surface adhesion properties using contact angle is given in the next section. Structural, morphological, optical, and surface properties of as grown TiO_2 thin films were studied by using X-ray Diffraction (XRD), Scanning Electron Microscope (SEM), UV-Vis Absorption Spectroscopy (UV-Vis), Atomic Force Microscopy (AFM) and X-ray Photoelectron spectroscopy (XPS) is also explained in the subsequent section. Formulae used in this thesis such as for contact angle, surface energy, energy band gap, Burstein shift etc. are given in the last section.

2.1. Synthesis of TiO_2 thin films

2.1.1. Materials: Titanium tetraisopropoxide ($\text{Ti}(\text{OC}_3\text{H}_7)_4$) (purity 98.99%), ethanol ($\text{C}_2\text{H}_5\text{OH}$) (purity 99.9%), triethanolamine ($\text{N}(\text{C}_2\text{H}_4\text{OH})_3$), iron (III) nitrate and cobalt (II) nitrate (purity 99%) were procured from Sigma-Aldrich and Merck, respectively. The reagents were used as received without further purification.

2.1.2. Preparation of TiO_2 sol

Titanium tetraisopropoxide ($\text{Ti}(\text{OC}_3\text{H}_7)_4$: TTIP), ethanol ($\text{C}_2\text{H}_5\text{OH}$) and triethanolamine ($\text{N}(\text{C}_2\text{H}_4\text{OH})_3$) were used as the starting materials. Mixing of the chemicals was carried out under ambient condition. In the synthesis process, addition of TTIP in ethanol prior to the introduction of triethanolamine induces immediate precipitation due to high reactive alkoxide. Therefore, triethanolamine a stabilizing agent in the process of hydrolysis was stirred first which was followed by the dropwise addition of chemical TTIP. In the chemical process, 17 mL of $\text{Ti}(\text{OC}_3\text{H}_7)_4$ added to a mixture of 67 mL of $\text{C}_2\text{H}_5\text{OH}$ and 4.8 mL of $\text{N}(\text{C}_2\text{H}_4\text{OH})_3$. The solution was then stirred continuously for 2 hours. In the above solution, was mixed with another mixture of 1 mL deionized water and 9 mL $\text{C}_2\text{H}_5\text{OH}$ was added drop wise. The solution was stirred for about two hours. After two hours, the solution was allowed to cool down to the room temperature, which was then left for ageing for about 48 hours.

After this time interval, there was formation of TiO_2 sol. The complete chemical reactions may be represented as:

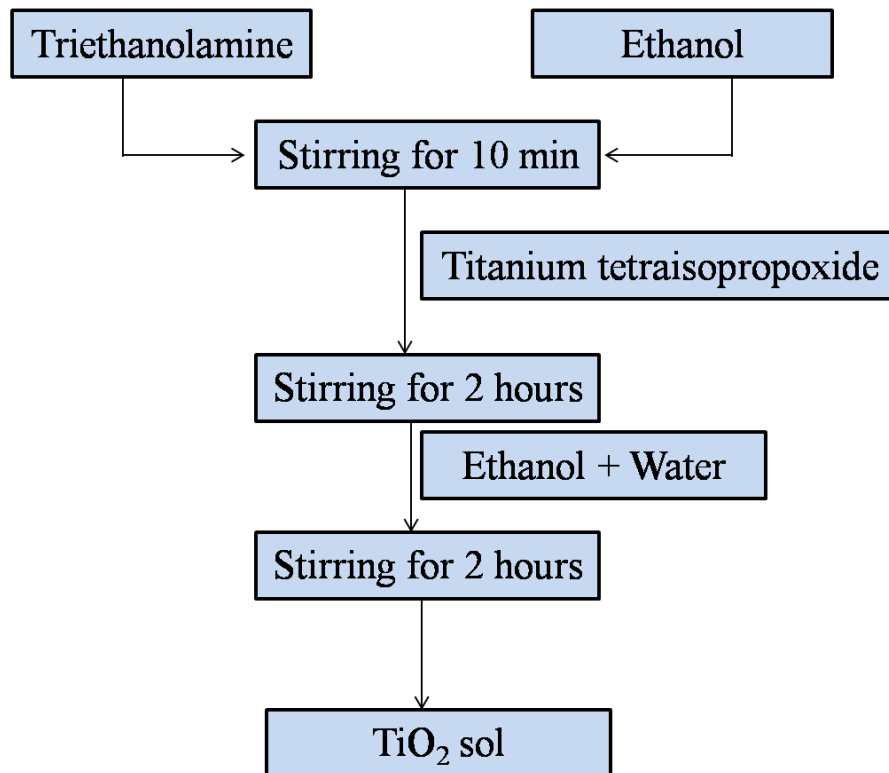
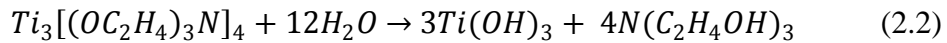
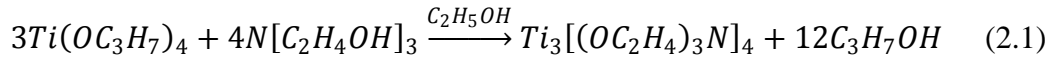


Fig.2.1:Flow chart for the formation of TiO_2 sol.

2.1.3. Role of stabilizing agent

The addition of the triethanolamine helps in the formation of a homogeneous solution avoiding the precipitation. Thus, the presence of triethanolamine in the solution retains its transparency of the thin films formed in this work. In fact, the films formed without using triethanolamine; there was formation of precipitate when ethanol was added to TTIP, which

resulted in the poor formation of the thin films when this solution was used for thin films on glass substrate. Also, the films were found to be opaque in appearance.

2.2. Thin film preparation

The fabrication of TiO₂ thin films was mainly dependent upon the two steps.

- (i) First, selection of substrates on which oxide was deposited. It depends upon the class of measurements considered for the samples.
- (ii) Second, deposition of TiO₂ thin film by dip coating method.

2.2.1. Substrates

The selection of substrate is very important because it can influence structure and properties of deposited thin film. In ideal case, all evaluation should be completed on the same substrate to formulate a good relation between results, although it is often not promising but here we have used glass substrate with same specifications.

2.3. Formation of TiO₂ thin film by sol-gel dip coating method

To coat thin film of TiO₂ on the surface of glass slides, the slides were cleaned before deposition of the TiO₂ films. For the cleaning, they were first washed ultrasonically in acetone, and then in ethanol and distilled water. In the next step, for the deposition of film, the cleaned slides were immersed in the solution, and then withdrawn with a constant withdrawal speed of 2.5 cm/min. In the last the films were annealed at 200°C for about 30 min in a furnace to remove the contaminations [123, 124].

2.3.1. Synthesis of Fe and Co doped TiO₂ thin films

Similar to the pure/undoped TiO₂ thin films, thin film of Ti_{1-x}Fe_xO₂ and Ti_{1-x}Co_xO₂ (where x=0 and 0.05) were also prepared using dip-coating method [125]. In this case, the precursor solutions of titanium (IV) isopropoxide (TTIP, Ti[OCH (CH₃)₂]₄, 98%, Aldrich) with Fe (NO₃)₃.9H₂O, and Co (NO₃)₂.6H₂O were formed separately to fabricate Fe and Co doped

TiO₂ thin films. Again triethanolamine (C₆H₁₅NO₃) was used as a stabilizing agent to prevent the precipitation of titanium precursor. Following the similar procedure as that of undoped TiO₂ films, triethanolamine (C₆H₁₅NO₃) was dissolved in ethanol (C₂H₅OH) to form a colorless solution, and then Ti [OCH(CH₃)₂]₄ was added dropwise with continuously stirring to form a clear pale-yellow sol. Afterwards, a mixture of ethanol and deionized water (9:1) was added to the prepared sol to avoid rapid precipitation of TiO₂. During the synthesis of sol-gel, the solutions of transition metals Fe and Co were added to the solution, separately.

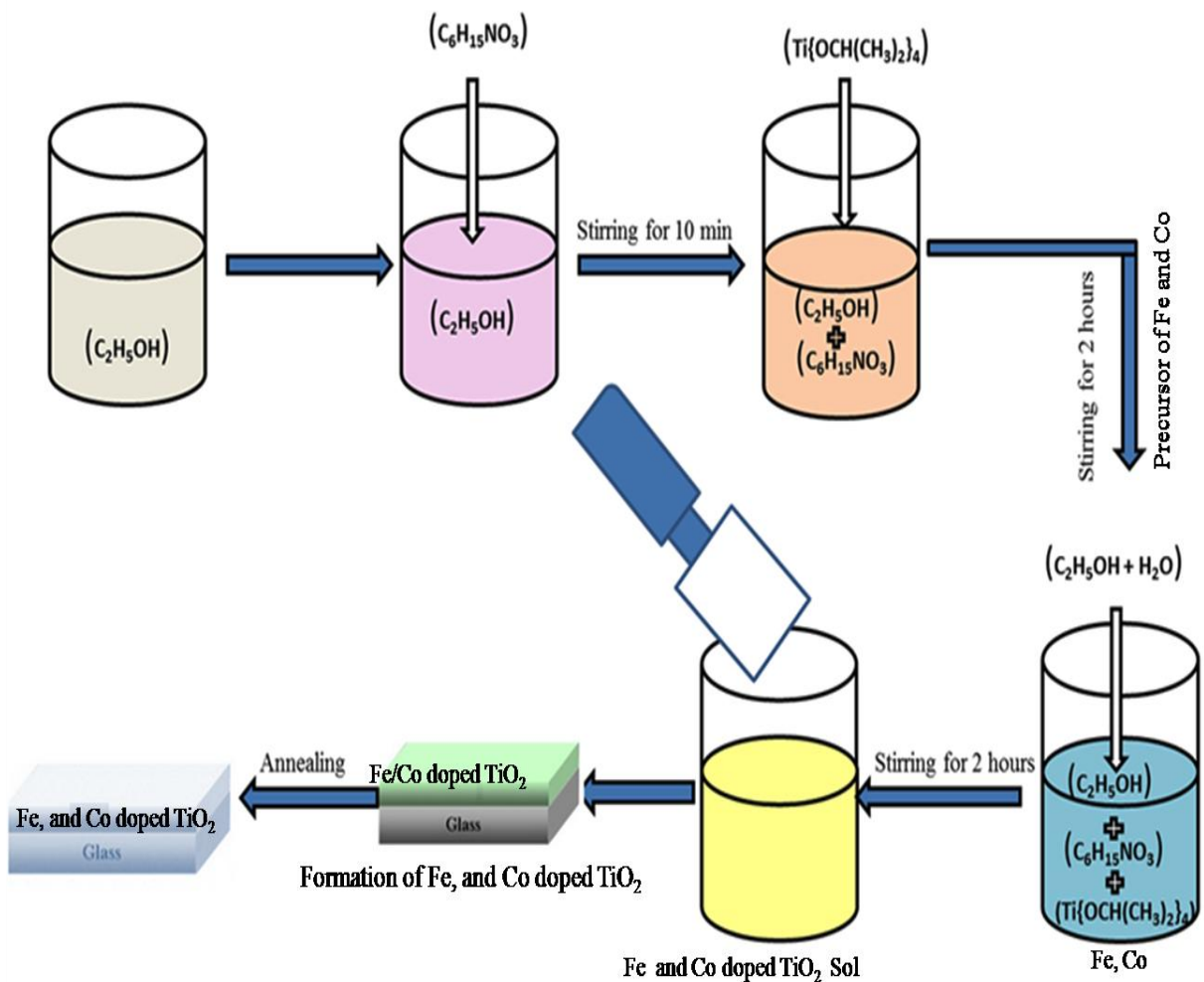


Fig.2.2: A schematic representation for TiO₂ sol formation.

The final solutions were stirred further for next 2 hours and allowed to age over night before coating on glass slides. Glass substrates were cleaned ultrasonically with sequentially deionized water, detergent, C₃H₆O and then C₂H₅OH. After coating the films were dried in air and annealed at 400°C for 2 hours in an oven.

2.4. Surface modification of TiO₂, Fe and Co doped TiO₂ thin films

As we discussed in the first chapter, that the plasma treatment is a clean and dry process to enhance the surface properties of the films [126, 127]. The formed thin films were treated in air plasma for varying treatment time such as; 0, 05, 10, 15, 30, 60, 120 and 180 seconds. The plasma was generated using air inside a vacuum coating unit (Model 12A4D). For the plasma formation, a vacuum of 0.3 mbar was created using rotary pump in the machine. The applied voltage was kept 30 V and the power was 24.6 Watt. These films after plasma treatment were studied for their wetting properties as discussed in the following sections. Before the wetting study, untreated and plasma treated films were characterized by XRD, EDX, AFM and XPS. The variation in the treatment time was thought to produce changes in the wettability of the treated films.

2.5. Contact angle measurements and surface energy estimation

Surface energy is directly related to surface wettability, more actively steady surface results in less wettable surface. In fact, enhanced wettability is attributed to the increase in the amount of polar groups [128, 129] variation in the roughness of treated films [130]. To estimate the change in the wettability of treated samples, variation in the contact angle of liquids was measured. In this experiment, we used deionized water and ethylene glycol as the test liquids. These two were selected as they have known surface tension components. Droplets of these liquids were placed on the samples surface using micropipette. In order to accuracy of results of the contact angles, liquid droplets were placed at many position of the surface of sample. After finding the contact angles, surface energy was estimated using the relation:

$$(1 + \cos\theta) \gamma_{LV} = 2 (\gamma_S^D + \gamma_{LV}^D)^{1/2} + 2 (\gamma_S^P + \gamma_{LV}^P)^{1/2} \quad (2.3)$$

Where θ is measured contact angle of different test liquids. The known surface tension of deionized water and ethylene glycol i.e. γ_{LV} and its two components such as polar γ_{LV}^P and dispersive γ_{LV}^D were used which are mentioned in the Table 2.1 [131, 132].

Table 2.1: Various parameter of the testing liquids.

Test Liquids	Polar γ_{LV}^P (mJ/m ²)	Dispersion γ_{LV}^D (mJ/m ²)	Surface tension γ_{LV} (mJ/m ²)
Deionized Water	51.0	21.80	72.8
Ethylene Glycol	19.0	29.0	48.0

The contact angle of H₂O and C₂H₆O₂ results a set of two equations of two unknowns γ_S^P and γ_S^D of TiO₂ surface. By solving these two equations, unknown γ_S^P and γ_S^D on the TiO₂ surface were calculated. Total surface energy i.e. γ_S were estimated by adding γ_S^P and γ_S^D using in the following equation:

$$\gamma_S = \gamma_S^P + \gamma_S^D \quad (2.4)$$

2.6. Characterization Techniques

2.6.1. X-ray Diffractometer (XRD)

The crystal structure of thin films was explored by X-ray diffractometer. When high energy X-ray was fallen on solid materials, a part of the incident beam would be spread in all direction by the atoms. A regular array of atoms made a crystalline solid which form a 3-dimensional

diffraction grating for the X-ray. As a result, the atomic arrangement in the crystal could be analyzed by X-ray diffraction. The distance between the atomic planes where X-rays are diffracted can be obtained from the Bragg condition given as:

$$2d\sin\theta = n\lambda \quad (2.5)$$

where θ is the peak angle position of diffracted X-rays and λ is the wavelength of X-rays. The distance between atoms varies regularly with kinds of atoms or ions. Therefore, if the distance between atomic planes is known, one can know kinds of constituents of the sample. The diffraction angle 2θ was varied in an appropriate range and the diffraction intensity was recorded as a function of 2θ . In principle, every crystal has its own indication: the location of the respective peaks rely on the size of the elementary cell and their crystal arrangement. To check whether the amorphous or crystalline phases present in the samples a standard database has been used [133]. Measurements were performed on a Rigaku diffractometer, with a Cu X-ray tube (Cu K α wavelength 1.54246 Å). Two types of diffraction configurations were used: grazing incidence and θ - 2θ . In the first case, the angle between the thin film surface and the incident x-ray beam was kept constant at a low value, 5° typically. In the second case, the angle between the thin films moved in such a way that only reflections from atomic planes parallel to the film surface were measured. The crystallite size (D) of nanoparticles and thin films have been calculated using Scherer's formula [28]:

$$D = k\lambda / \beta \cos\theta \quad (2.6)$$

where λ is the wavelength of the x-rays used, β the full width at half maximum of the preferred XRD peak, and θ the Bragg angle. Also from XRD data, the average strain (ϵ_{str}) can be calculated using Stokes-Wilson equation:

$$\epsilon_{str} = \beta / 4 \tan\theta \quad (2.7)$$

2.6.2. Scanning Electron Microscopy (SEM)

In SEM, a high energy focused beam is used to different signals at the surface of solid species. The interaction between electrons and sample surface give very important information regarding the different variables like; orientation of materials, external morphology, chemical composition and the crystal structure. During characterization, selected area was used to collect the data which give 2-dimensional images. Area ranging from approximately 1 cm to 5 microns in width can be imaged in a scanning mode using conventional SEM techniques (magnification ranging from 20X to approximately 30,000X, spatial resolution of 50 to 100 nm). SEM is also capable of performing analyses of selected point locations on the sample; this approach is especially useful in qualitatively or semi-quantitatively determining chemical compositions (using EDS), crystalline structure, and crystal orientations (using EBSD). In our case, for the variation in the sample morphology and elemental identification with the change of doping conditions as well as the plasmatreatment conditions with exposure time, we characterized our samples using SEM which was installed with EDX.

EDX is an investigative technique used for the analysis of the different elements that were present on the sample surface. X-ray was emitted when a high energetic electron beam incident on the sample surface. We can detect each element on the sample and their stoichiometry via knowing the nature of X-ray generated. Element with atomic number less than four are difficult to detected by EDX whereas the elements whose atomic number are lies between 4-92 were easily detected and analyzed. An atom within the sample contains ground state electrons in discrete energy levels. The elemental composition of the specimen is measured, because the energy of X-rays is characteristic of energy difference between the two shells and of the atomic structure of the elements present, an electron beam strikes the surface of a sample. The energy of the beam is typically in the range of 10-20 KeV. An EDX can be used in various fields like environmental testing, materials identification, home inspection metallography, etc.

2.6.3. Optical characterizations

UV-VIS-Spectrophotometer

Since the surface properties also affect the optical properties of the films, the UV-Vis spectrophotometer was used to study the variation after plasma treatment/exposure. In the absorption process, photons of a known energy excite an electron from a lower to a higher energy state. Thus, by placing a semiconductor specimen at the output of a monochromator and studying the changes in the transmitted radiation, one can discover all the possible transitions an electron can make and learn much about the distribution of states.

The instrument automatically records a graph of absorbance versus wavelength within a spectral range of 200 to 1100nm. A beam of selected wavelength is passed through the sample. Visible, infrared or ultraviolet light from the lamp enters the monochromators, which disperse the light and select the wavelength chosen by the operator for the measurement. Light of selected wavelength strikes a rotating mirror, which directs the light beam alternately through the sample and along a reference path. The two light beams coverage on the detector. Relative intensities of two beams which strike the detector provide a measure of the amount of light absorbed or transmitted by the sample. The absorption spectrum is obtained by an automatic recorder with a scan drive system which changes the wavelength setting of the monochromators and drives the recorder chart. From UV-visible plot

2.6.4. X-ray Photoelectron Microscopy

To understand the variation in electronic structure with the plasma treatment, the plasma treated and untreated samples were investigated using X-ray photoelectron spectroscopy (XPS). XPS is based on the measurement of the energy of electrons emitted from a surface bombarded by a beam of X-rays. Like in the EPMA technique, each atom has its own signature. One of the most important capabilities of XPS is its ability to measure shifts in the binding energy of core electrons resulting from a change in the chemical environment of the emitting atom. In this way, the degree(s) of oxidation of each atomic species can, in principle, be measured. The depth penetration of this chemical analysis is only few nanometers, thus surface contamination and

surface oxidation have a great influence on the results and samples must be carefully prepared to obtain valuable information. The XPS studies were performed on samples deposited on silicon using a SCIENTAESCA 300 system equipped with a rotating anode, Al K α X-ray source, an X-ray monochromator and a hemispherical electron energy analyzer. X-rays are directed onto the sample and the resulting photoelectrons are then focused onto the entrance slit of a concentric hemispherical analyzer. Here a negative and positive potential are applied to the outer and inner cylinders, respectively, such that the central line between the cylinders is a line of zero potential. Scanning the potentials allows control of the energy of electrons that can pass through the analyzer and onto the detector, usually a channel electron multiplier (channeltron). In order to check the variation in the peak area of respective peak, the percentage area was calculated by the following formula:

$$\text{Percentage area} = \frac{\text{Area of specific peak}}{\text{Total area of all the peaks}} \times 100 \quad (2.8)$$

2.6.5. Atomic Force Microscopy (AFM)

The variations in the surface morphology (3D) were also investigated using AFM. AFM is the most basic of scanning probe techniques which provides topographical information and used to study over a range of materials like semiconductors, conductors and insulator. AFM is a real-space imaging method that enables one to characterize and manipulate surfaces, nanostructures and molecules at the nanometer length scale, and in some cases down to the atomic scale. AFM can be performed in either contact Mode (CM) or tapping Mode (TM) [134, 135]. Different AFM imaging modes rely on the interaction of a tip located at the end of a cantilever with the surface. This interaction influences the cantilever properties which can be detected with a motion sensor. A standard AFM image consists of a raster scan of n lines with on each line n measurement points. In constant force mode, the force applied by the tip on the sample is kept constant, this is done by adjusting the distance between the tip and sample surface in a feedback loop. This signal is also used to image the surface topography. In tapping mode, the tip is oscillating in vertical direction at its resonance frequency. Tip–surface interactions will result in

a change of the oscillation amplitude and resonance frequency. These signals or the adjustments of the tip-sample distance can again be used to image the surface.

2.7. Formulae:

In the thesis, to estimate different parameters of the formed TiO₂ films, the following formulae were used.

1. Surface energy of unexposed and plasma exposed TiO₂ films were calculated by following equation [25]:

$$(1 + \cos\theta)\gamma_{LV} = 2(\gamma_S^D + \gamma_{LV}^D)^{1/2} + 2(\gamma_S^P + \gamma_{LV}^P)^{1/2} \quad (2.9)$$

where θ is average value of apparent contact angle. The standard values of total surface tension (γ_{LV}), and its polar (γ_{LV}^P) and dispersive (γ_{LV}^D) components for water and ethylene.

2. Total surface energy was estimated according the following Young's equation

$$\gamma_S = \gamma_S^P + \gamma_S^D \quad (2.10)$$

3. Young's contact angle is generalized in terms of apparent contact angle (*Wenzel* contact angle) as:

$$\cos\theta_a = r \cos\theta_y \quad (2.11)$$

where θ_a is apparent contact angle, θ_y is the *Young's* contact angle and r is the *Wenzel* roughness factor, defined as the ratio of actual surface area and projected area.

4. Absorption coefficient depends on optical band gap, given by:

$$(ah\nu)^{1/2} = C(h\nu - E_g) \quad (2.12)$$

Where $h\nu$ is the incident photon energy, C is a constant and E_g represents the optical band gap.

5. Optical energy band gap all synthesized TiO₂ thin films have been calculated using the formula:

$$E_{eV} = hc / \lambda \quad (2.13)$$

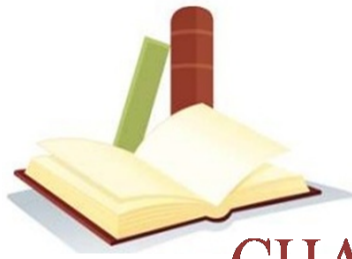
Where h = Planck's constant and E = energy band gap of thin films.

6. Burstein Moss effect, which explains blue shift occurred by a shift of fermi level into the CB, and enhancing optical band gap energy by

$$\Delta E_g^{BM} = \frac{\hbar^2 K_F^2}{2} \left[\frac{1}{m_e^*} + \frac{1}{m_h^*} \right] \quad (2.14)$$

Where m_h^* and m_e^* are the effective mass of hole and electron in the respective bands, and K_F is fermi wave vector.

Note: A detailed discussion of the formulae listed above is given in the corresponding chapters of the thesis



CHAPTER III

Superhydrophilic TiO_2 Thin Film by Nanometer
Scale Roughness and Dangling bonds

This chapter reports an increase in the hydrophilic property of titanium dioxide (TiO_2) thin films. In this chapter, we describe an experiment performed to enhanced hydrophilicity of TiO_2 thin films using air plasma treatment. As in the study of hydrophilic property, the surface energy plays an important role so in this chapter we have enhanced surface energy which has been examined through the measurement of contact angle variation in a sessile drop method. We observed that the hydrophilicity of plasma exposed TiO_2 films depends upon both the roughness of surface and formation of dangling bonds on the surface of films. The performed experiment for antifogging properties of plasma treated films give direct application/results of the superhydrophilic wetting characteristics to TiO_2 films.

3.1. Introduction

For solid surfaces, wettability is one of the crucial resources which play a very significant function in every day life. Formation of water droplet on transparent solid surface scatter light and reduces optical transmission, which can be a major issue for the everyday use of windshields, eyeglasses and goggles and reduces the efficiency of medical/analytical instruments, solar energy panels and other industrial equipments. To prevent fogging, immense research on the control of surface wetting/dewetting behavior, typically using super hydrophobicity and super hydrophilicity, has been reported over the past decades. In recent years, materials properties related to their surfaces have been extensively studied to understand their wettability for many applications as anti-fogging behavior, surface cleaning, applications in dye sensitized solar cells, as a photocatalyst, and gas sensing etc. [136-142]. To exhibit these properties, TiO_2 has been found most suitable material. This material is used in hydrophilic coatings; however, it is found that this material shows hydrophilicity in the presence of UV radiations only, and in the absence of UV irradiation it does not show any hydrophilicity. [143]. It is found that when TiO_2 is placed in the dark or in visible light, there occurs recombination of photo generated charge carriers with the time of nanoseconds [144]. In our daily life there are many objects which needs their surface to be hydrophilic, examples belong to surfaces of car mirrors, building glasses, self-cleaning objects etc. [145]. Therefore, to achieve the required hydrophilicity of the surface there is a need of controlling the properties of the material which as to be used as a coating material.

The simple way to estimate the wetting ability of a surface is to measure the contact angle of test liquids. It is found that the surface shows perfect wetting if the water contact angle is less than 10° [146] and perfect water repellent if it is greater than 150° [147]. Generally, the wetting is ascribed by the surface smoothness, in both wetting case i.e. perfect wetting and perfect water repellent. In these two cases, the mechanism is different, but the concept of wetting in the presence of UV light remains same. In the irradiation process of smooth surfaces, when UV light is irradiated on the material surface it is absorbed due to the incident energy which is sufficient to jump an electron the band gap of the material.

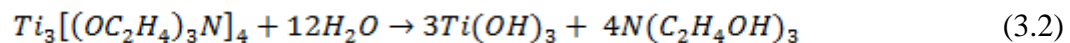
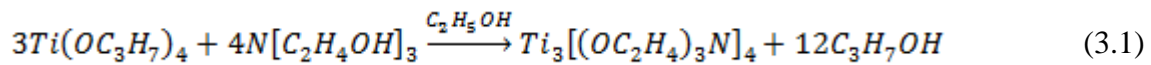
Thus in the absorption process, there is generation of electron/hole pairs. These produced electrons reduce Ti^{4+} to Ti^{3+} state and the produced holes oxidize O^{2-} . In this process, the oxygen atoms are ejected out for the lattice and in place oxygen vacancies are produced. In the process of wetting when a water drop is placed on TiO_2 in UV light, the oxygen vacancies are occupied by the water molecules, and thus OH group is adsorbed on its surface, making the surface hydrophilic [148, 149]. Again, if the film is kept in the dark, the absorbed OH is replaced with the oxygen in air, and the surface becomes hydrophobic again [150]. For smooth surfaces, the water contact angle is simply Young's contact angle or the intrinsic contact angle which is symbolized by θ_y . Alteration in the value of θ_y described the wetting transition whether it is hydrophobic or hydrophilic. Historically this phenomenon was studied by *Wenzel* and latter supported by *Cassie* and *Boxter*. There are two defined wetting regimes which are named as *Wenzel* regime and *Cassie* regime. The *Wenzel* regime states that the liquid which is used as droplet spreads over all the surface irregularities, and in *Cassie* regime, there is impregnation or rolling of water droplet. In the state of rolling of a droplet on the surface it is called *Cassie* regime; whereas, if it impregnates the surface irregularities it is called *Cassie* impregnation regime or the state of super hydrophilicity. In the wetting of surfaces, surface roughness is an important factor. In fact, the interfacial area of solid and gas is replacing with the interfacial area of solid and liquid after wetting. This change in the interface conditions relay upon mainly the texture etiology. Every individual surface possesses surface energy and therefore the variation in the wetting property of a surface depends upon the alteration in the surface energy, and the total energy of liquid/vapor interface [151].

Various approaches have been adopted in regard of TiO₂ to enhance its hydrophilicity such as making of porous surface and texturing of surface, which in fact shows better hydrophilicity in comparison to its smooth surface [145]. In some of the approaches, incorporation of PEG or the nanoparticles has been done to make them hydrophilic. These porous TiO₂ thin films as superiority reveal hydrophilic activities still in the visible light in a certain degree. Other than these approaches, there are reports involving exposure of TiO₂ surface to photons, corona plasma, electrons, flame, ions etc. Generally, in the process of the surface modification, if plasma is used it alters simply the surface properties without altering the bulk properties; therefore, this method as compared to other is most appropriate for surface modification [152, 153]. Also, the plasma treatment is an economical, dry and contamination free approach allowing uniformity over the treated surface [154, 155]. In the process of the plasma treatment, basically there is generation of electrons, positive charge particles along with the neutral particles, which is accelerate to the surface of interest. The accelerated particles get strike on the surface and causes break of the surface bonds, thus producing dangling (free) bonds. In this process, some of the oxygen based functionalities; such as such as -COOH, -C=O, -OH are also generated, which then helps in the wetting of surface [156]. Kim *et al.* [157] addressed O₂ or N₂ plasma exposure in order to enhance the performance of dye sensitized solar cell and revealed a strong adhesion of TiO₂ with dye which consequences in the decrease of oxygen vacancies on the surface of TiO₂. This chapter reports that the plasma generated surface roughness (nanometer range) and the produced dangling bonds produces significant effect on the wetting property of TiO₂ thin films. It is observed in the experiments that the generated nanometer scale roughness along with the dangling bonds changes its surface energy which is determining by calculating the contact angle of test liquids on the surface. To observe the variation in the surface energy of TiO₂ films, they were treated to the plasm for varying treatment time. These films were then investigated for the variation in the contact angle and hence the surface energy. The roughness of the surface was estimated using AFM studies, where we found that with raising the plasma treatment time the surface roughness also increased. For the first 10 seconds of the plasm exposure time, there is effect of dangling bonds only and afterwards the surface roughness becomes prominent resulting in the enhanced wetting behavior of the treated films.

3.2. Experimental method

3.2.1. Fabrication of TiO₂ thin films

TiO₂ thin films were deposited on the cleaned glass substrate. Initially, the sol of TiO₂ was formed by the following method; C₁₂H₂₈O₄Ti were mixed with a mixture of C₂H₆O and C₆H₁₅NO₃ in 1:4:4 ratios with continuous stirring. To the above solution, a mixture of H₂O and C₂H₅OH was added drop wise with constant stirring. This mixture was stirred for 2 hours, and then it was left to cool down to the normal environmental temperature. Thus, formed liquid was left for aging for about 48 hours, which resulted in the TiO₂ sol. This sol was then used to form thin films on glass substrates, which were cleaned ultrasonically. The cleaned glass substrate after dipping the sol was withdrawal with a speed of 2.5cm/min. Then the formed films were annealed at 200°C for about 30 minutes [158, 159]. Films thickness could be controlled by controlling the withdrawal speed, in our case it is about 350nm, thickness of the films when measured by a stylus profilometer. The involved chemical reactions can be represented as;



3.2.2. Surface modification of thin films by plasma exposure

The formed films were treated in air plasma for varying time intervals such as, 0, 5, 10, 15, 30, 60, 120 and 180 seconds. The plasma was generated in a vacuum coating unit (Vacuum coating unit; Model 12A4D) by applying a voltage of 30 volts and power 24.6 watt. The pressure inside the chamber was kept 0.3 mbar throughout the treatment process. These resulted films were examined for the change in their wetting behavior. Also, these were characterized by XRD for structural properties, EDX for elemental composition, AFM for surface roughness and XPS for surface chemistry variations. To evaluate the variation in wetting properties, γ_s was estimated with the help of change in contact angle of test liquids deionized water and ethylene glycol. The surface tensions of these test liquids were known. In the contact angle measurement, drop of diameter about 0.1 μ l was positioned on the surface of treated films. Different measurements on the contact angle of a single liquid were taken, which were then averaged for different locations.

Thus measured contact angle was used to determine the surface energy of the films by means of the subsequent equation [160]:

$$(1 + \cos\theta)\gamma_{LV} = 2(\gamma_S^D \gamma_{LV}^D)^{1/2} + 2(\gamma_S^P \gamma_{LV}^P)^{1/2} \quad (3.3)$$

In this equation ‘ θ ’ represents the average contact angle. Table 3.1 shown the standered values of surface tension (γ_{LV}), its polar (γ_{LV}^P) and dispersive (γ_{LV}^D) components for deionized water and ethylene glycol, respectively [161, 162].

Table 3.1. Surface tensions of deionized water and ethylene glycol.

Test Liquids	Polar γ_{LV}^P (mJ/m ²)	Dispersion γ_{LV}^D (mJ/m ²)	Surface tension γ_{LV} (mJ/m ²)
Deionized Water (H ₂ O)	51.0	21.80	72.8
Ethylene Glycol (C ₂ H ₆ O ₂)	19.0	29.0	48.0

The measured contact angles for the test liquids gave 2 equations having two unknowns ‘ γ_S^P ’ and ‘ γ_S^D ’ for the TiO₂ surface. By elucidating these two equations, the unknown components ‘ γ_S^P ’ and ‘ γ_S^D ’ were calculated, by adding ‘ γ_S^P ’ and ‘ γ_S^D ’ the total surface energy was measured according the following Young’s equation:

$$\gamma_S = \gamma_S^P + \gamma_S^D \quad (3.4)$$

Finding the super wetting behaviour of these films, they were also investigated for antifogging behavior. In this experiment, the samples were exposed to hot water vapors.

3.3. Results and discussion

3.3.1. Structural analysis

Figs. 3.1(a, b) illustrate the XRD spectra of prepared and plasma treated TiO₂ thin films. The characteristics peak were found at the diffraction angle of (2 θ) 25.3° which indicates that the prepared TiO₂ were amorphous in nature [163], as thin films of TiO₂ were annealed at 200°C.

2θ angle and FWHM of (101) diffraction peak remains almost unaffected with plasma exposure, as shown in Fig. 3.1(b). Therefore, these XRD analyses revealed that there is an insignificant impact on the TiO_2 crystalline structure.

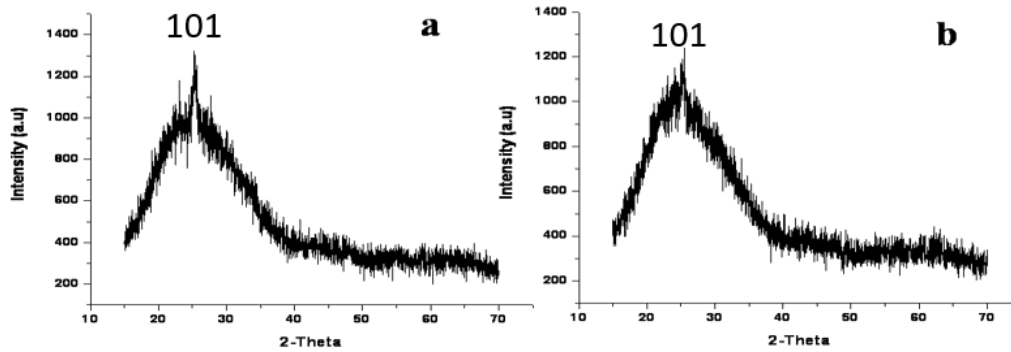


Fig.3.1: XRD of (a) prepared TiO_2 thin film and (b) plasma exposed TiO_2 thin film.

EDX analysis was also performed, to check which elements were present in the synthesized TiO_2 thin films. Figs. 3.2(a, b) shows the EDX spectrum of prepared and plasma exposed films. Particularly oxygen and titanium were recognized with strong signals as shown in Fig. 3.2(a) and no other impurities were detected. Atomic percentage of O: Ti: 62:33 (around in the ratio of 1:2) also confirmed the formation of TiO_2 .

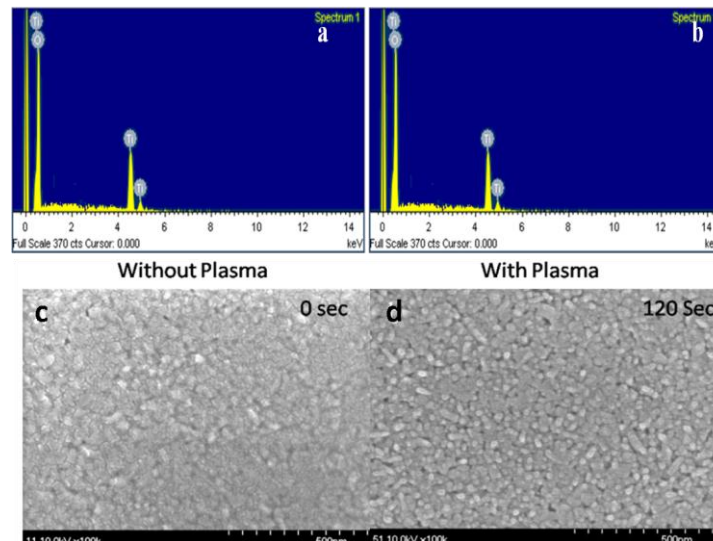


Fig.3.2: (a, b) Illustrating EDX spectrum (to detect the different elements present on the surface of TiO_2) (c, d) SEM images of undoped and plasma doped TiO_2 thin films.

Fig. 3.2 (c, d) shows the SEM image of unexposed and plasma exposed TiO_2 thin films. These images show that the films are composed of small grains with grain size range of 20-40 nm. Also the films are coarse, dense, and the surface of the films remains almost same even after the exposing to the plasma.

3.3.2. Wetting Behaviour: experimental data and its interpretation

The deviation in the contact angle of TiO_2 , measured for various plasma treatment time (0, 5, 10, 30, 60, 120 and 180 seconds) is depicted in Fig. 3.3. Droplet images corresponding to H_2O and $\text{C}_2\text{H}_6\text{O}_2$ on unexposed and plasma exposed TiO_2 thin films were shown in Fig. 3.3(a) and 3.3(i) respectively. Fig. 3.3(a-e) indicates that as the plasma treatment times were increased, reductions in the values of contact angle were also occurred. Similarly, Fig. 3.3(j-m) shows the reduced contact angle value of $\text{C}_2\text{H}_6\text{O}_2$ droplet with plasma treatment time.

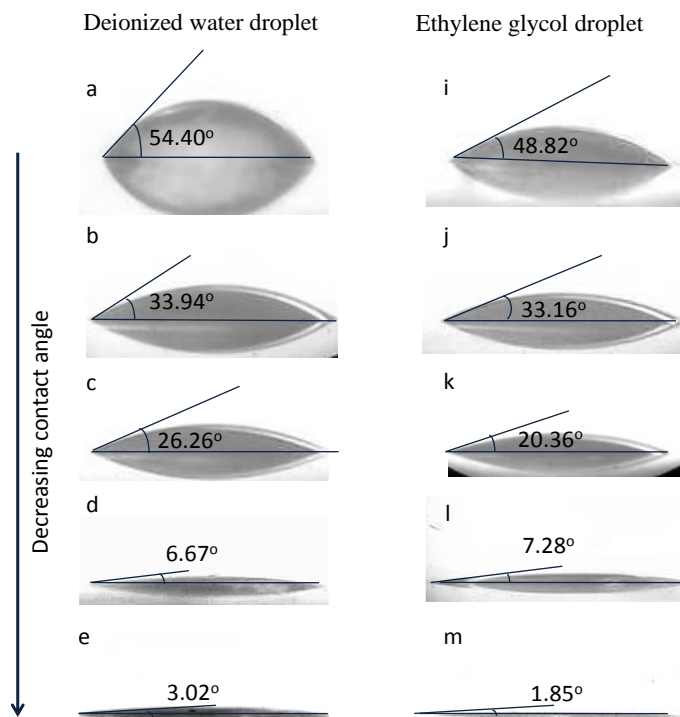


Fig.3.3: Test liquids behavior and contact angles of H_2O (left) and $\text{C}_2\text{H}_6\text{O}_2$ (right).

Different intervals of plasma treatment alter the apparent contact angle as summarized in Table 3.2. The contact angle of deionized water for untreated TiO_2 film was 54.40° and for ethylene glycol it was 48.82° . With plasma treatment time of 180 seconds on the surface of TiO_2 thin

films, contact angle reduced to 3.02° for deionized water and 1.85° in case of ethylene glycol. Change in the components of surface energy and thus total surface energy was also considered, after evaluating the contact angle for different intervals of plasma treatment time which are shown in Table 3.2. Here we examined that contact angle value for plasma exposure time more than 180 seconds stay similar as observed for 180 seconds. However, at the beginning, as the plasma exposure time was somewhat enlarged, the contact angles were quickly decreased as depicted in Fig. 3.3(b) and 3.3(j). “This shows that within first 10 seconds of exposure time, the water contact angle decreased from 54.40° to 33.94° and ethylene glycol contact angle decreased from 48.82° to 33.16° , whereas after 10 seconds it decreased slowly as shown in the Table 3.2.

Table 3.2. Effect of plasma exposure time on the contact angle and corresponding surface energy of TiO₂ films.

Time	Contact Angle (Degree)		Polar Component (mJ/m ²)	Dispersive Component (mJ/m ²)	Surface Energy (mJ/m ²)
	Deionized Water	Ethylene Glycol			
0	54.40	48.82	47.12	2.26	49.38
5	49.20	39.05	47.68	2.67	50.35
10	33.94	33.16	71.19	2.64	73.84
20	28.82	24.37	71.99	2.91	74.91
30	26.26	20.36	72.99	3.00	76.00
40	22.32	16.54	76.03	3.05	79.08
50	20.18	15.20	77.90	3.06	80.97
60	19.50	14.88	78.52	3.06	81.58
120	6.67	7.28	85.58	3.09	88.68
180	3.02	1.85	88.92	3.12	88.92

Genuinely a water contact angle consideration is enough for wettability applications. Analogous to the variation in the contact angle values, the polar component ' γ_{LV}^P ' of surface energy also display a quick increase in its value; on the other hand, the dispersive component ' γ_{LV}^D ' approximately identical as shown in column 5 of Table 3.2. “This rapid decrease in the contact

angle is regarded as wetting transition; a detailed discussion related to the wetting transition is given in next sections". TiO₂ thin film with apparent contact angle < 90° resides in partial hydrophilic regime without any plasma exposure time, but after plasma exposure time of 180 seconds the films become superhydrophilic, which shows increasing wettability as observed by significant decrease in contact angle value. For this increased wetting behavior with plasma exposure time, two inferences are responsible: formulation of surface dangling bonds and nanometer scale surface roughness. Certain numbers of Ti and O dangling bonds are being on the surface of TiO₂ thin films, therefore H⁺, OH⁻ ions and alternative ionic group can be adsorbed/chemisorbed to the surface of TiO₂ surface [164]. Most common dangling bonds particularly available on the unsaturated surface are OH species, O₃⁻, O⁻, Ti³⁺ defects state, and O vacancies [165].

3.3.3. Atomic force microscopy observation

AFM were used to examine the differences in the surface roughness and topography formed by the plasma exposure. Explanation for the increased surface roughness with exposure time can simply be understood. Plasmas comprised of certian reactive group namely: radicals, neutral molecules, ions, and electrons would act together strongly with surface, provide several degrees of freedom for the modification of chemical and physical properties of material [166]. AFM images explain a variation in the surface roughness upon the plasma treatment. The distinctive AFM images of the prepared and plasma exposed TiO₂ films are shown in Fig. 3.4. Fig. 3.4(a)) clearly indicates the consistent distribution of TiO₂ on the substrate without any plasma exposure and has roughness 4.6nm which is relatively smooth. While with increasing the plasma treatment time, another AFM images, (Fig. 3.4(b-e)), demonstrate an alteration in topography. Two major reasons which are responsible for the increased surface roughness ascribed as; creation of few nano/micro-dents and aggregation of nanoparticles on the plasma exposed TiO₂ thin film as presented in Fig. 3.4(d) and 3.4(e). Here, in these images the black mark represents the etched area by plasma whereas the bright mark exhibits the arrangement of bigger nanoparticles. As plasma, takes along all the particles into the close network result in a dense packing [166]. Plasma results in the agglomeration of naoparticles which were responsible for the increased particles size. Only some molecular layers were distored as the roghness of

TiO₂ thin films changes (around 10nm) [167]. There were formations of micro and nano-dents when different plasma particles were bombarded with each other and concluded the loss of thin films by etching [168, 169]. Variation in the surface roughness of TiO₂ thin films after plasma treatment was attributed to the aggregated particles and the etched area created by plasma. Root mean square surface roughness were obtained during the AFM characterization of TiO₂ films which were mentioned in Fig. 3.4. Surface roughness of untreated TiO₂ film was about 4.6nm, which shows a gradually increment with different intervals of plasma treatment time and reached to 19.83nm.

Now we try to explain the wetting on the basis of surface roughness. From the contact angle measurements we observed that the wettability of TiO₂ surface increased rapidly within first 10 seconds of plasma exposure time; however, it did not happen in the case of surface roughness. The surface roughness, as observed by AFM analysis does not vary significantly within first 10 seconds of plasma exposure time. This indicates that along with the surface roughness there should be another factor which influences the wettability. No doubt the surface becomes rough when it is exposed with plasma, but at the same time the plasma also creates dangling bonds on the surface layer [170]. These dangling bonds along with surface roughness should increase wettability of the surface. From the AFM images, it is observed that the surface roughness of unexposed film was 4.6nm which increased to 6.6nm when the sample was exposed to plasma for 10 seconds. The change in surface roughness i.e. 2.0nm looks inadequate to explain the observed rapid change in wettability of the surface for corresponding exposure time. Even the surface exposed for 30 seconds shows merely 8.24nm of surface roughness (as shown in Fig. 3.4(c)), there is no micro-dent observed on the film surface. For larger exposure time above 30 seconds, the surface roughness increased further and there exists some micro-dents/particles as observed in AFM images (Fig. 3.4(d) and 3.4(f)). Based upon this observation, we can divide the surface of the exposed samples in two categories: one having very small surface roughness (Fig. 3.4(a-c) and the other having high surface roughness associated with particles/micro-dents (Fig. 3.4(d) and 3.4(f)). In the first category, the surface roughness is very small thus the samples exposed from 0 second to 30 seconds may be considered as almost flat surfaces. The total surface energy of a flat surface is estimated by measuring the Young contact angle. In flat surfaces, the wetting is termed by the polar ' γ_{LV}^P ' and dispersive ' γ_{LV}^D ' components of the total surface energy. The polar and dispersive components are shown in the Table 3.1. We found that the change in the polar component of the surface energy is analogous to the change in the contact angle of the test liquids on the surface. For first 10 seconds, the polar component changed rapidly and thus the contact angle. The other component 'dispersive component' of the surface energy decreases with the treatment time as estimated and shown in the table. Therefore, the increase in the polar component, and thus the total surface energy enhances the wetting property of the as prepared TiO₂ films. [160].

In the literature, surface roughness is the most important thing mentioned for the wetting property of any surfaces; however, in our case we found that the formation of the dangling bonds

along with the nanometer scale roughness on the surface after plasma treatment also enhances the wetting characteristic of the surface. In the first 10 seconds of the treatment time, there is formation of dangling bonds, and surface roughness is small enough as observed from AFM analysis. Further treatment in the air plasma enhances surface roughness as obviously the dangling bonds on the surface that enhances the wetting rapidly estimated the rms value of the surface roughness, which is mentioned in Fig. 3.5. From the measurements, it is concluded that for 0 to 10 seconds, plasma creates only dangling bonds, which causes the wetting of the surface for the short treatment time. Thereafter, surface roughness increases, as estimated from the rms values, which in addition to the dangling bonds makes the TiO₂ films superhydrophilic.

We know that Young's contact angles were measured for the flat surfaces in order to calculate the total surface energy [160]. ' γ_{LV}^P ' and ' γ_{LV}^D ', components of surface tension for flat surfaces were illustrated in Table 3.1. Here, the variation in the surface energy is estimated by the change in the value of corresponding componets of surface tension ' γ_{LV}^P ' and ' γ_{LV}^D '. Therefore, the sum of these two components (' γ_{LV}^P ' and ' γ_{LV}^D ') gives the total surface energy i.e. the improved total surface energy promotes the wetting of TiO₂ surface [160].

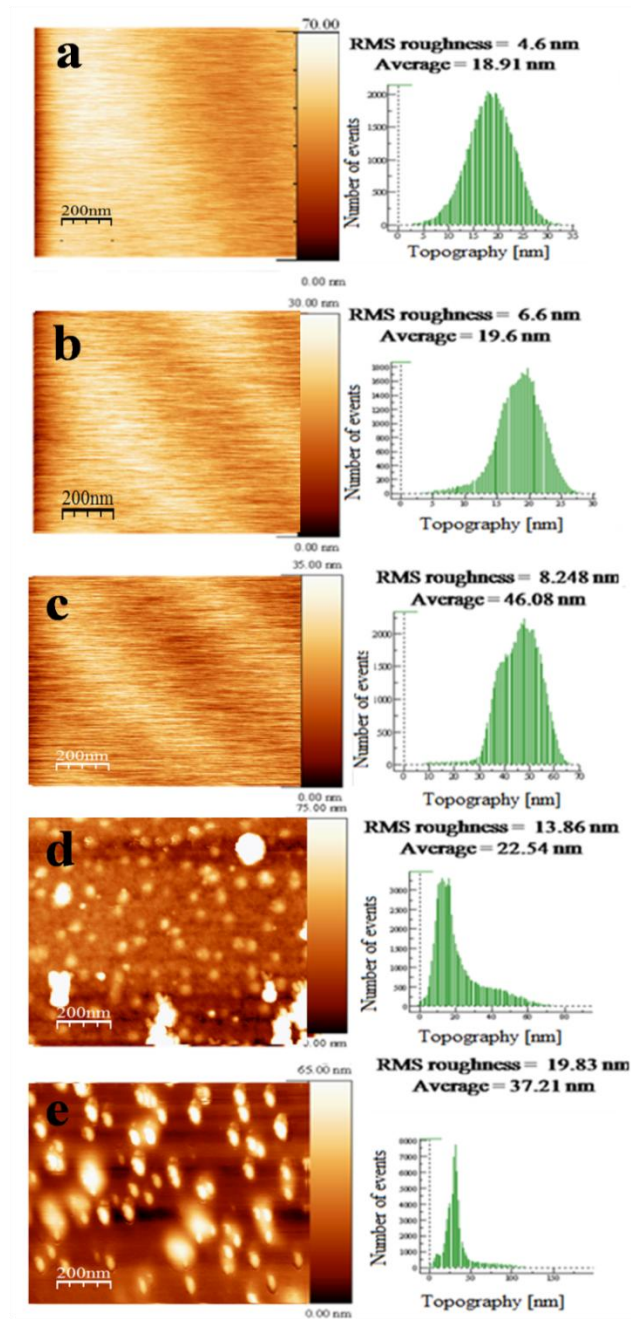


Fig. 3.4: AFM images of unexposed and exposed TiO₂ film with glow discharge plasma for (a) 0 sec, (b) 10 sec, (c) 30 sec, (d) 120 sec, and (e) 180 sec.

For wetting transition, surface roughness was investigated as a significant factor, but in our case the observed value for this factor is very low as compared to the other reports which shows their values in the micrometer range. Initially, when plasma treatment time changes from 0 to 10 seconds, there was formation of free bonds i.e dangling bonds in conjunction with small surface

roughness. Surface area of TiO_2 thin films were enhanced as the dangling bonds and surface roughness increased with plasma treatment time. The wettability of TiO_2 thin films were quickly improved by two main important factors i.e nanometer scale roughness and dangling bonds present on the surfafce of thin films. Fig. 3.5 represents the variation of the root mean square surface roughness of TiO_2 thin films with different plasma treatment time. The most decisive point in this study is that as the plasma treatment time chnaged from 0 to 10 seconds, there is only the creation of dangling bonds that are responsible for the wetting of TiO_2 thin film. But there is a little change in the surface roughness of thin films which are not sufficient for the explanation of wetting properties. With different plasma treatment time, the increased surface roughness along with the dangling bonds makes the thin film superhydrophilic.

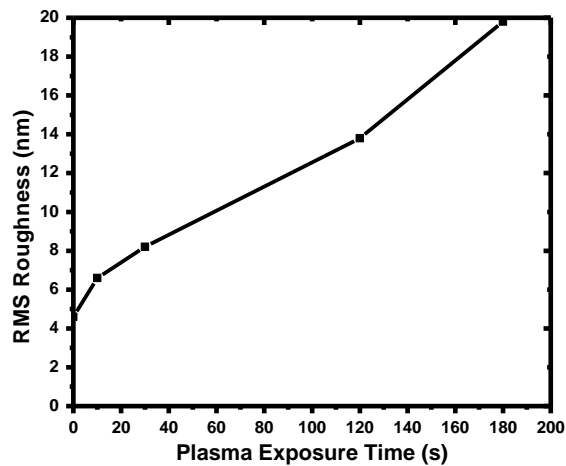


Fig. 3.5: Root mean square values of the plasma treated TiO_2 thin films as a function of plasma treatment time.

The formation of dangling bonds and their reason to cause the wetting can be understood as follows. In the process of plasma formation, the accelerated atmospheric ions get collide with the gas (air in our case), and creates positive and negative ions in the plasma chamber. These created ions along with the neutral species form plasma. When a voltage is applied inside the chamber, the accelerated charged particles strike on the surface of TiO_2 causing bonds to break. Since the surface atoms have broken bonds from their neighboring atoms or molecules, this reduces the bond length of surface atoms with the underneath atoms, which results in the inward pulling of the surface atoms. In case of the small particles, this reduction in the bond length becomes important, and affects the lattice constant of the whole solid particle [171]. Thus, by the

reduction of lattice constant, there is an additional energy possessed by the particle which is known as the surface energy. Therefore, when TiO₂ film is exposed to the air plasma free or dangling bonds are formed on its surface. These free bonds enhance the surface energy of TiO₂ surface. Thus, when some object is brought close to the unsaturated surface might satisfy some of these bonds to reduce the surface energy to bring the whole system in the equilibrium. Wetting characterer of a surface can also be explained by these unsaturated bonds. When a drop is placed on such as surface some of the bonds are satisfied by the process chemisorption of H₂O with the surface [172]. The change in the wetting character can be measures by the change in contact angle of the test liquid on such a surface. Larger the dangling bonds more is the wetting charterer of a surface, and hence the reduced contact angle.

3.3.4. Explanation for the wetting properties

Here we explain the wetting behavior of plasma treated TiO₂ thin films. For the films treated for 180 seconds in the air plasma shown a decrease in the contact angles of the test liquids i.e. for water it reduced to 3 degrees and for ethylene glycol it reduced to 1 degree. The change in the wetting property of treated thin film can be explained by *Cassie-Wenzel* model [173]. According to the models, the films which were not exposed to air plasma show partial hydrophilic property, but when they were exposed to the plasma, enter the *Cassie* impregnating regime as they show perfect wetting characteristic.

Again, in the *Wenzel* model, depending upon the wetting situation of the solid surface, the surface can get wetted partially (it will be partially hydrophilic if the contact angle is less than 90 degrees and partially hydrophobic if the contact angle is greater than 90 degrees). Now this state is basically intermediate as the wetting characteristic of the surface may move towards either side of the wetting (superhydrophilic or hydrophobic). These changes relay upon the chemical and physical properties of the solid surface [151]. The measured contact angle is termed as *Wenzel* contact angle. In case of the rough surfaces the generalization of the Young contact angle is given as:

$$\text{Cos}\theta_a = r \text{Cos}\theta_y \quad (3.5)$$

where θ_a is the measured contact angle, θ_y is *Young's* contact angle and r is known as the *Wenzel* roughness factor, which is defined by the area ratio of actual surface and projected surface. In

case of the rough surfaces the measurement of Young contact angle is difficult; therefore, the above equation shows a relation between the Young contact angle and the apparent contact angle. This relation is linear, showing that the value of apparent contact angle is proportional to the Young contact angle.

From this relation, for the flat surface the value of r is 1, showing that on the flat surfaces both the Young contact angle and the apparent contact angles are same.

If the roughness increases, i.e. r increases and Young contact angle is less than 90 degrees, the surface results in the increased wettability or the hydrophilic one. For this type of the surface, from the relation 3.5, the apparent contact angle also decreases. And in case, if the value of the Young contact angle is more than 90 degrees, for the increased roughness the wettability again increases. We also found that the surface roughness increases with plasma treatment as observed by AFM measurements. For untreated films, the apparent contact angle is 54.40° (as measured by contact angle measurement experiments), indicating that the Young contact angle can not be greater than 90 degrees for any value of the roughness factor r . This observation of contact angle shows that the untreated films are in the hydrophilic regime of the Wenzel model. After plasma treatment, the roughness increases and at the same time the measured contact angel increases, this indicates that the value of Young contact angle should lie below 90 degrees. Since there are small creaks on the surface produced after the plasma treatment, these can promote the wetting of the surface as mentioned in other studies too [174]. Therefore, the roughness of the surface and the defects makes the liquid droplets to spread over the surface as soon as it is placed over it. The change in the surface energy and the contact angles is shown in Fig. 3.6. In the Fig. 3.6(a), there is a sudden drop in the contact angle well below the 10 seconds of the treatment time. An analogous variation can be seen in the plots for surface energy shown in Fig. 3.6(b). These variations in the contact angle and the corresponding surface energy are due to the creation of polar groups ' γ_{LV}^P ' by the plasma treatment time. The variation in the hydrophilicity estimated by the alteration in the contact angle is suitable to the above mentioned increased surface roughness and the formation of free bonds 'dangling bonds' on the surface layer of the film after plasma treatment. We found that the untreated films possess 49.38mJ/m^2 value of the surface energy and 47.12mJ/m^2 and 2.26mJ/m^2 values of polar ' γ_{LV}^P ' and dispersive ' γ_{LV}^D ' components, respectively The value of the surface energy increased to 88.68mJ/m^2 after the films was exposed

to plasma for 180 seconds. The observed enhancement in the surface energy is attributable to the formation of dangling bonds and surface roughness by plasma treatment. In the measurement of contact angle three different locations were chosen on the film surface, which were then averaged to estimate contact angle.

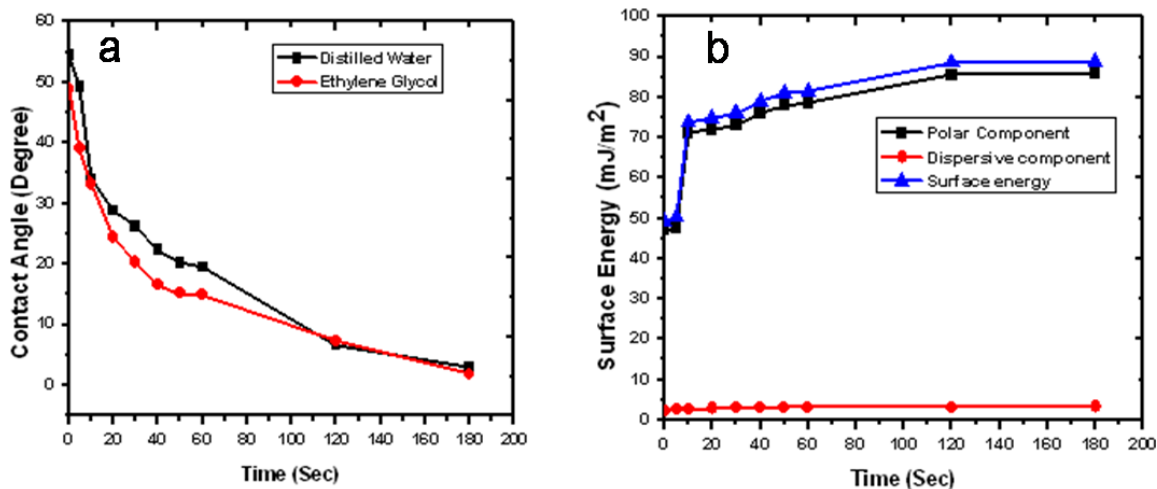


Fig.3.6: Difference in contact angle (a) surface energy and its ' γ_{LV}^P ', ' γ_{LV}^D ' component (b) with plasma treatment time.

3.3.5. XPS analysis

The samples were investigated using XPS measurements. Fig. 3.7 shows the survey spectra of untreated and plasma treated thin films. In these spectra, signals Ti, O and C (C1 peak is supposed to come from the impurity). One another feature can be seen from the survey spectra that the peaks corresponding to Ti2p and O1s increases till 10 seconds of treatment time, and afterward there is no variation observed.

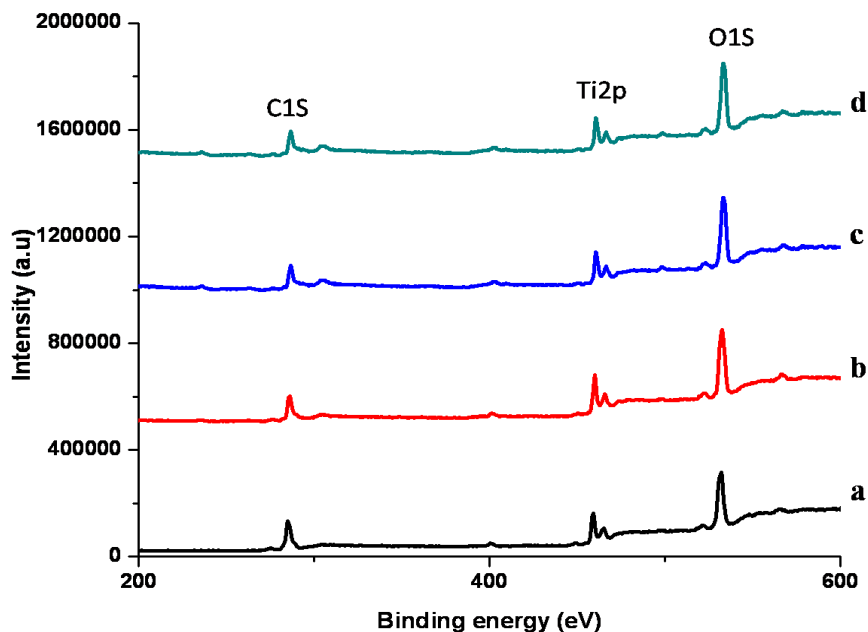


Fig.3.7: XPS survey spectra of TiO₂ thin films (a) 0 sec, (b) 10 sec, (c) 30 sec, and (d) 120 sec.

Further this XPS spectrum is analyzed to find the variation in the surface states upon treatment, which is shown in Fig. 3.8. The untreated and plasma treated films are shown by high resolution spectrum in Fig. 3.8(a) and 3.8(b). These two plots are for Ti2p of the treated and untreated films. The spectrums are fitted in peaks corresponding to titanium dioxide (Ti⁴⁺) and titanium sub oxide (Ti³⁺) in Ti2p_{1/2} and Ti2p_{3/2}, respectively. In the reports, the range of the binding energy of TiO₂ is from 458.5 to 459.9eV [175]. The peaks in the untreated films are fitted at 464.8eV (Ti⁴⁺2p_{1/2}), 464.8eV (Ti⁴⁺2p_{3/2}) and 459.0eV (Ti³⁺2p_{3/2}). In the case of plasma treated films, the peaks are fitted at 464.8 (Ti⁴⁺2p_{1/2}), 459.1eV (Ti⁴⁺2p_{3/2}) and 460.4eV (Ti³⁺2p_{3/2}). To estimate the change in the stoichiometry, change in the surface area of the corresponding peak was measured in the XPS plots. We found that there is 16% increase in the surface area of Ti³⁺ peak and a decrease of 28% in the area of Ti⁴⁺ peak. The reduction of Ti⁴⁺ resulting in the formation of Ti₂O₃ is inferred to increase the surface area of Ti³⁺ peak. The factors causing the reduction of Ti⁴⁺ may be the creation of oxygen vacancies or the electrons generated in the plasma.

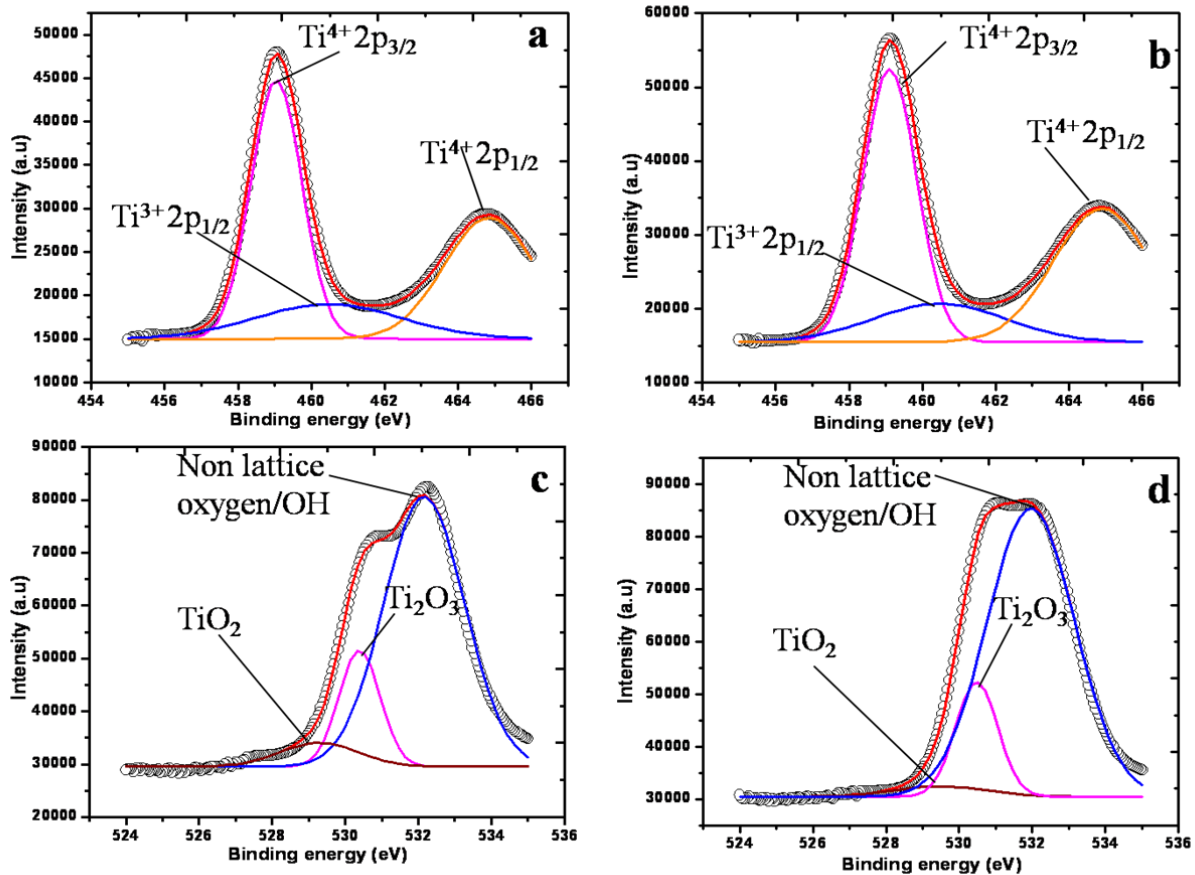


Fig.3.8: XPS spectra of Ti₂p (a, b) and O1s (c, d) core level for TiO₂ thin films.

In the XPS studies, we also analyzed O1s state to estimate the variation in the atomic state of the oxygen. Both the untreated and plasma treated films for O1s peak of XPS are shown in the Fig. 3.8(c) and 3.8(d). Again, these spectra are shaped with 3 peaks at binding energy of 529.3eV, 530.3eV and 532.1eV, which appear for both the untreated and plasma treated films. These peaks correspond to the oxygen in Ti₂O₃ and non-lattice state [176, 177]. The observed higher binding energy can be inferred due to the hydroxyl groups on the surface or water on the surface, and a small contribution of the remanent Ti-OH bonds during the synthesis [178]. In this case too, stoichiometric change was predictable by the surface area change of the relative peak as in case of the titanium. We observed that there is a decrease of 50.7% in the peak at 529.4 eV, and increase of 530.4eV and 531.9eV, respectively. The reduction in the peak area at 529.4eV represents the decrease percentage of the O²⁻. Also, the increase in the rest of the two peaks

surface area indicates an increase in OH⁻ groups, and the non-lattice oxygen. These defect states may be created due to the bombardment of ions in the plasma or the generated UV irradiation in minute amount. In fact, in the process electrons and holes are generated. Thus, generated electrons may have reduced Ti⁴⁺ to Ti³⁺, and the holes would have captured by the oxygen atoms (lattice) on the surface, which results in the decrease of the surface oxygen as observed in the XPS. There is formation of oxygen vacancies on the surface of TiO₂ as well [179].

In the XPS, the variation is observed only for the first 10 second of treatment time, and no variation is observed for further treatment time, indicating the surface defects are generated mainly for the first 10 seconds of treatment time, and for latter time it is only the surface roughness which varies as seen from AFM. Thus, for the samples treated for 10 seconds in plasma, it only the surface defects which causes the wetting, and after 10 seconds the surface roughness also take part in the wetting characteristic of the surface. In our case, we found that the nanometer surface roughness is more prominent to cause the superhydrophilic nature of the TiO₂ films.

3.4. Antifogging experiment

The antifogging is needed due to the problems observed in the higher humidity environment. And in fact, this is dependent to the temperature conditions, as the vapor reaches to the saturation limit with the change in the temperature conditions. If it is cool, it gets saturated on the surface of the substrates and creates a problem to see through it. In this regard, a superhydrophilic surface can be used to prevent fogging as the water diffused on the hydrophilic surface and forms a thin layer rather than forming droplets. In our experiments, we investigated our samples for their antifogging application as shown in Fig. 3.9. In this figure, the left side is plasma treated TiO₂ thin film which remains unfogged due to the formation of thin water layer on it, whereas on the right side is the normal glass slide which covers with the droplets and gets fogged. In the left side, we can read letters clearly, whereas on the right side it is difficult to read the letters through the slide. Thus the plasma treated TiO₂ films show perfect antifogging ability as observed in this work.

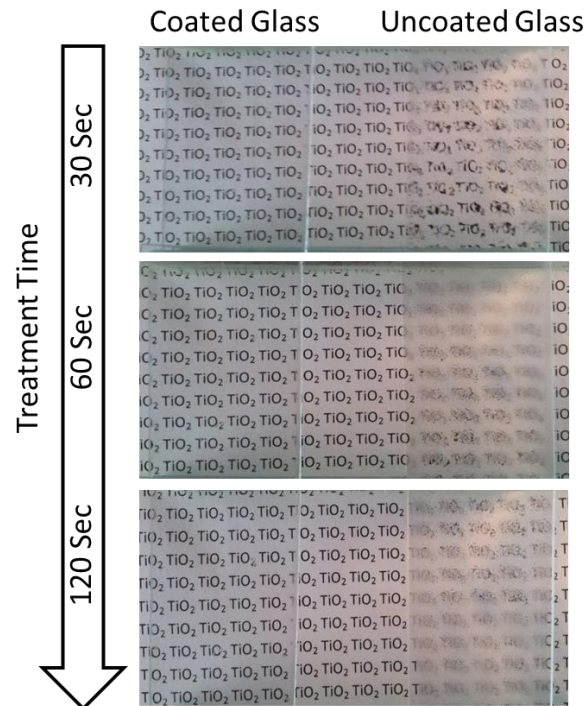


Fig.3.9: Illustration of antifogging properties of uncoated and TiO_2 coated glass and plasma exposed samples for (a) 30 sec, (b) 60 sec and (c) 120 sec.

It is reported that the antifogging behavior appears if the water contact angle remains less than 7° [180]. We found that the value of the water contact angle is 3° which shows enhanced hydrophilic properties of the plasma treated TiO_2 films. These films can be used in many applications such as surface of mirrors, windows glass and windshields of automobiles etc.

3.5. Summary

TiO_2 films when treated with air plasma show superhydrophilic nature. The plasma treatment causes a reduction in the contact angle and thus the surface energy of the TiO_2 surface. In the plasma treatment, there is formation of dangling bonds for initially, which creates nanometer scale surface roughness for prolonged time. The created dandling bonds and the surface roughness cause an enhancement in the surface properties of the as fabricated TiO_2 thin films. These films when used for antifogging application show a remarkable transmission in the fogged conditions. Therefore, TiO_2 films with the enhanced surface properties, having changed surface states and surface roughness can be a significant material for many technological applications.



CHAPTER IV

Enhancement of Optical Properties of TiO_2
Thin Films as a Result of Oxygen Vacancies
and Ti^{3+} States by Air Plasma Treatment

This chapter explains the enhancement in the optical properties of TiO₂ thin films. TiO₂ thin films; undoped and having moderate doping of Fe and Co were fabricated using sol-gel method. These films exhibited significant enhancement in the optical properties upon air plasma treatment. The moderate doping has facilitated the formation of charge trap centers by avoiding the formation of charge recombination centers. In fact, enhancement in absorbance and optical absorption region as revealed by the formation of Ti³⁺ and oxygen vacancies in the band gap of TiO₂ films was observed in the plasma treated films. The samples were treated in plasma with varying treatment time. With the increasing treatment time Ti³⁺ and oxygen vacancies increased in the Fe and Co doped TiO₂ films leading to increased absorbance; however, the increase in optical absorption region/red shift (from 3.22 to 3.00eV) was observed in Fe doped TiO₂ films, on the contrary Co doped TiO₂ films exhibited blue shift (from 3.36 to 3.62eV) due to Burstein Moss shift.

4.1. Introduction

Metal oxides semiconductors are of indispensable consequence for the scientists, as their adjustable distribution brings diverse magnetic, chemical, structural, electronic, and optical properties. They are also considerable as functional materials because of their admirable stability under intense condition and ease of large scale fabrication. Coatings are applied as films to the surface for a variety of different applications. Among various metal oxide semiconductors, TiO₂ is considered as a prime candidate due to its many peculiar properties [181, 182] for diverse applications. It is the most suitable candidate for photocatalytic applications due to its biological and chemical inertness, strong oxidizing power, non-toxicity and long-term stabilization against photo and chemical corrosion [183]. Thin films of TiO₂ have valuable applications in LEDs, gas sensors, heat reflectors, transparent electrodes, thin film photo-anode to develop new photovoltaic, photo-electrochemical cells, solar cells and water splitting [184-190]. In anodic applications, it is a preferred material because of its low density/molar mass and structural integrity over many charge and discharge cycles [191]. However, the efficiency

of pure TiO_2 is substantially low because of its large band gap and quick recombination of electrons/holes pairs. The key issue to improve the performance of TiO_2 relies on efficient light harvesting, including the increase of its photo-efficiency and expansion of photo-response region and to ensure efficient number of photo-generated electrons/holes reaching to the surface before their recombination. To meet these desired performances, the bands structure modification of TiO_2 is preferred.

Generally, three fundamental approaches are implemented for band structure modification viz. doping with metallic/non-metallic elements or co-doping of metallic and non-metallic elements [181,192-194], modification via introducing defects such as oxygen vacancies and Ti^{3+} in the band gap [195, 196] and surface modification by treatment methods [191,197-199]. In the metallic doping, among the range of dopants such as Ni, Mn, Cr, Cu, Fe etc. [183, 200-203] the Fe is found most suitable due to its half field configuration. Similarly, from non-metallic dopants S, C, F, N etc. [204-207] the N is preferred one. In the case of metallic dopants, there are some contradictory reports that show disadvantage of thermal and chemical instability of TiO_2 . Also, their high doping although enhances the band gap but at the same time reduces optical/photocatalytic activity because of increasing carrier recombination centers [208-211]. What is the mechanism of observed photo-response of doped/modified TiO_2 ; it is still a question, however a generally accepted concern states that the photo absorption of a material is explained better by the introduction of defects in the lattice of TiO_2 . For example, Ti^{3+} and oxygen vacancies [212] create trap centers, rather than the recombination centers unlike the high doping case, and results in the variation of band gap of pristine TiO_2 .

On the other hand, surface modification methods including surface hydrogenation [213], vacuum activation [212] and plasma treatment [214] are also accomplished. In the hydrogenation method, the surface of TiO_2 is terminated with hydrogen leading to an enhanced photocatalytic activity [215] in visible region; however, it is still unknown that how does the hydrogenation modify a surface to enhance its optical performance (photocatalytic activity) [216]. The drawback of the hydrogenation method is that it

requires high temperature and the obtained TiO₂ film are black in color [215], which makes the films unable for many optoelectronic applications, such as a transparent electrode in optoelectronic devices. Both the vacuum activation and plasma treatment methods create highly stable Ti³⁺ and oxygen vacancies [212, 214]. In vacuum activation method, the sample may exhibit higher absorption intensity but it appears brown in color [215] that makes it unable for transparent electrode applications. Finally, in case of plasma treatment methods, generally hydrogen gas is used to create oxygen Ti³⁺ and vacancies in TiO₂ but it is always avoidable to use such a hazardous and expensive gas. Except hydrogen there are little reports on the use of argon [217], oxygen [218] and nitrogen plasma [219] for surface modification of TiO₂. We know that the implementation of gas in the treatment chamber may be hazardous and cost effective; therefore, it is always required to avoid the use of hazardous gas, and to implement a simple and low-cost approach to meet the requirements. In this regard, treatment by air plasma may be an effective approach. However, to the best of our knowledge there is no report on the application of air plasma for the surface modification of TiO₂ film.

In this chapter, the band structure modification of thin transparent films of TiO₂ was done by implementing simply the air plasma and thus creating Ti³⁺ and oxygen vacancies in TiO₂ films. The effect of air plasma treatment was studied in conjunction with metallic doping. First, Fe and Co-TiO₂ thin films were formed on glass substrates which were subsequently treated in air plasma. Considering the drawback of high metallic doping (formation of recombination centers), in this study a moderate amount of dopants was used to enhance the optical properties of TiO₂ thin film and thereafter the air plasma was applied to enhance them further. The moderate amount of metallic dopant not only favors the separation of electrons/holes but also narrows the band gap of TiO₂ [183]. We observed that simultaneous effect of the joint approaches increases photo absorbance as well as extends photo response region of the films towards both the visible and UV spectrum. The doped films of TiO₂ were treated in plasma with varying treatment time. The moderate doping of Fe and Co elements reduces band gap minutely in both the cases

but when treated with air plasma a significant change in the optical properties was observed due to the formation of Ti^{3+} and oxygen vacancies in the band gap.

4.2. Experimental methods

TiO_2 , Fe doped TiO_2 ($Ti_{0.95}Fe_{0.05}O_2$) and Co doped TiO_2 ($Ti_{0.95}Co_{0.05}O_2$) thin films were fabricated on glass substrate using sol-gel dip coating method. Titanium (IV) isopropoxide (TTIP, $Ti[OCH(CH_3)_2]_4$, 97%, Aldrich) was used as precursor solution. First of all, triethanolamine $C_6H_{15}NO_3$, a stabilization agent was dissolved in C_2H_5OH which resulted in a colorless solution. In this solution, the precursor solution $Ti[OCH(CH_3)_2]_4$ was added dropwise to form a pale yellow solution with a continuous stirring. To avoid the precipitation of TiO_2 , C_2H_5OH and H_2O was added in a ratio 9:1. Now during the sol gel synthesis, solutions of ferric nitrate ($Fe(NO_3)_3 \cdot 9H_2O$), and cobalt nitrate ($Co(NO_3)_2 \cdot 6H_2O$) were added separately as the dopant in TiO_2 . These solutions were stirred for 2 hours and allowed for ageing overnight. Then glass substrates cleaned with H_2O , C_3H_6O and C_2H_5OH were coated with the aged solution. Coated films were dried and annealed at $400^\circ C$ to form transparent thin films. It should be noted that the dopants concentration was controlled just by controlling the concentration ratio of the dopants with respect to the concentration of precursor solution. The fabricated films were treated in air plasma, generated in a vacuum coating unit (Hindhivac model: 12A4D), for varying treatment time; 0, 10, 30, and 60 seconds, respectively. The air plasma was generated at reduced pressure of 10^{-3} mbar in the vacuum chamber. During the treatment process the applied bias voltage was 30 volts with a power of 22.7 watt. After treating in plasma, the samples were analyzed for optical, structural, morphological and surface properties.

4.3. Materials characterization

The optical (absorbance, shift in absorption edge and band gap) properties of the films were studied by UV-Vis spectrophotometer (Perkin-Elmer Lambda 750). The band

gap of Fe and Co doped thin films was calculated by using the absorbance spectra by plotting $(\alpha h\nu)^{1/2}$ against $h\nu$, where $h\nu$ being incident photon energy. Surface morphology was studied using SEM and elemental confirmation was done using EDX. The structural analysis of the samples was done using XRD (company name Rigaku, with Cu $k\alpha$ radiation, $\lambda=1.5406 \text{ \AA}$), and to observe the effect of plasma treatment on surface states, XPS: (VG Multilab 2000, Thermo electron corporation, UK) studies were performed.

4.4. Results and discussion

4.4.1. Structural and morphological studies

After fabricating thin films of pure TiO_2 , Fe and Co doped TiO_2 were treated in air plasma for 0, 10, 30 and 60 seconds, which were analyzed for surface morphology and crystal structure variations using SEM and XRD. Fig. 4.1 shows the SEM image of pure and doped TiO_2 thin films exposed in the air plasma from 0 to 60 seconds. These images show that the films are composed of small grains with grain size range of 20-40 nm. Also the films are course, dense, and the surface of the films remains almost same even after the exposing to the plasma. To detect the presence of doped elements Fe and Co, the films were investigated by EDX as shown in Fig. 4.2. EDX spectrum of pure TiO_2 film represents in Fig. 4.2(a). Here, the elements Ti and O are detected. Fig. 4.2(b) is EDX spectrum of Fe doped TiO_2 film, in this spectrum element Fe with Ti and O is detected. Similarly, Fig. 4.2(c) is EDX spectrum of Co doped TiO_2 film, containing Co element with Ti and O.

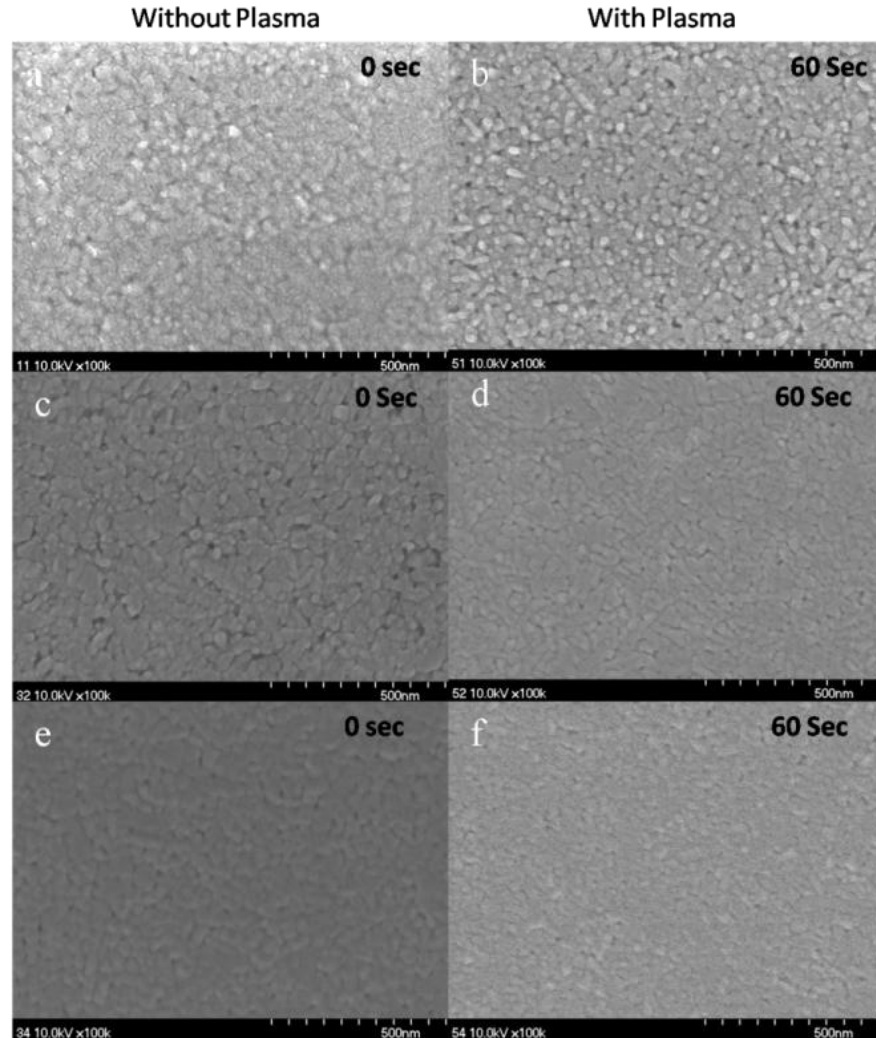


Fig.4.1: SEM images of TiO₂, Fe doped TiO₂ and Co doped TiO₂ thin films (a) pure TiO₂ film, (b) pure/treated TiO₂ film; plasma treatment time 60 seconds, (c) Fe doped/untreated TiO₂ film, (d) Fe doped/treated TiO₂ film; plasma treatment time 60 seconds (e) Co doped/untreated TiO₂ film, (f) Co doped/treated TiO₂ film; plasma treatment time 60 seconds.

The atomic percentage of the dopants was evaluated by using EDX. In the EDX spectra of Fe doped TiO₂ films, the atomic percentage of Fe, Ti and O was found as 1.66%, 12.93% and 85.41%, respectively, which closely resembles to the percentage of elements in Ti_{0.95}Fe_{0.05}O₂". Similarly, in case of Co doped TiO₂, the obtained atomic percentage of

Co, Ti and O in EDX was 1.33%, 23.33% and 75.35%, respectively, which confirmed the formation of $\text{Ti}_{0.95}\text{Co}_{0.05}\text{O}_2$ thin films.

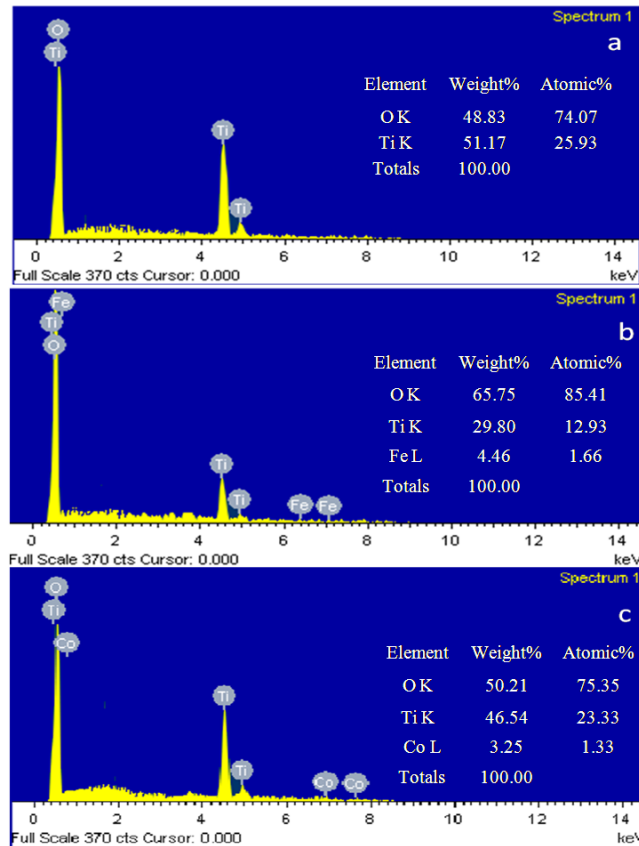


Fig.4.2: EDX spectrum of thin film of (a) pure TiO_2 , (b) Fe doped TiO_2 , and (c) Co doped TiO_2 .

For structural analysis, XRD spectra of doped thin films for extreme treatment time 0 and 60 seconds were shown in Fig. 4.3. Fig. 4.3(a, b) represents XRD pattern of Fe doped and Fig. 4.3(c, d) represents XRD patterns of Co doped TiO_2 thin films for 0 (untreated) and 60 seconds of plasma treatment time. Since there is no detection of Fe and Co signals, it indicates that all the Fe and Co ions in the respective samples gets incorporated into the structure of TiO_2 by replacing some of Ti ion and located at the interstitial sites [220]. Absence of sharp peak in XRD patterns represents amorphous phase of TiO_2 thin films [125]. After plasma treatment 2θ angle and FWHM of the peaks remain almost

unchanged, indicating negligible effect on the film structure. XRD indicates that plasma treatment does not create any change in the crystal structure of Fe and Co doped TiO₂ thin films. The obtained low signal-to-noise ratio in the above XRD spectra is due to the low crystallinity of the films and small crystallite size [221].

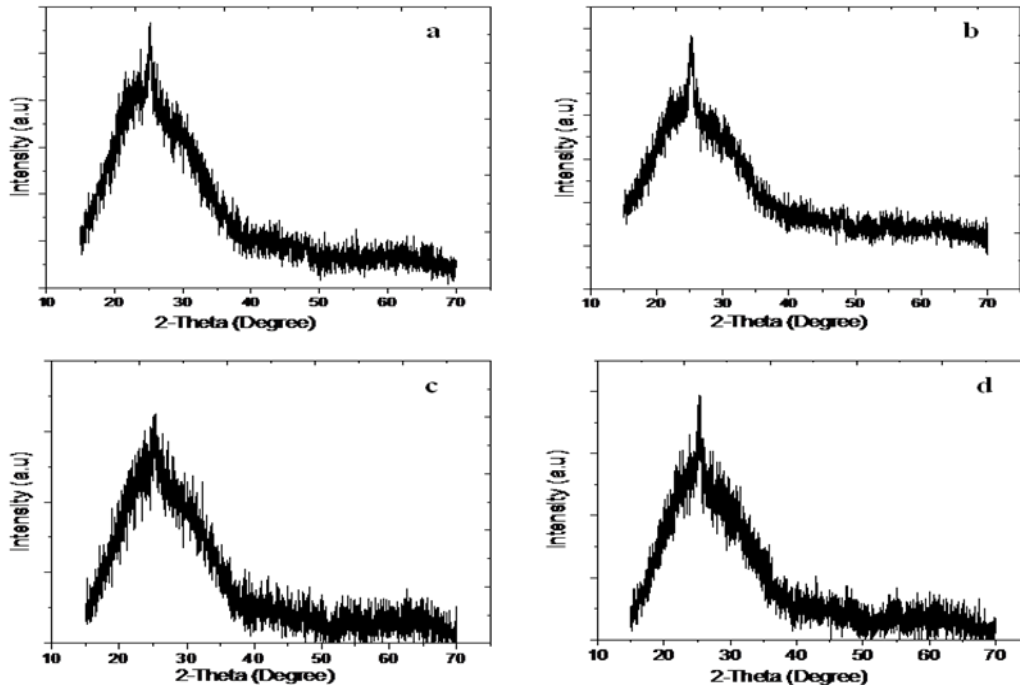


Fig.4.3: X-ray diffraction spectra of (a) Fe doped/untreated TiO₂ film; plasma treatment time 0 second, (b) Fe doped/treated TiO₂ film, plasma treatment time 60 second, (c) Co doped/untreated TiO₂ film, plasma treatment time 0 second and (d) Co doped/treated TiO₂ film; plasma treatment time 60 second.

Similarly, Fig. 4.4(a, b, c) represents the XRD spectra of pure TiO₂, Fe doped TiO₂, and Co doped TiO₂ samples treated at other treatment time i.e. 30 seconds. It reveals that the crystal structure of TiO₂ thin films remains unchanged after the different plasma treatment time or the synthesis process.

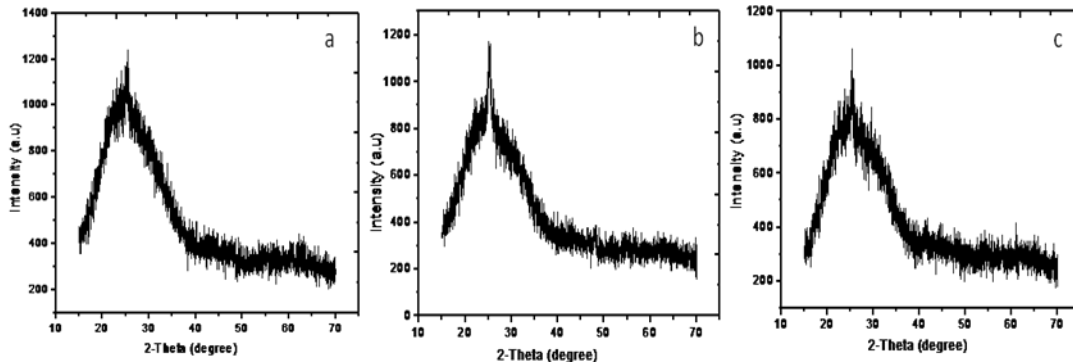


Fig.4.4: X-ray diffraction spectra of thin films for 30 seconds of plasma treatment (a) pure TiO₂, (b) Fe doped TiO₂, and (c) Co doped TiO₂ film.

4.4.2. Optical studies

In order to check the variation in optical properties of TiO₂ thin films by doping and subsequent air plasma treatment the film was analyzed by UV-Vis spectrophotometer. A summary of the change in absorption edge and corresponding band gap is mentioned in Table 4.1. Pure TiO₂ film (undoped and untreated) showed absorption edge at 367nm and band gap 3.37eV, whereas Fe doped TiO₂ film showed a shift in the absorption edge to 385nm, with a decreasing in the band gap to 3.22eV. Similarly, Co doping shifts absorption edge from 367nm to 369nm with a reduction in the band gap to 3.36eV. The observed red shift in absorption edge and narrowing band gap in both the dopants cases is similar to other reports on metallic doping [183]. In both the cases, samples were doped with a moderate (5%) concentration of Fe and Co forming Ti_{0.95}Fe_{0.05}O₂ and Ti_{0.05}Co_{0.05}O₂, respectively. We could have tuned the optical properties further by increasing the dopant concentration but that would form recombination centers [208]; therefore, to avoid the formation of recombination centers, a further tuning in the optical properties was done by treating these moderately doped TiO₂ films in air plasma. The films were treated in air plasma for treatment time (0, 10, 30 and 60 seconds), and investigated for the shift in absorption edge and band gap variation. With increasing treatment time, the absorption edge of Fe doped TiO₂ films shifts continuously from

385nm (for 0 seconds treatment time) to 413nm (for 60 seconds treatment time), with a corresponding band gap change from 3.22eV to 3.00eV, showing a significant increase in the absorption region. In case of Co doped TiO₂ films, the absorption edge shifts from 369 to 342nm (for 60 seconds treatment time) with a corresponding band gap change from 3.36 to 3.62eV, which shows an increase in the optical band gap/UV absorption region probably due to the Burstein-Moss effect [222] explained latter.

Table 4.1. Variation in absorption edge and band gap of Fe and Co doped TiO₂ thin films with plasma treatment time.

Plasma treatment time [sec]	Absorption edge [nm]		Band gap [eV]	
	Fe doping	Co doping	Fe doping	Co doping
0	385	369	3.22	3.36 by doping
10	396	360	3.13 ↓	3.44 ↓
30	402	345	3.08 ↓	3.59 ↓ by plasma treatment
60	413	342	3.00 ↓	3.62 ↓

From the Table, it is observed that the change in optical properties of TiO₂ films appears at two levels; by the doping of Fe and Co, and then by plasma treatment. However, here it should be noted that the change in the band gap due to the doping is smaller as compared to the subsequent band gap changes by plasma treatment. While discussing the effect of doping on the change of band gap, we know that the reduction may take place due to either the increasing grain size of highly crystalline sample [223] or the formation of electronic energy levels within energy band gap [224]. The XRD results indicated the samples to be amorphous, thus the first reason can be discarded. Therefore, Fe³⁺ and Co²⁺ ions substitute Ti⁴⁺ ions in TiO₂ matrix and cause a change in the band gap by forming their mid gap energy levels in the respective samples along with the formation of Ti³⁺ and oxygen vacancies. The electronic transition from valance band to dopant level and then from dopant level to conduction band, and/or from valance band to oxygen level and then form oxygen level to Ti³⁺ level/ dopant level effectively causes a red shift in the absorption edge, showing reduced band gap [225-227].

In many cases, the localized level of t_{2g} state of the doping element even lies in the middle of band gap (in case of, Cr, Mn or Fe as the doping materials), and at the top of the valance band (in case of Co is used as a dopant) [228]. Next, the variation in the absorption edge/band gap with plasma treatment time is due to the increase in the Ti^{3+} and oxygen vacancies.

Fig. 4.5 shows variation in the absorption spectra of Fe doped TiO_2 thin film treated for different plasma treatment time (10, 30 and 60 seconds (Fig. 4.5(b-d)) with respect to untreated one (Fig. 4.5(a). There is a continuous change in the absorbance, absorption edge and band gap of the films with plasma treatment time. The absorbance of the film increased from 60% (untreated film) to 87% (treated for 60 seconds) along with a red shift in the absorption edge and band gap narrowing by 0.22eV (Tauc plot shown in the inset of Fig. 4.5(a-d)). The band gap and absorption edge were estimated using the following equations [229]:

$$(\alpha h\nu)^{1/2} = C(h\nu - E_g) \quad (4.1) \quad \text{and}$$

$$E_{ev} = hc / \lambda \quad (4.2)$$

Where α is absorption coefficient and E_g is band gap energy.

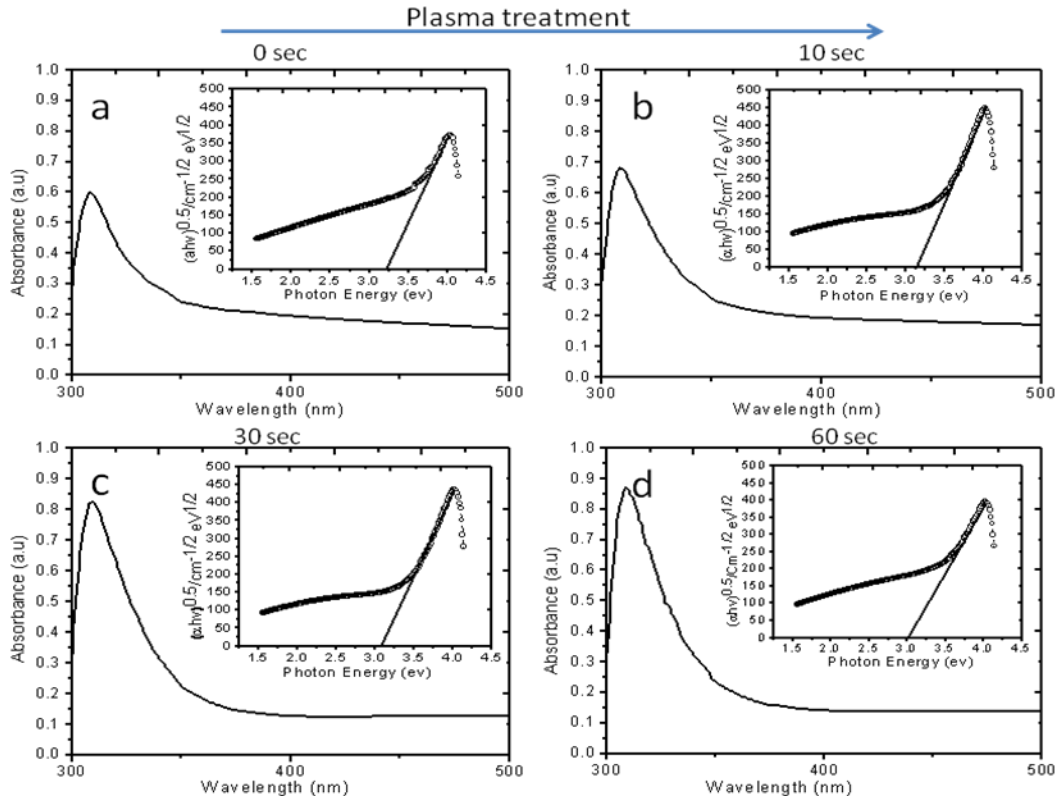


Fig.4.5: Optical absorption spectra and Tauc plot ($(\alpha h\nu)^{1/2}$ versus $h\nu$ plots) in the inset for (a) Fe doped/untreated TiO_2 film; plasma treatment time 0 second, (b) Fe doped/treated TiO_2 film; plasma treatment time 10 second (c) Fe doped/treated TiO_2 film; plasma treatment time 30 second and (d) Fe doped/treated TiO_2 film; plasma treatment time 60 second.

Similarly, the variation in absorption spectra of Co doped TiO_2 thin film treated for 0 to 60 seconds is shown in Fig. 4.6(a-d). In this case, doping shows a red shift due to the presence of Co levels in the energy gap of TiO_2 , whereas after plasma treatment the film shows continuous blue shift with increasing treatment time. This overall shift (due to treatment in plasma for 60 seconds) in the band gap is 0.26eV. The observed blue shift can be explained by Burstein-Moss effect [222], resulted by the change in the position of fermi level into the conduction band. The general equation that represents the enhancement in the band gap energy is given by:

$$\Delta E_g^{BM} = \frac{\hbar^2 K_F^2}{2} \left[\frac{1}{m_e^*} + \frac{1}{m_h^*} \right] \quad (4.3)$$

Where m_h^* and m_e^* are the effective mass of hole and electron in the respective bands, and K_F is fermi wave vector. In our case, the shift of fermi level into the CB leads to the energy band widening. With increasing carrier concentration, the absorption edge shifts to shorter wavelength region.

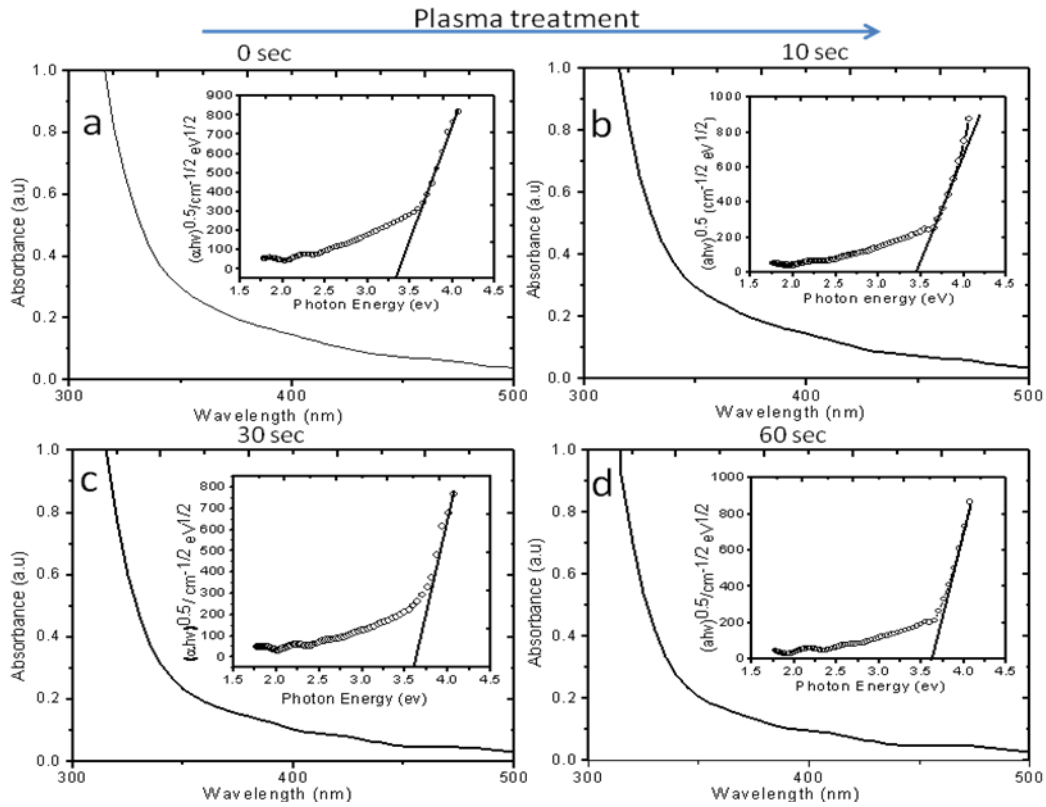


Fig.4.6: Optical absorption spectra and Tauc plot ($(ah\nu)^{1/2}$ versus $h\nu$ plot) in the inset for (a) Co doped/untreated TiO_2 film; plasma treatment time 0 second, (b) Co doped/treated TiO_2 film; plasma treatment time 10 second, (c) Co doped/treated TiO_2 film; plasma treatment time 30 second and (d) Co doped/treated TiO_2 film; plasma treatment time 60 second.

The overall variation in the band gap of TiO_2 thin film due to the doping (Fe and Co) and air plasma treatment is plotted in Fig. 4.7. In the plasma treatment region, a remarkable change in the band gap values can be observed with treatment time.

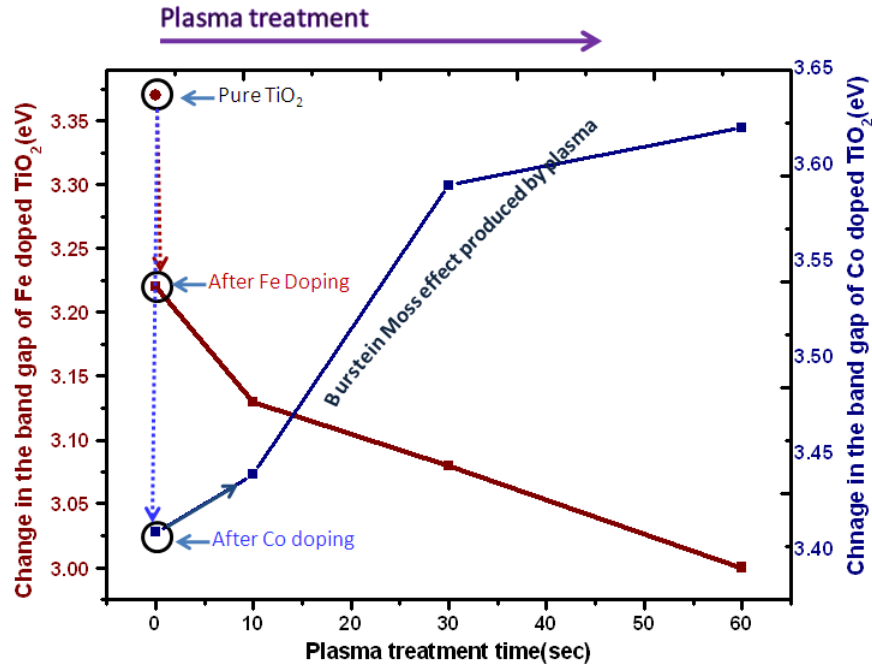


Figure 4.7: Plots for variation of optical band gap of Fe and Co doped TiO₂ thin film with plasma treatment time.

4.4.3. Surface characterization

4.4.3.1. X-ray photoelectron microscopy (XPS) study

To understand the mechanism for the change in the band gap of Fe and Co doped TiO₂ films with plasma treatment time, the films were investigated by XPS. The XPS being surface sensitive technique provides information about the change in chemical state of film constituting species. Here, the variation in the chemical state of elements ‘O’ and ‘Ti’ with plasma treatment time was analyzed in detail to correlate it with the observed variations in the band gap of the films. Figs. 4.8(a, b) show XPS survey spectra of untreated and plasma treated Fe and Co doped TiO₂ thin films, respectively. In these spectra, C1s is probably an instrumental impurity. The intensities of O1s and Ti2p peaks increase with the increasing plasma treatment time, indicating an increase in these states with treatment time.

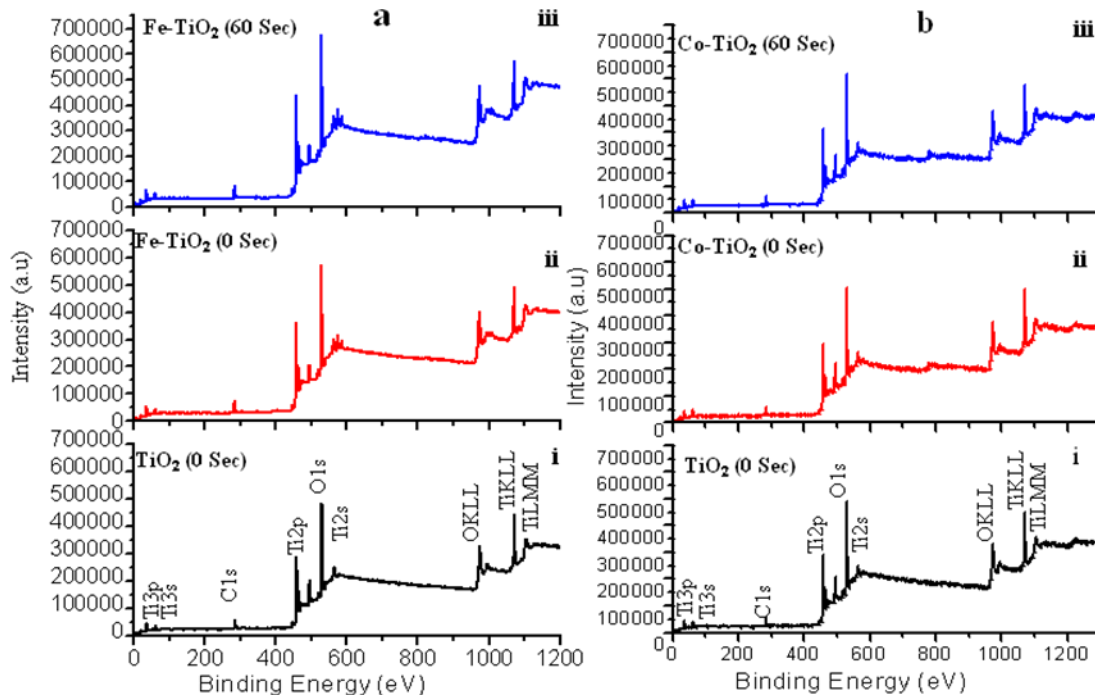


Fig.4.8: XPS survey spectra in a(i) pure TiO₂ film indicating all the peaks of elements present in the sample, here the appeared carbon peak is instrumental impurity, a(ii) Fe doped/untreated TiO₂ film; plasma treatment time 0 seconds, a(iii) Fe doped/treated TiO₂; plasma treatment time 60 seconds, b(i) pure TiO₂ film which is similar to a(i), b(ii) Co doped/untreated TiO₂ film; plasma treatment time 0 seconds, and b(iii) Co doped/treated TiO₂ film; plasma treatment time 60 seconds.

Fig. 4.9(a) shows high resolution XPS spectrum of pure TiO₂ film. In this spectrum, the doublet ‘Ti2p_{3/2} (binding energy 458.6eV) and Ti2p_{1/2} (binding energy 464.4eV)’ arises from spin orbit-splitting. These peaks are consistent with Ti⁴⁺ in TiO₂ lattice [230]. Also, the shoulder Ti2p_{1/2} at binding energy 460.2eV is corresponding to Ti³⁺ [231] in Ti₂O₃. This indicates that both TiO₂ and Ti₂O₃ are formed in the film. After doping with Fe, the high resolution XPS spectrum (Fig. 4.9(b)) shows a slight shift in the position along with a variation in the original peaks. The peaks in the Fe doped samples are now located at binding energies 458.4 (Ti2p_{3/2}), 464.3eV (Ti2p_{1/2}) and 459.0eV (Ti2p_{1/2}), respectively as shown in Table 4.2.

Table 4.2. XPS data of different chemical states of O, Ti, Fe and Co elements on the surface of untreated TiO₂, Fe doped/treated TiO₂ and Co doped/treated TiO₂ where O_L represents lattice oxygen, O_s represents sub oxide and O_{NL} non lattice oxygen/ oxygen vacancies.

Sample	Plasma treatment time (sec)	Ti ⁴⁺ (eV)		Ti ³⁺ (eV)		O1s (eV)			Total Percentage of oxygen vacancies	Binding energy of metal ions(eV)	
		Ti2p3/2	Ti2p1/2	Ti2p3/2	Ti2p1/2	O _L	O _s	O _{NL}		2p3/2	2p1/2
TiO ₂	0	458.6	464.4	—	460.4	529.9	530.3	531.3	35	2p3/2	2p1/2
Ti _{0.95} Fe _{0.05} O ₂	0	458.4	464.3	—	459.0	529.8	—	531.9	53.9	710.1	724.6
	60	458.5	464.4	—	459.0	529.7	—	531.5	61.9	711.3	724.8
Ti _{0.95} Co _{0.05} O ₂	0	458.6	464.4	460.4	457.9	530.1	—	531.1	43.4	781.0	796.9
	60	458.5	464.3	460.6	457.4	530.1	—	531.8	54.2	781.2	796.6

The shift in the position of these peaks indicates an influence of Fe addition on the electronic state of Ti element; probably some of the Ti ions get substituted with Fe ions in the lattices. After doping, the area of Ti (III) peak increased by 81% and that of the peak Ti (IV) decreased by 19%. The increment in Ti (III) peak indicates that either Ti₂O₃ is formed in large amount or some mixed oxide structure with Fe (having oxidation state Ti (III)) is formed after doping. Meanwhile, the decreasing area of Ti (IV) indicates a reduction of TiO₂ in the sample, and probably formation of Ti-O-Fe structure in the TiO₂ lattice through the substitution of transition metal ions. Observed shift in the peaks also indicates interaction between Ti and Fe atoms and an overlapping of their 3d orbital [232]. This causes an electronic excitation from Fe to Ti in the optical absorption experiment, which indicates a narrowing in the band gap of Fe doped TiO₂ film (as observed in the optical analysis).

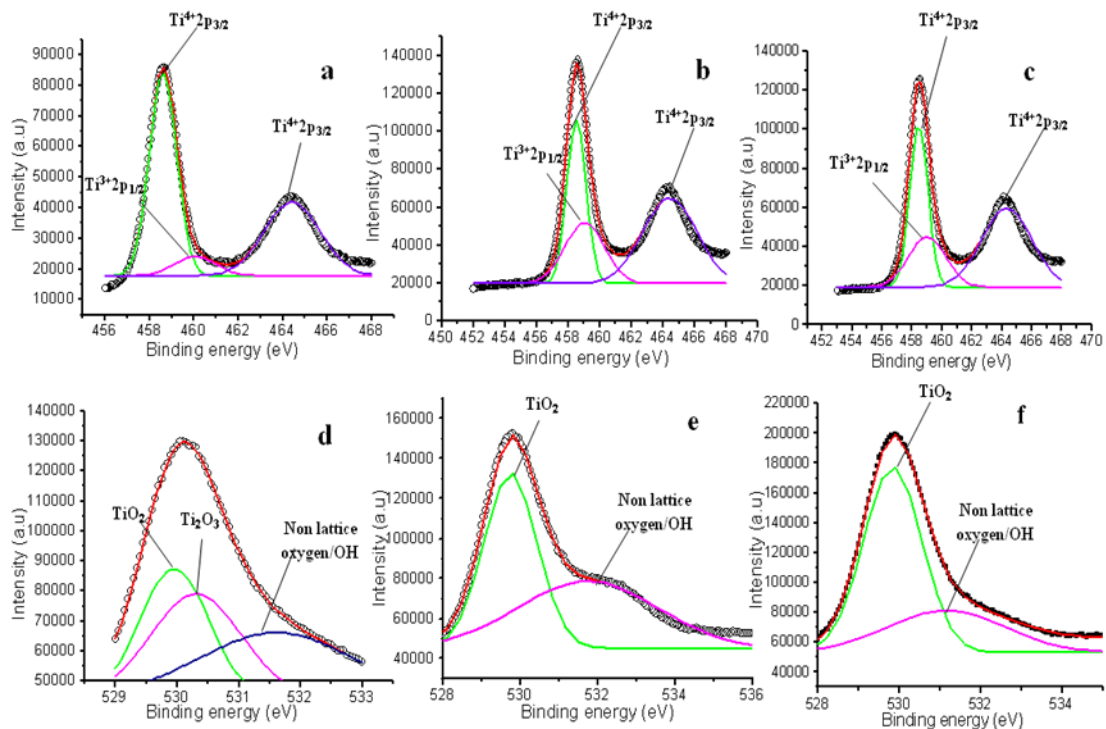


Fig.4.9: High resolution XPS spectra of Ti2p and O1s in (a) pure/untreated TiO₂ film, (b) Fe doped/untreated TiO₂ film; plasma treatment time 0 second, (c) Fe doped/treated TiO₂ film; plasma treatment time 60 seconds, (d) O1s for pure/untreated TiO₂ film, (e) O1s for Fe doped/untreated TiO₂ film; plasma treatment time 0 second, and (f) O1s for Fe doped/treated TiO₂ film; plasma treatment time 60 seconds.

After doping, the film was treated in air plasma. In the XPS results, only the sample which was treated for 60 seconds in plasma is demonstrated. The XPS shows a further increase in the peak corresponding to Ti³⁺ at 459.0eV (Fig. 4.9(c)) and a decrease in the peak area of Ti⁴⁺. The transformation in the stoichiometry was predictable by the variation in the peak area of relative peaks. The peak area of Ti³⁺ increases by 20% and that of Ti⁴⁺ decreases by 12%. The increase in the peak area of Ti³⁺ indicates that after plasma treatment there is removal of oxygen from the lattice, which shows a relative increase in Ti³⁺ in the XPS spectrum. On the other hand, decreasing peak area of Ti⁴⁺ is inferred due to the reaction of Ti⁴⁺ with electrons coming either from the oxygen vacancies or by the plasma [125]. Now, as observed in optical analysis, the band gap of

Fe doped films (3.22eV) decreased to 3.00eV (for 60 seconds of treatment time), this is correlated with the increasing carrier/electrons density due to plasma treatment. As we know that in the doped samples, the possible reasons of red shift/decreasing band gap is the introduction of donor states in the energy gap. In the present case, the band gap decreases further with increasing treatment time, while the concentration of the dopant was kept constant, which is due to the change in the surface states of the constituents i.e. Ti element and oxygen vacancies.

Next, the O1s spectrum of pure TiO₂ thin film is shown in Fig. 4.9(d), which is fitted with three peaks. The peaks at binding energies 529.9eV, 530.3eV and 531.3eV are attributed to lattice oxygen, Ti₂O₃ and non-lattice oxygen [233, 234]. Similarly, for the doped sample, O1s spectrum of Fe doped TiO₂ thin film fitted with two peaks is shown in Fig. 4.9(e). In this spectrum, only two peaks at binding energies 529.8eV, and 531.9eV are observed which are attributed to lattice oxygen and surface adsorbed OH group, whereas the peak 530.3eV corresponding to Ti₂O₃, disappears. This indicates that in the doping process TiO₂ is formed along with some mixed oxide. Yet again, the transformation in the stoichiometry was predictable by the change in area of relative peaks. In case of Fe doped TiO₂ film, the area of the peak at 529.7 increases by 64% and that of the peak at 531.5eV increases by 54%.

After plasma treatment, the binding energy of lattice oxygen (O in TiO₂) shifts slightly from 529.8eV to 529.7eV (Fig. 4.9(f)), whereas its area increases by 35%. Also, the area of peak at 531.5eV (non-lattice oxygen/OH) increases by 15% as shown in Table 4.2. The increase in the area of non-lattice oxygen indicates the formation of oxygen vacancies in the lattice. This result is analogous to the XPS spectrum of Ti2p (Fig. 4.9(c)).

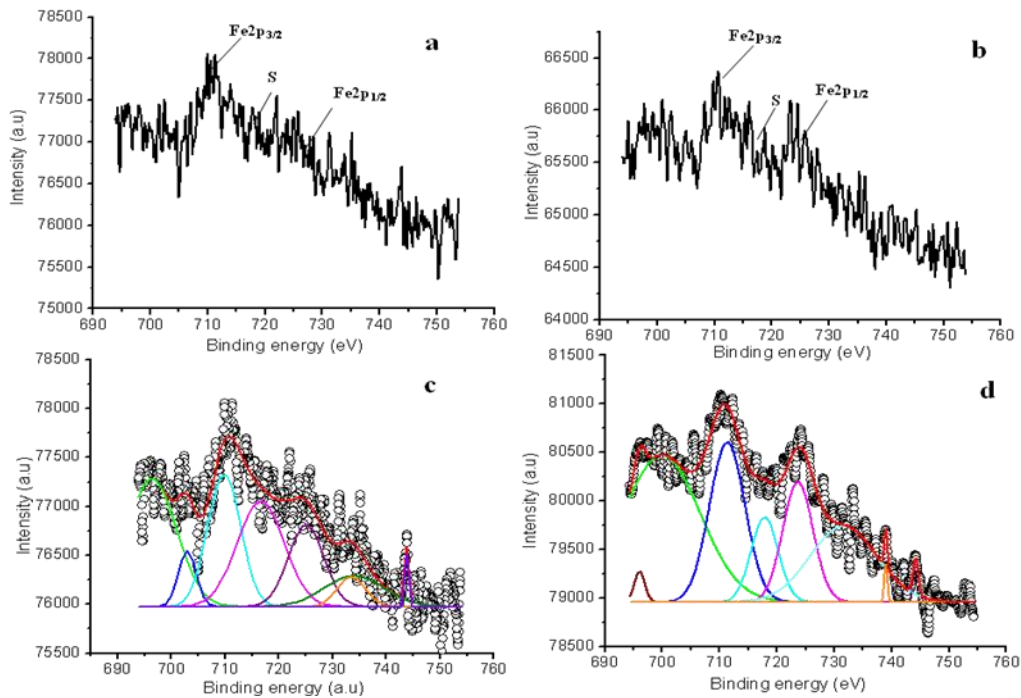


Fig.4.10: High resolution XPS spectra of Fe2p in (a) Fe doped/untreated TiO₂ film; plasma treatment time 0 second, (b) Fe doped/treated TiO₂ film; plasma treatment time 60 seconds, (c) and (d) are Gaussian fit of (a) and (b).

Fe doping results in a minor shift in the binding energy, indicating that Fe ions are better dispersed in the substitutional sites of TiO₂ lattice and produce more mixed oxide structure, probably Fe-O-Ti. Fig. 4.10(a) shows high resolution XPS spectrum (for Fe2p_{3/2}) of Fe doped TiO₂ film. After plasma treatment, the high resolution XPS spectrum of Fe2p_{3/2} is shown in Fig. 4.10(b). These spectra are fitted with Gauss-peak shapes as shown in Fig. 4.10(c, d). The deconvoluted XPS spectrum of Fe2p_{3/2} (Fig. 10(c, d)) contains main peaks at 710.1eV and 724.6.1eV corresponding to Fe2p_{3/2} and Fe2p_{1/2}, respectively. The appearance of these peaks supports the presence of Fe in Fe³⁺ ionic state [235]. Further, after plasma treatment the shift in the binding energy of Fe2p_{3/2} from 710.1eV to 711.3eV also indicates the presence of Fe³⁺ species, irrespective of the particular oxide (i.e., Fe₂O₃, Fe₃O₄, and FeOOH). Shake up satellite at 716.9eV also supports that Fe is presented in Fe³⁺ state (oxide) [235]. These shake-up satellites are

associated with Fe3d-O2p hybridization. Thus, XPS analysis confirmed that Fe ions are doped into TiO₂ matrix in the form of Fe-O-Ti. From the XPS analysis, we confirmed that by increasing the plasma treatment time the concentration of Ti³⁺ and oxygen vacancies also increases.

The Co doped samples after plasma treating show adverse effect on the band gap of the doped TiO₂ film. In this case, band gap increases with the increasing treatment time as observed in optical studies. To investigate this divergent behavior, the samples were analyzed via XPS; Fig. 4.11 shows high resolution spectra. Here, Fig. 4.11(a) is XPS spectrum of pure TiO₂, and for Co doped sample is shown in Fig. 4.11(b). As discussed above in the case of Fe doped sample, here also the XPS of pure TiO₂ is fitted with three peaks corresponding to titanium dioxide (Ti⁴⁺) and titanium sub oxide (Ti³⁺) in Ti2p_{1/2} and Ti2p_{3/2}, respectively. These peaks are fitted as Ti⁴⁺2p_{1/2} at 464.4eV, Ti⁴⁺2p_{3/2} at 458.6eV and Ti³⁺ 2p_{3/2} at 460.2eV as illustrated in Table 4.2. The line separation between Ti2p_{1/2} and Ti2p_{3/2} is 5.8eV, which is consistent with the standard binding energy of TiO₂ [230]. In this case the Ti2p spectrum (Fig. 4.11(b)) is fitted with four peaks as 464.4 for Ti⁴⁺2p_{1/2}, 458.6eV for Ti⁴⁺2p_{3/2}, 460.4 for Ti³⁺2p_{1/2} and 457.9eV for Ti³⁺2p_{3/2}, [236], respectively. In comparison to the pure TiO₂, the area of Ti³⁺ peak in Co doped TiO₂ increases by 26%, while that of the peak Ti⁴⁺ decreases by 7%, indicating a reduction in the formation of TiO₂, which is similar to the case of Fe doped samples.

After the plasma treatment (Fig. 4.11(c)), binding energies of the mentioned peaks are shifted slightly to the positions such as 464.3eV (Ti⁴⁺2p_{1/2}), 458.5eV (Ti⁴⁺2p_{3/2}), 460.6eV (Ti³⁺2p_{3/2}) and 457.4eV (Ti³⁺2p_{1/2}), respectively. The change in stoichiometry was estimated by the change in peak area of respective peaks.

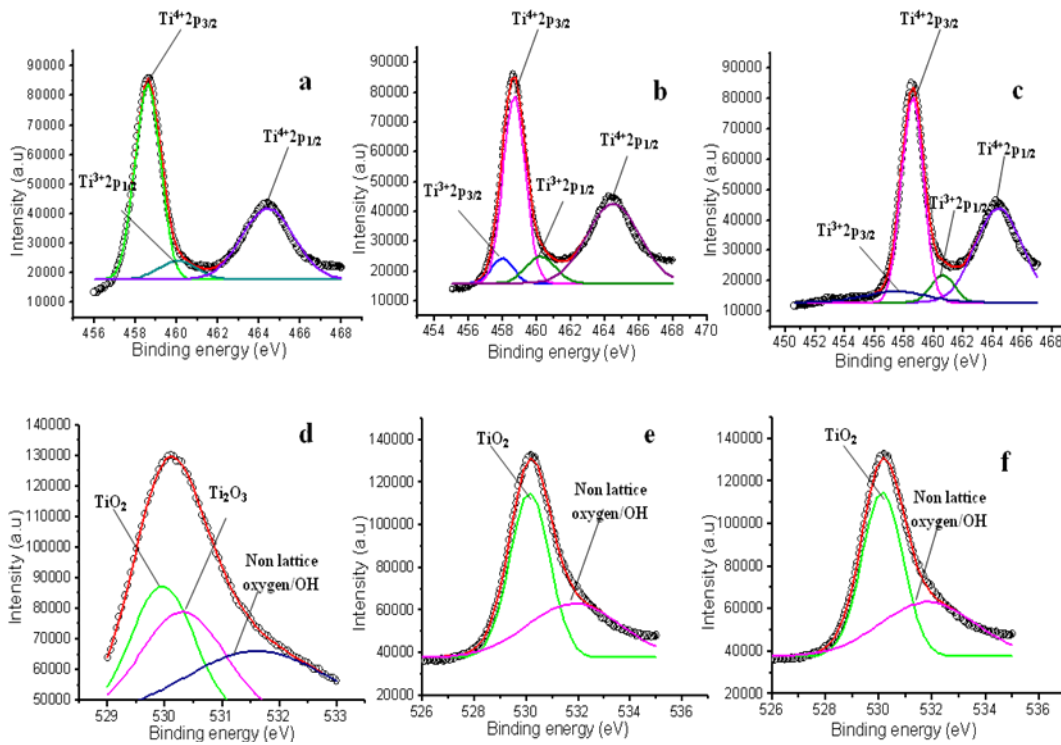


Fig.4.11: High resolution XPS spectra of Ti2p and O1s in (a) pure/untreated TiO₂ film, (b) Co doped/untreated TiO₂ film; plasma treatment time 0 second, (c) Co doped/treated TiO₂ film; plasma treatment time 60 seconds, (d) O1s for pure/untreated TiO₂ film, (e) O1s for Co doped/untreated TiO₂ film; plasma treatment time 0 second, and (f) O1s for Co doped/treated TiO₂ film; plasma treatment time 60 seconds.

After plasma treatment, we observed that the peak area of Ti³⁺ increases by 30%, whereas, peak area of Ti⁴⁺ decreases by 12%. Further, this is predictable due to the reaction of Ti⁴⁺ with the electrons coming either from the oxygen vacancies or by plasma. Further, the high resolution O1s XPS spectrum obtained for Co doped sample is shown in Fig. 4.11(d-f). The spectrum is shaped with three peaks i.e. 529.9eV, 530.3eV and 531.6eV that correspond to lattice oxygen of TiO₂, oxygen in Ti₂O₃ and non-lattice oxygen, respectively.

The change in stoichiometry was estimated by change in the peak area of relative peaks. With the doping of Co, the lattice oxygen (corresponding to TiO₂) peak at 529.9 shifts to

the position 530.3eV, and the area of the peaks at 530.3eV and 531.6eV increases by 51% and 24%, respectively. The original peak at 530.3eV (Fig. 4.11(d)) corresponding to Ti_2O_3 disappears after doping (Fig. 4.11(e)), which is due to the formation of mixed oxide structure. Further, with the increasing treatment time, the areas of the peaks at 530.3eV and 531.6eV ((Fig. 4.11(f)) increases by 24% and 25%, respectively.

Next, Fig. 4.12(a) corresponds to high-resolution XPS spectra of Co2p region of Co doped TiO_2 thin films and Fig. 4.12(b) shows high-resolution XPS spectra with plasma treatment. Fig. 4.12(c, d) represent deconvoluted XPS spectra of doped TiO_2 and plasma treated TiO_2 thin films, respectively. The core level binding energies of peaks $Co2p_{1/2}$ and $Co2p_{3/2}$ are 796.9eV and 781.0eV, respectively. The satellite peaks at 787eV and 802eV reveal high spin Co(II) state with complex transitions [237]. These results are an indication that Co does not precipitate as metallic Co on the film surface. After plasma treatment, the satellites peaks shift slightly to the 785.3eV and 802.3eV. Also, the binding energies of $Co2p_{1/2}$ and $Co2p_{3/2}$ are shifted to 796.6eV and 781.2eV, respectively. These latter spectra are typical of compounds containing high-spin Co^{2+} ions [238,239], revealing the presence of CoO (Co^{2+}), $CoTiO_3$ (Co^{2+}), Co_2O_3 (Co^{3+}) or mixed valence Co_3O_4 (Co^{2+} and Co^{3+}) in the surface. The presence of strong satellites indicates that Co atoms in the doped TiO_2 film are in 2+ oxidation state, referring the possible formation of CoO or $CoTiO_3$ inside the film.

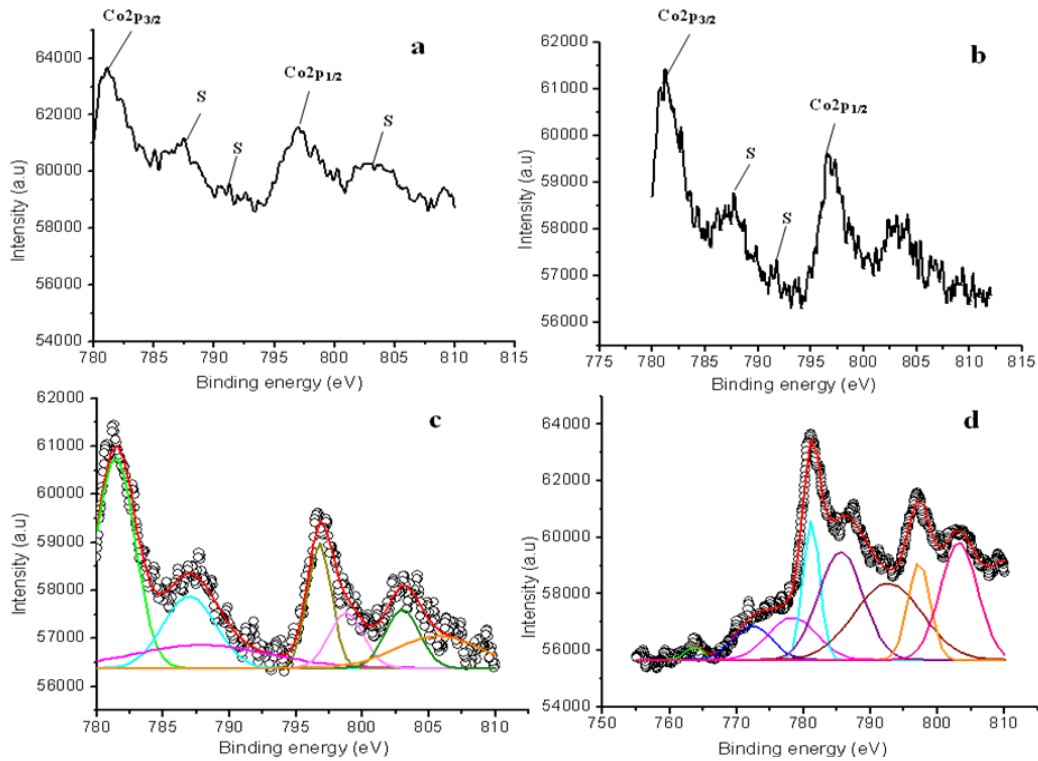


Fig.4.12: High resolution XPS spectra of Co2p in (a) Co doped/untreated TiO₂ film; plasma treatment time 0 second, (b) Co doped/treated TiO₂ film; plasma treatment time 60 seconds, (c) and (d) are Gaussian fit of (a) and (b).

Now we discuss the probable reason of band gap narrowing in TiO₂ film with Fe doping, and widening in the case of Co doping after plasma treatment. As reported, the iron dopant acts as an acceptor impurity in TiO₂ lattice [240]. Thus, when the TiO₂ film is doped with Fe, the acceptor levels of Fe along with oxygen vacancies are created in the band gap of TiO₂ [241]. In our case, as discussed above Ti³⁺ is also formed which also creates energy level in the band gap, contributing to the reduction of band gap. The energy level position of Ti³⁺ lies just below the conduction band since Ti³⁺ acts as a donor level in the band gap [212]. Next, when this Fe doped TiO₂ film was treated in air plasma, the Ti³⁺ levels and oxygen vacancies increases further with the treatment time, whereas no change in the dopant levels occurs as the dopant concentration was kept constant.

The increase in Ti^{3+} levels and oxygen vacancies would further reduce the band gap of Fe doped TiO_2 film. In case of Co doping, there is formation of Co acceptor levels along with Ti^{3+} and oxygen vacancies levels in the band gap that reduces the band gap of Co doped TiO_2 film. But in this case when the film was treated with plasma we observed continuous widening in the band gap with treatment time. The observed increase in the band gap can be explained by Burstein-Moss effect. The probable reason for Burstein-Moss shift in this case is that with the treatment time the Ti^{3+} levels and oxygen vacancies increases more as compared to Fe doped case. By plasma treatment for 60 seconds the Ti^{3+} increases by 20%, oxygen vacancies increase by 15% in case of Fe doped TiO_2 , whereas Co doped TiO_2 Ti^{3+} increases 30%, oxygen vacancies increase 25%. These created levels donate more electrons and thus shift the fermi level to the conduction band, which increases the band gap of Co doped TiO_2 film. However, the precise reason of the observed divergent behavior of Co doped TiO_2 films than Fe doped TiO_2 films is not clear but the most suitable reason looks the on-site coulomb interaction/repulsion [242] in case of Co doped TiO_2 films. When Co^{2+} ion substitutes Ti^{4+} ions, the balance of charge is compensated by oxygen vacancies located near Co ion [243]. The production of oxygen vacancies is equivalent to the addition of two electrons per Co ion [244]. In case of Co doping the number of oxygen vacancies produced with the plasma treatment is more than that of Fe doped case; that may be the reason of on-site Coulomb interaction requiring large Coulomb energy to add electrons to the Co ion in the optical transition that results to the blue shift in the absorption spectra. The proposed mechanism for both the Fe and Co doped TiO_2 is illustrated in Fig. 4.13.

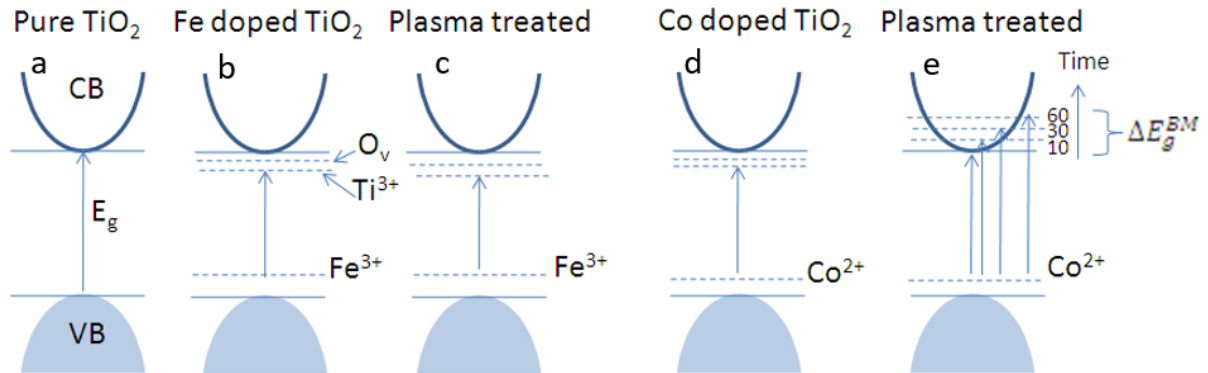


Fig.4.13: Schematic diagram of the energy levels of (a) pure/untreated TiO₂ films, (b) Fe doped/untreated TiO₂ film, (c) Fe doped/treated TiO₂; for 60 seconds of treatment time, (d) Co doped/untreated TiO₂ film, (e) Co doped/treated TiO₂ film; for 10, 30 and 60 seconds of treatment time, indicating Burstein Moss effect. (O_v represents oxygen vacancies)

4.5. Summary

We observed that the treatment by air plasma leads to significant change in the optical properties of TiO₂ thin films. Unlike the other treatment methods, this approach possesses transparency of TiO₂ thin film and alters optical properties. The charge separation centers i.e. oxygen vacancies and Ti³⁺ is created with the doping of metallic Fe and Co elements; however, they are significantly enhanced by the air plasma treatment. In Fe doped TiO₂ thin film, the formation of oxygen vacancies and Ti³⁺ causes enhance absorbance and red shift due to the formation of energy levels in the band gap, whereas in Co doped TiO₂ the Burstein-Moss shift is effective to make blue shift in the absorption spectra. Conclusively, we can say that the joint approaches i.e. low level/moderate doping and safe and low-cost air plasma treatment resulted in enhanced optical properties of transparent TiO₂ thin films, making them efficient candidate for transparent electrode applications.



CHAPTER V

Photocatalytic Activity of Fe and Co Doped TiO_2 Thin Films

In this chapter, we briefly discuss the formation of undoped and doped TiO₂ films for photocatalytic activity. In the introduction, we describe different approaches applied for photocatalytic viability of TiO₂ nanostructures and related drawback associated with TiO₂ in the photocatalytic performance. In the next section, we discuss the formation of doped TiO₂ films and their implementation for photocatalytic performance in sun light irradiation. Finally, in the last section the chapter ends with the summary.

5.1. Introduction

TiO₂ is of great importance because of its lifetime, chemical inertness and the fact that it is simply synthesised and fabricated by simple chemical processes [245]. Nonetheless, films of TiO₂ have been widely studied due to their physical possibilities and multifunctional applications. Aforementioned properties make TiO₂ a significant material in numerous applications, including water splitting, pigments, photocatalytic degradation of organic contaminants, dye sensitized solar cells, self-cleaning, and perovskite solar cell [246-251] etc. Current advancement in research on TiO₂ photocatalyst has considerably raised the practical significance of photocatalysis, because of its strong oxidation as well as moderate reduction potential. Photocatalytic ability of pure TiO₂ is very low by cause of the limited UV region of the arriving solar energy under solar irradiation [252]. Generally, under the illumination of light electron/hole pairs are formed, which are responsible for the photocatalytic activity. These electron/hole pairs originate several chemical reactions by introducing radical species on TiO₂ surface [253]. Due to enhanced fast recombination rate of generated electron/hole pairs along with its wide band gap ($E_g = 3.2$ eV), TiO₂ shows limited response in the visible light, and thus a low quantum efficiency [254]. Therefore, to enhance the photocatalytic activity of TiO₂, it is crucial to reduce the rate of electron/hole recombination, reduction in the band gap, which would improve its sensitivity in the visible range [255-258]. To address the above-mentioned obstacle, doping is one of the important ways to enhance its optical and electronic properties. Doping with nonmetals, metals or coupling with semiconductors, etc. have been reported in many studies [259]. Among all these, metal doping in TiO₂, is most effective that not only to enhance the optical response from UV to visible range, but also reduced the electron/hole pair recombination during photocatalytic activity [260-262]. It is also found that doping with transition metals

formed new intra-bands inside the TiO₂ matrix, which reduced their band gap and consequently promote the optical response of TiO₂ in UV and visible range [263, 264]. However, in TiO₂ the existence of oxygen vacancy is extensively studied which normally widen the absorption edge of TiO₂ towards visible region [265]. It has been reported that when dopant act as acceptor in TiO₂, generates oxygen vacancies for the charge compensation.

Khan *et al.* [266] has reported the consequence of defects on the optical, electronic and structural properties of anatase TiO₂. They found that Cr 3d states reduced the recombination rate of electron/hole pair which improve the visible light absorption and separate the photoexcited carriers resulting in the increased photocatalytic activity. Formation of oxygen vacancy makes it complicated to elucidate the actual reason for the enhanced photocatalytic activity, as the increase in the photo activity can be ascribed to the formation of oxygen vacancies or to the elemental doping. Khan *et al.* [267] studied the importance of oxygen vacancies, creation of hydroxyl radicals, Ti³⁺ centers and Fe³⁺ impurity energy levels in doped catalysts visible light response, and concluded that the Fe³⁺-TiO₂ decreases the electron/hole pairs and improved photocatalytic activity.

In this chapter, we have synthesized undoped; Fe and Co doped TiO₂ thin films simply by dip coating method. The films after formation were annealed at 500°C for 2 hours. Both the dopant metal and plasma generated oxygen vacancies affect the band gap of TiO₂ films, and thus their photocatalytic activity. Structural properties of as synthesized samples show that the dopants in TiO₂ exhibit no tendency and/or precipitate in different phase during the synthesis process. Similarly, the UV-Visible spectra show decrease in the band gap of Fe and Co doped TiO₂ films. XPS analysis reveals the presence of Ti, O, Fe and Co in the synthesized samples.

5.2. Experimental section

Similar to the pure/undoped TiO₂ thin films, thin film of Ti_{1-x}Fe_xO₂ and Ti_{1-x}Co_xO₂ (where x=0 and 0.05) were also prepared using dip-coating method. In this case, the precursor solutions of titanium (IV) isopropoxide (TTIP, 98%, Aldrich) with ferric nitrate, and cobalt nitrate were formed separately to fabricate Fe and Co doped TiO₂ thin films. Again, triethanolamine (C₆H₁₅NO₃) was used as a stabilizing agent to prevent the precipitation of titanium precursor. Following the similar procedure as that of undoped TiO₂ films, triethanolamine (C₆H₁₅NO₃) was

dissolved in ethanol (C_2H_5OH) to form a colorless solution, and then $C_{12}H_{28}O_4Ti$ was added dropwise with continuously stirring to form a clear pale-yellow sol. Afterwards, a mixture of ethanol and deionized water (9:1) was added to the prepared sol to avoid rapid precipitation of TiO_2 . Fig. 5.1 illustrate the synthesis of Fe doped TiO_2 thin films. The final solutions were stirred further for next 2 hours and allowed to age over night before coating on glass slides. Same procedure was followed for the preparation of Co doped TiO_2 thin films were. Glass substrates were cleaned ultrasonically with sequentially deionized water, detergent, C_3H_6O and then C_2H_5OH . After coating the films were dried in air and annealed at $400^\circ C$ for 2 hours in an oven.

5.2.1. Photocatalytic activity experiment

Methylene blue (MB) ($C_{16}H_{18}ClN_3S$), an extensively used dye, was working as a representative dye pollutant to check the photocatalytic activity of TiO_2 films. The undoped and doped (Fe and Co) TiO_2 films were investigated for their photocatalytic performance in the sun light. In the experiments about 0.40 g of TiO_2 powder was coated on glass slides to make thick films of the material. The coated slide of TiO_2 (undoped and doped) was dipped in a MB solution of 6.50×10^{-5} M and irradiated for varying time intervals. Investigation of photocatalytic degradation of MB dye in the sun light was done by analyzing the change in optical absorption of the prepared samples. The absorbance of the peak at 650nm is used to evaluate the absorption of MB solution.

5.2.3. Sample characterization

The samples were characterized for morphology by using field emission electron microscope (FE-SEM), structural properties using X-ray diffractometer (XRD), and optical properties by using UV-Vis spectrophotometer and surface properties by using X-ray photoelectron spectroscopy (XPS).

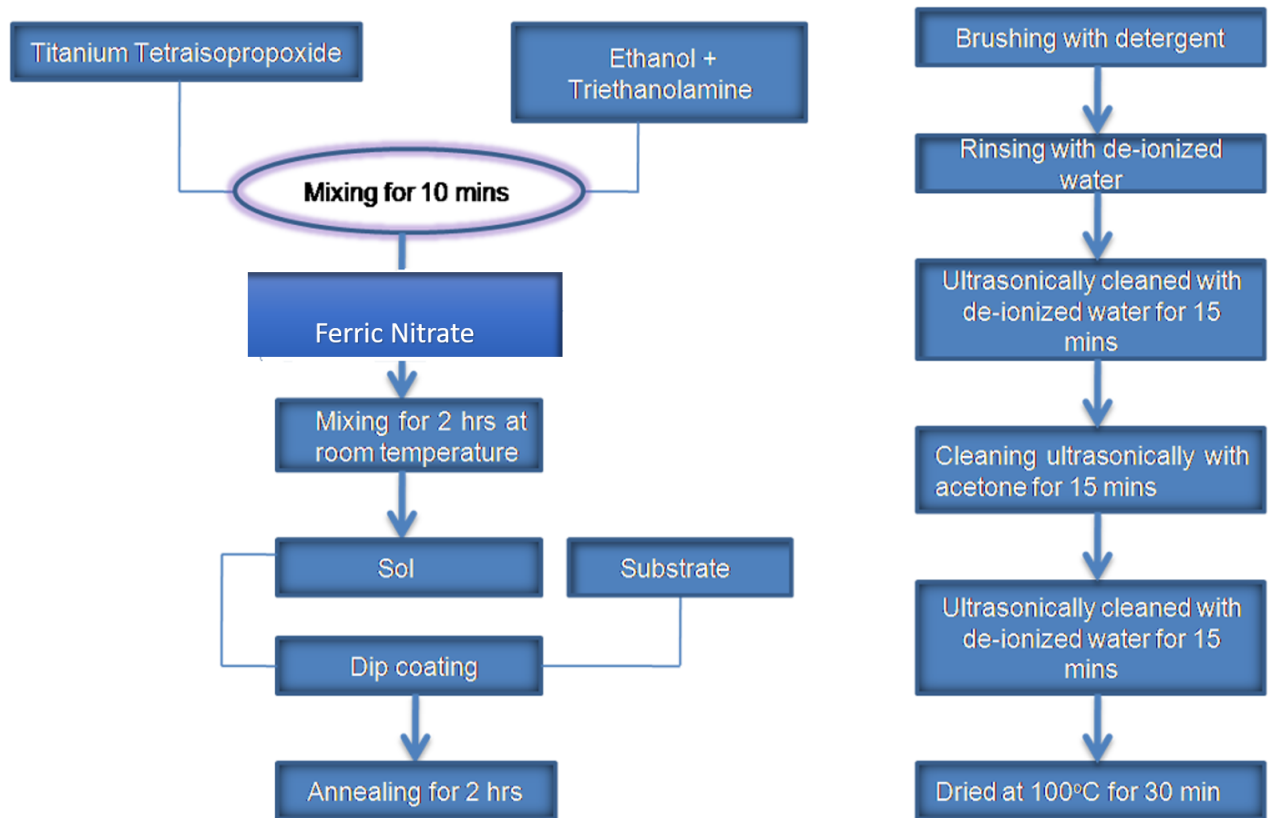


Fig.5.1: Schematic diagram of the preparation of undoped, Fe and Co doped TiO₂ films (left) and cleaning of the glass substrate (right).

5.3. Results and discussion

5.3.1. XRD analysis

To check the structural properties of thicker films, XRD analysis was performed on the as-deposited TiO₂, Fe and Co doped TiO₂ films were illustrated in Fig. 5.2(a, b, c). These spectra were corresponding to amorphous phase of TiO₂, indicating no considerable peak present in the synthesized samples. The prepared TiO₂ films were annealed at 500°C. A diffraction peak of anatase and rutile phase of TiO₂ formed after heating at 500°C in some cases [268]. Fig. 5.2(b, c) clearly indicate that, no characteristics peaks for Fe and Co were detected. The reason may be; (i) Fe³⁺ are well implanted into TiO₂, (ii) Fe content cannot be found because it is under diffractometer detection limits, or (iii) the formed Fe can have an amorphous state [269, 220].

Similarly, Co ions in the respective samples get embedded into the structure of TiO_2 by replacing some of Ti ions, and locate at interstitial sites [220].

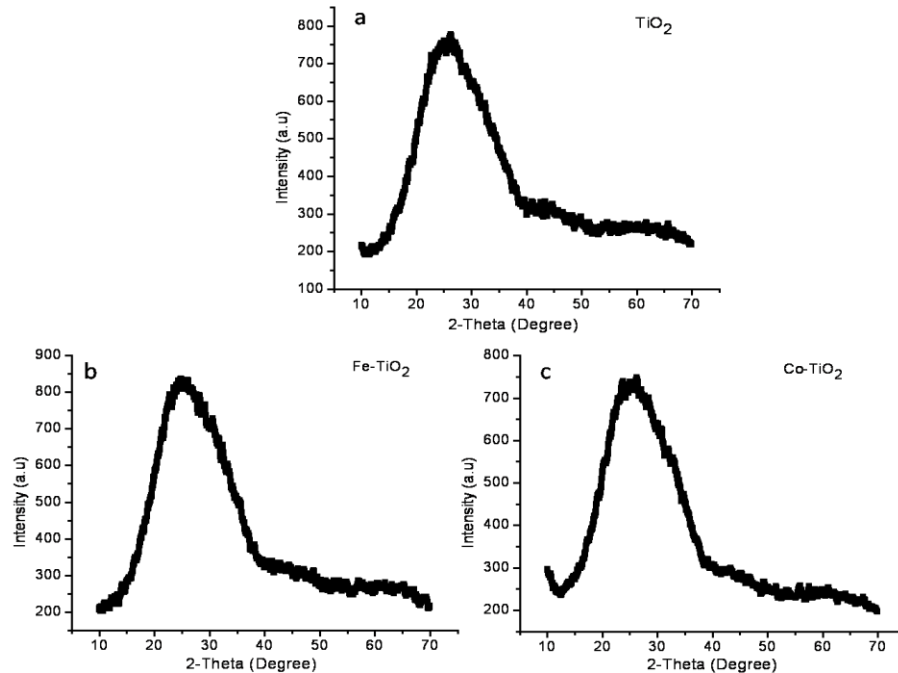


Fig.5.2: XRD pattern of (a) pure TiO_2 , (b) Fe doped TiO_2 and (c) Co doped TiO_2 films.

5.3.2. Morphological analysis

Fig. 5.3 shows the SEM micrograph of TiO_2 , Fe and Co doped TiO_2 film. The films appear to be dense and flat. To check elemental composition, the synthesized samples were characterized by EDX. The EDX analysis confirmed that Fe and Co was distributed throughout the film with slight variations. In the EDX of Fe doped TiO_2 films, the atomic percentage of Fe, Ti and O were found as, 2.37%, 9.77% and 87.86%, respectively, which closely approximate to the percentage of elements in $\text{Ti}_{0.96}\text{Fe}_{0.04}\text{O}_2$. Similarly, in case of Co doped TiO_2 , the obtained atomic percentage of Co, Ti and O in EDX was 2.75%, 10.17% and 87.08% respectively, which corresponds to the formation of $\text{Ti}_{0.96}\text{Co}_{0.04}\text{O}_2$ films.

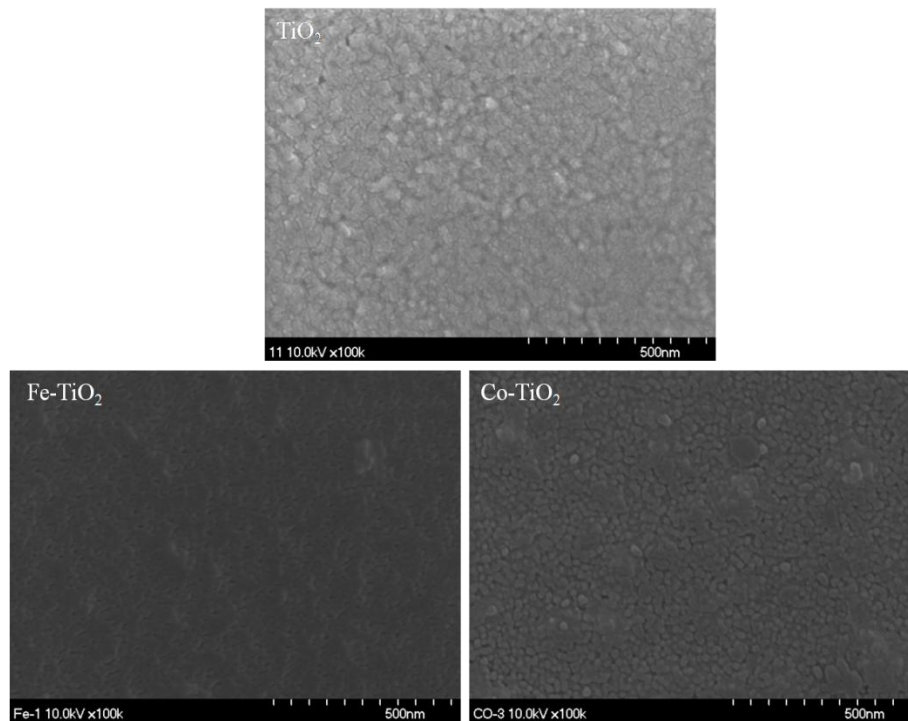


Fig.5.3: SEM micrograph of pure TiO₂, Fe doped TiO₂ and Co doped TiO₂ thin films.

5.3.4. XPS analysis of pure and doped TiO₂ films

XPS analysis was performed to confirm the elemental and chemical states of as synthesized samples. The corresponding XPS survey scans are shown in Fig. 5.4 (a, b). The binding energies found in the XPS spectra are calibrated using C 1s (284.8 eV). The peaks for carbon impurities may arise from the chamber contamination in the XPS equipment itself. All peaks in the Fig. 5(a, b) were attributed to Ti, O, C, Fe and Co.

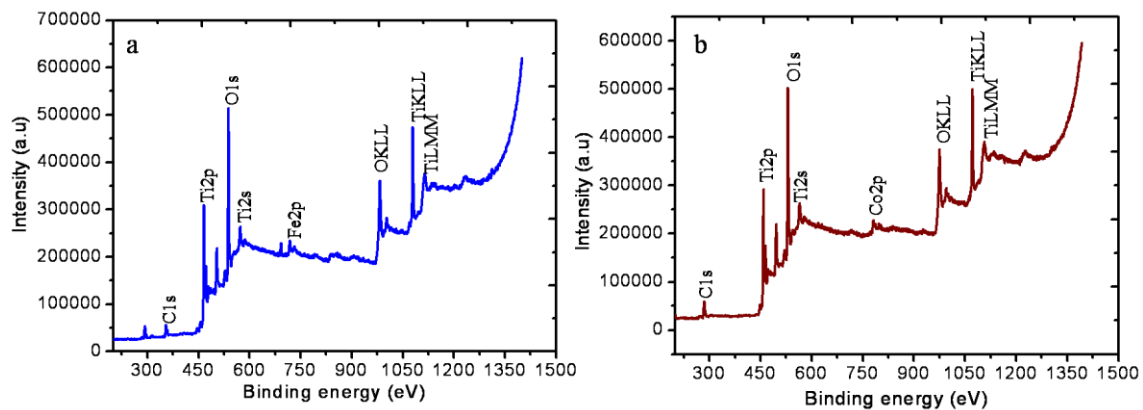


Fig.5.4: XPS survey spectra of (a) Fe doped TiO₂ and (b) Co doped TiO₂ film.

5.4. Photocatalytic performance of undoped and doped TiO₂ films

Variation of absorption spectra of MB solution after different time interval of sunlight irradiation in the presence of pure, Fe and Co doped TiO₂ films are shown in Fig. 5.5. From the Fig. 5.5(a), it was observed that pure TiO₂ film does not show any change in the absorbance with the sun light irradiation time. The solution samples were collected for time 0, 1 and 2 hours. The small decrease in the absorbance (Fig. 5.5 (a)) can be observed for 2 hours of irradiation time. In the case of Fe doped TiO₂ (Fig. 5.5(b)), the change in the absorption spectra with irradiation time is such as that in the first 1 hours of irradiation, the absorption peak intensity (at 650nm) decreases from 0.15 to 0.097. In the next hour, there is no change in the peak intensity indicating that the Fe doped TiO₂ degrades MB dye to a certain extent within first 1 hour of irradiation, and thereafter there is no degradation in the MB. This result is correlated with the observed change in the band gap of TiO₂ when doped with Fe (3.22 to 3.00eV) as discussed in the chapter IV. As we found, that the presence of Fe by doping and oxygen vacancies by plasma treatment affects the band gap of the films. Now, also in the case of Co doping (Fig. 5.5(c)), there is variation in the absorption peak value with the irradiation time. In this case, the absorption intensity decreases from 0.15 to 0.12. The values are higher than those in the case of Fe doping. In both cases (Fe and Co doped TiO₂) the observed change in the absorption peak is because of the creation of oxygen vacancies on the surface of thin films, which in general effects the band gap and thus the absorbance of the films. However, in Co doped films, the degradation of MB dye cannot be explained on the bases of band gap, because in this case the band gap increased (3.36 to 3.62eV) with the treatment time as shown in chapter IV, which should affect adversely the degradation of dye. Therefore, in this case it is only the oxygen vacancies, which produces trap centers to avoid the recombination of photo-generated charge careers, and thus the enhanced photocatalytic activity.

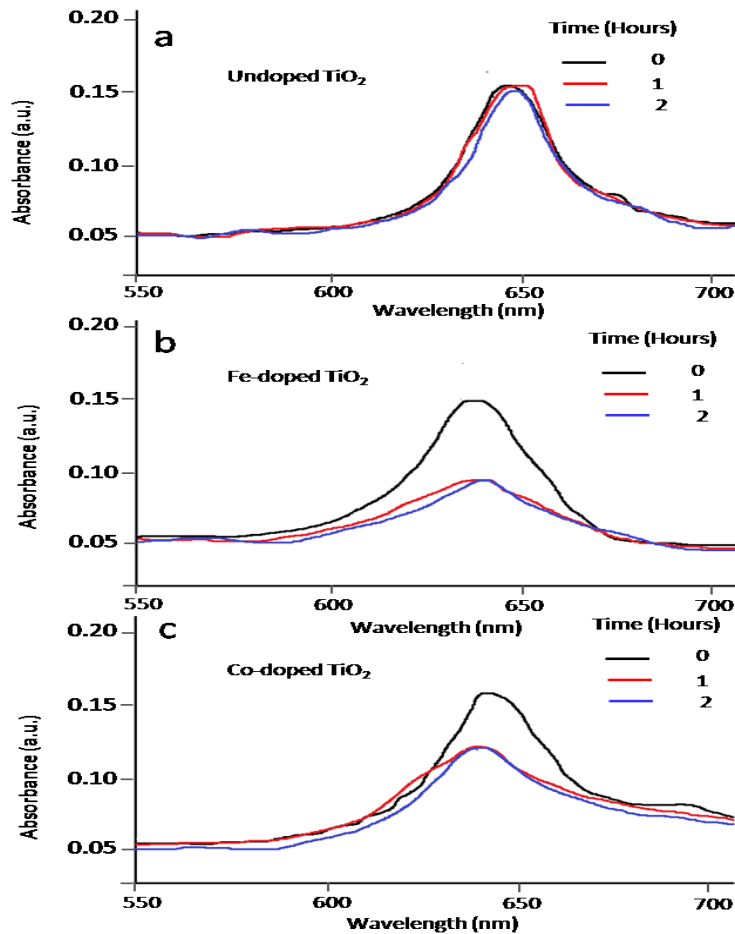


Fig.5.5: Sunlight degradation of Methylene Blue (a) undoped TiO₂, (b) Fe doped TiO₂ and (c) Co doped TiO₂ films.

Fig. 5.6 shows the variation of relative concentration C/C_0 of MB dye with sunlight irradiation time. Here, the initial concentration of MB dye is represented by C_0 and final concentration after the equilibrium is C . In this image, for the undoped TiO₂ films, there is negligible degradation of MB dye; whereas, in case of Co doped TiO₂ there is 30% degradation and for Fe dopant it increases to 50%. The photocatalytic efficiency was calculated using the formal $\eta = (1 - C/C_0) \times 100$.

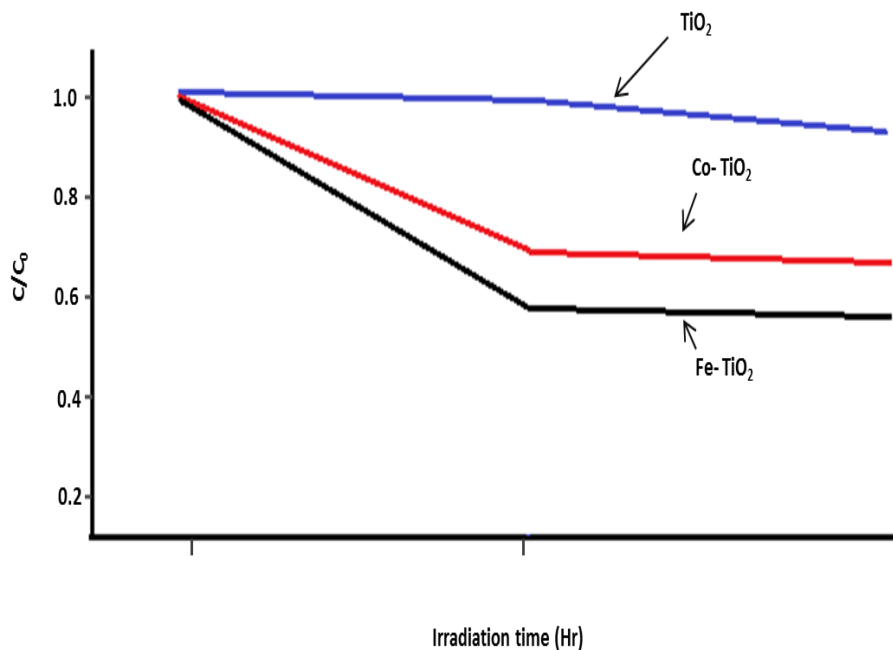


Fig.5.6: Photocatalytic activity of undoped, Fe and Co doped TiO₂ films under sunlight irradiation.

Photocatalytic mechanism

Here, a brief explanation of the photocatalytic mechanism of undoped and doped TiO₂ films is presented. Initially, the solution was kept in dark for 30 minutes, the adsorption-desorption of MB on the surface of TiO₂ films takes place. This solution was then irradiated in the sun light which should create electron/hole pairs in TiO₂ matrix. In photocatalysis, the absorption of a photon excites an electron to the conduction band (CB) generating a hole in valence band (VB) (Eq. 5.1). Thus, generated electron/hole pairs can be trapped as O-defect sites and Ti³⁺ in the TiO₂ or they can recombine, dissipating energy [270]. Alternatively, the electron/hole can shift to the catalyst surface and start redox reactions with adsorbates [271]. The produced holes react with electron rich surface hydroxyl groups; the water molecule in the solution, and form $\cdot\text{OH}$ in the solution (Eq. 5.2&5.3), which are extremely powerful oxidants. Electrons when react with the dissolved oxygen molecules in the solution, reduced to form superoxide radical anions $\text{O}_2^{\cdot-}$ (Eq. 5.4). The hydroxyl radicals can consequently oxidize organic species, yielding H₂O and CO₂ (Eq. 5.8) [272]. Thus, produced radicals ($\cdot\text{OH}$ and $\text{O}_2^{\cdot-}$) participate in the degradation of the pollutant MB dye [273].

The observed no change in the absorbance peak of pure TiO₂ film is analogous to the reported showing its wide band gap then to absorb the visible light. In the absorption spectra, small degradation is due to the 3 to 5 % UV portion of the sun light. In another two cases of Fe and Co doped films, there is an absorbance of degradation of the MB dye. However, the degradation in both the cases cannot be explained on the similar bases i.e. band gap reduction, since as studied from the UV-Vis analysis the reduction in the band gap occurs only in the case of Fe doped TiO₂ films; whereas, in another case Co doped TiO₂, UV-Vis results show increased band gap (as discussed in the chapter IV). To explain the photocatalytic activity in these two different cases, oxygen vacancies play an important role [274]. These oxygen vacancies introduced mid-energy levels in the band gap which by trapping the photo-generated charge carriers reduces their recombination (as explained in chapter IV), and hence increases the photocatalytic performance. Therefore, the Fe doped TiO₂ degrades MB dye due to the reduction of its band gap by Fe doping and the oxygen vacancies by plasma, while Co doped TiO₂ works as the photocatalytic due to the creation of oxygen vacancies after plasma treatment.

The generation of electron/holes pair under UV and visible light can be explained from the following equation [275, 276]:



Fig. 5.7 represents the proposed mechanism for generation of photo induced electrons/holes which were responsible for the degradation of MB molecules.

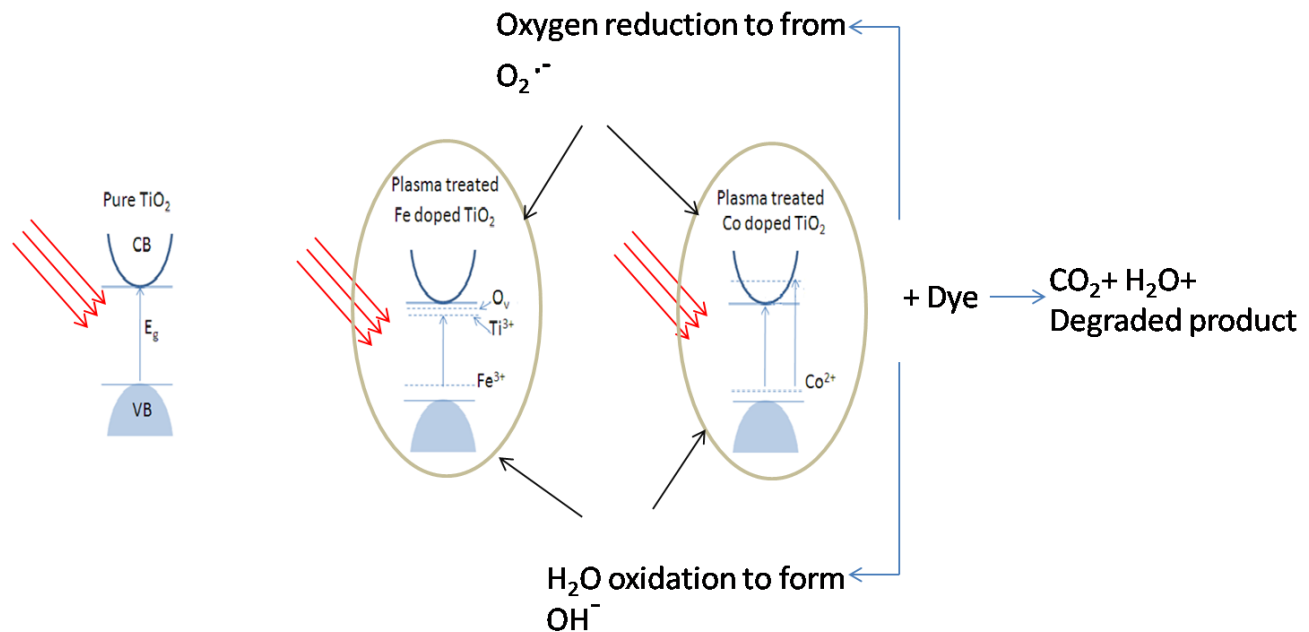


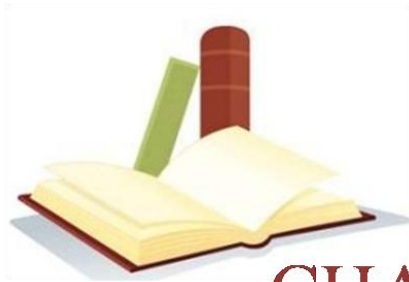
Fig.5.7: Representation of degradation mechanism by undoped, Fe doped and Co doped TiO₂ films in the sunlight.

It is inferred that plasma induced oxygen vacancies participate in the new photoexcitation reactions. Electron may be excited from the VB to the oxygen vacancy which results in excellent visible light absorption and high quantum efficiency. For the separation of photo induced charges, oxygen vacancies seem to be highly valuable. The increase in oxygen vacancy may also enhance the surface OH group; advantageous for photocatalytic reactions. Thus, the oxygen vacancies reduce the recombination of electron/hole pairs either by trapping the VB electron or promoting the trap electron to the CB [267].

From the absorption spectra of Fe doped sample there was 50% degradation of MB dye, while in the case of Co doped sample it was about 30%. The difference in the degradation capabilities may be elucidated to the difference in their degradation parameters (band gap and vacancies in Fe doped samples, and only oxygen vacancies in Co doped sample). In Fe doping, the formation of Ti³⁺, oxygen vacancies as well as Fe³⁺, and Fe²⁺ states improve photocatalytic activity by trapping charge carries.

5.5. Summary

In summary, we demonstrate photocatalytic activity of dip coated undoped, Fe and Co doped TiO₂ films after plasma treatment. The Fe doped TiO₂ films show 50% degradation of MB dye due to the decrease in the band gap of TiO₂ and creation of oxygen vacancies, and Fe³⁺, and Fe²⁺ states. In case of Co doped TiO₂ films, the absorption edge shifted toward lower wavelength results in the widening of the band gap. In this case, observed 30% degradation of methylene blue is due to the creation of oxygen vacancies only. As a conclusion, the generation of oxygen vacancies by air plasma can enlarge the photocatalytic activity of doped TiO₂ films. This approach may be used for a wide range of applications, such as photo electrochemical cells, antibacterial coating, self-cleaning materials, water splitting, etc.



CHAPTER VI

Summary and Future Scope

Summary

We have found that air plasma treated TiO₂ thin films have shown good superhydrophilicity, excellent antifogging properties, enhanced optical and photocatalytic properties due to the change in surface states of undoped as well as doped TiO₂ thin films. The observed properties can be suitable for many technological applications such as; photocatalysis, anti-fogging, dye sensitized solar cells, gas sensing, surface cleaning, heat reflectors, LEDs, thin film photo-anode to develop new photovoltaic, transparent electrodes, photo-electrochemical cells, and water splitting etc.

As the summary of the thesis, a low temperature and economical method i.e. sol-gel method has been adopted to prepare TiO₂ sol. After the formation of TiO₂ sol, thin films of TiO₂ were prepared on the glass substrate by dip coating method. In order to tune properties of these films, the films were treated in air plasma with different plasma treatment time: 0, 5, 10, 15, 30, 60, 120 and 180 seconds. The plasma was generated using air inside a vacuum coating unit (Model 12A4D). For the plasma formation a vacuum of 0.3 mbar was created using rotary pump in the machine. The applied voltage was kept 30 V and the power was 24.6 Watt. After exposure in air plasma, the samples were analyzed for their wetting behavior, optical properties, antifogging properties, surface morphology and structural properties. Both the untreated and plasma treated thin films were characterized by using contact angle measurement, XPS, AFM, XRD, XPS and UV-Visible Spectroscopy.

To recognize the consequence of plasma treatment on the wetting properties of thus formed films, they were analyzed using sessile drop method. The decrease in the contact angle of test liquids (H₂O and C₂H₆O₂) with the increasing plasma exposure time, revealed an increase in the surface energy of the films.

These films when examined for their hydrophilic properties showed super hydrophilicity. In the analysis, we found that dangling bonds, commonly; Ti³⁺, O₃⁻, O⁻, OH species, O vacancies and nanometer scale surface roughness created by the plasma are the responsible factors for superhydrophilicity. The presence of dangling bonds facilitates OH⁻, H⁺ ions and other ionic species to be chemisorbed/adsorbed on the surface of TiO₂ film. While investigating through XPS, the presence of dangling bonds due to the enhancement of oxygen vacancies and Ti³⁺ states via plasma treatment was confirmed. The increase in Ti³⁺ state indicated formation of Ti₂O₃ by the reduction of Ti⁴⁺ state, and decrease in Ti⁴⁺ state due to the reaction of Ti⁴⁺ with electrons

from the plasma or by formation of oxygen vacancies resulted from plasma treatment. In the investigations for surface morphology by AFM reveal that increasing plasma treatment time also enhances surface roughness, which is due to the formation of nano/micro-dents on the treated film as well as the formation of aggregated nanoparticles. In the process of plasma treatment, small nanoparticles in the intimate contact aggregate results in the formation of slightly bigger nanoparticles, causing the surface roughness. However, the surface roughness occurs only a few molecular layers (approximately 10nm) of TiO₂ film surface. As observed from the AFM results, the bombardment of plasma particles leads to the formation of micro and nano-dents as well. Thus, formed TiO₂ thin films have shown superior superhydrophilic nature under the antifogging experiments by exposing the film to hot water vapor. In the experiment, plasma exposed superhydrophilic TiO₂ thin film remained clear for several minutes due to the formation of a continuous water film on the surface, whereas a simple glass substrate gets fogged.

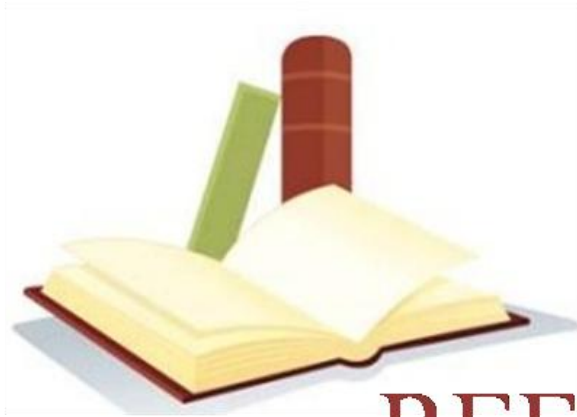
In another set of experiments doped TiO₂ films were prepared using the above-mentioned technique. For structural characterization of these films done by XRD indicated amorphous nature of the films. From the XRD analysis it is concluded that the dopants Fe and Co get incorporated in the TiO₂ structure by replacing Ti ions, and locate at the interstitials site in the lattice. XRD indicated that plasma treatment does not create any change in the crystal structure of Fe and Co doped TiO₂ thin films.

While investigating the optical properties, the doped films after plasma exposure showed enhanced optical properties. We found that the plasma exposure enhances optical absorbance and absorption region, while keeps the films transparent. Also, we found that a moderate doping of Fe and Co avoids the formation of charge recombination centers, and when exposed to air plasma there is a formation of Ti³⁺ and oxygen vacancies in the band gap of TiO₂ films resulting in the variation of optical properties. However, the observed increase in the optical absorption region/red shift (3.22 to 3.00eV) in Fe doped TiO₂ films indicated reduction in the band gap; whereas, on the contrarily, Co doped TiO₂ films exhibited blue shift (3.36 to 3.62eV) and thus a broadening in the band gap due to Burstein Moss shift. The broadening in band gap in the case of Co doped thin films is the formation of relatively larger number of Ti³⁺ levels and oxygen vacancies increases as compared to Fe doped samples. These created levels donate more electrons and thus shift the fermi level into the conduction band, which increases the band gap of

Co doped TiO₂ film. The formed oxygen vacancies by air plasma treatment also lead to the photocatalytic activity of Fe and Co doped thin films.

Future Scope

- ✚ The present study has been carried out for TiO₂ thin film fabricated by sol-gel dip coating method. The work can be further extended using TiO₂ films deposited by RF sputtering and electron beam evaporation.
- ✚ Additional study on the TiO₂ films such as annealing in H₂ or D₂ gas at high temperature can further alter the surface states and thus the film properties.
- ✚ By the study of doping materials into TiO₂ films their electron mobility could be enhanced to make them a suitable candidate as a photo-anode in the solar cells applications.
- ✚ Similar studies can be done for other metal oxide semiconductor thin films.



REFERNCES

References

- [1] Dowling, Ann, et al. "Nanoscience and nanotechnologies: opportunities and uncertainties." *London: The Royal Society & The Royal Academy of Engineering Report* 61 (2004): e64
- [2] Macoubrie, Jane. "Public perceptions about nanotechnology: Risks, benefits and trust." *Journal of Nanoparticle Research* 6.4 (2004): 395-405.
- [3] Currall, Steven C., et al. "What drives public acceptance of nanotechnology?" *Nature Nanotechnology* 1.3 (2006): 153-155.
- [4] Castellini, O. M., et al. "Nanotechnology and the public: Effectively communicating nanoscale science and engineering concepts." *Journal of Nanoparticle Research* 9.2 (2007): 183-189.
- [5] Satterfield, Terre, et al. "Anticipating the perceived risk of nanotechnologies." *Nature nanotechnology* 4.11 (2009): 752-758.
- [6] Heitbaum, Maja, Frank Glorius, and Iris Escher. "Asymmetric heterogeneous catalysis." *Angewandte Chemie International Edition* 45.29 (2006): 4732-4762.
- [7] S.Kaskel, F. Schuth, K. S. W. Sing, J. Weitkamp, *Wiley-VCH: Weinheim*, 2002, **2**, **1190-1249**.
- [8] Kitagawa, Susumu, Ryo Kitaura, and Shin-ichiro Noro. "Functional porous coordination polymers." *Angewandte Chemie International Edition* 43.18 (2004): 2334-2375.
- [9] Sharma, Navneet, et al. "Preparation and catalytic applications of nanomaterials: a review." *RSC Advances* 5.66 (2015): 53381-53403.
- [10] Su, Shao, et al. "Nanomaterials-based sensors for applications in environmental monitoring." *Journal of Materials Chemistry* 22.35 (2012): 18101-18110.
- [11] Fujishima, Akira. "Electrochemical photolysis of water at a semiconductor electrode." *nature* 238 (1972): 37-38.
- [12] Alivisatos, A. Paul. "Perspectives on the physical chemistry of semiconductor nanocrystals." *The Journal of Physical Chemistry* 100.31 (1996): 13226-13239.
- [13] Alivisatos, A. Paul. "Semiconductor clusters, nanocrystals, and quantum dots." *Science* 271.5251 (1996): 933.
- [14] Burda, Clemens, et al. "Chemistry and properties of nanocrystals of different shapes." *Chemical reviews* 105.4 (2005): 1025-1102.

References

- [15] Murray, Christopher B., C. R. Kagan, and M. G. Bawendi. "Synthesis and characterization of monodisperse nanocrystals and close-packed nanocrystal assemblies." *Annual Review of Materials Science* 30.1 (2000): 545-610.
- [16] Chen, Xiaobo, et al. "Doped semiconductor nanomaterials." *Journal of nanoscience and nanotechnology* 5.9 (2005): 1408-1420.
- [17] Wolf, S. A., et al. "Spintronics: a spin-based electronics vision for the future." *Science* 294.5546 (2001): 1488-1495.
- [18] Fernandez-Garcia, M., et al. "Nanostructured oxides in chemistry: characterization and properties." *Chemical Reviews* 104.9 (2004): 4063-4104.
- [19] Hass, D. D., J. F. Groves, and H. N. G. Wadley. "Reactive vapor deposition of metal oxide coatings." *Surface and Coatings Technology* 146 (2001): 85-93.
- [20] Graham, John L., et al. "An investigation of nanostructured vanadia/titania catalysts for the oxidation of monochlorobenzene." *Catalysis today* 88.1 (2003): 73-82.
- [21] Niranjana, R. S., et al. "Nanostructured tin oxide: Synthesis and gas-sensing properties." *Materials chemistry and physics* 92.2 (2005): 384-388.
- [22] Eguchi, K., et al. "Electrical properties of ceria-based oxides and their application to solid oxide fuel cells." *Solid State Ionics* 52.1-3 (1992): 165-172.
- [23] Schiller, S., et al. "Methods and applications of plasmatron high rate sputtering in microelectronics, hybrid microelectronics and electronics." *Thin Solid Films* 92.1-2 (1982): 81-98.
- [24] Lee, Seung-Chul, et al. "Fabrication of tin oxide film by sol-gel method for photovoltaic solar cell system." *Solar energy materials and solar cells* 75.3 (2003): 481-487.
- [25] Di Paola, A., et al. "Photocatalytic degradation of organic compounds in aqueous systems by transition metal doped polycrystalline TiO₂." *Catalysis Today* 75.1 (2002): 87-93.
- [26] Kennedy, Bruce A., ed. *Surface mining*. SME, 1990.
- [27] Brock, Thomas, Michael Groteklaes, and Peter Mischke. *European coatings handbook*. Vincentz Network GmbH & Co KG, 2000.
- [28] Ghosh, T. B., SampaDhabal, and A. K. Datta. "Erratum: On crystalline size dependence of phase stability of nanocrystalline TiO₂." *Journal of Applied Physics* 95.1 (2004): 408-408.

References

- [29] Beltran, A., L. Gracia, and J. Andres. "Density functional theory study of the brookite surfaces and phase transitions between natural titania polymorphs." *The Journal of Physical Chemistry B* 110.46 (2006): 23417-23423.
- [30] Zhang, Qinghong, Lian Gao, and JingkunGuo. "Effects of calcination on the photocatalytic properties of nanosized TiO₂ powders prepared by TiCl₄ hydrolysis." *Applied Catalysis B: Environmental* 26.3 (2000): 207-215.
- [31] Sclafani, A., L. Palmisano, and M. Schiavello. "Influence of the preparation methods of titanium dioxide on the photocatalytic degradation of phenol in aqueous dispersion." *Journal of physical chemistry* 94.2 (1990): 829-832.
- [32] Tanaka, Keiichi, Mario FV Capule, and TeruakiHisanaga. "Effect of crystallinity of TiO₂ on its photocatalytic action." *Chemical Physics Letters* 187.1 (1991): 73-76.
- [33] Photocatalysis, Fundamentals. "Applications, ed. N. Serpone and E. Pelizzetti." (1989).
- [34] Wahlbeck, Phillip G., and Paul W. Gilles. "Reinvestigation of the phase diagram for the system titanium–oxygen." *Journal of the American Ceramic Society* 49.4 (1966): 180-183.
- [35] Hwang, D. K., et al. "Scratch resistant and transparent UV-protective coating on polycarbonate." *Journal of sol-gel science and technology* 26.1-3 (2003): 783-787.
- [36] Kim, Jin-Woong, et al. "Titanium dioxide/poly (methyl methacrylate) composite microspheres prepared by in situ suspension polymerization and their ability to protect against UV rays." *Colloid and Polymer Science* 280.6 (2002): 584-588.
- [37] Mahltig, B., et al. "Optimized UV protecting coatings by combination of organic and inorganic UV absorbers." *Thin Solid Films* 485.1 (2005): 108-114.
- [38] Popov, A. P., et al. "TiO₂ nanoparticles as an effective UV-B radiation skin-protective compound in sunscreens." *Journal of Physics D: Applied Physics* 38.15 (2005): 2564.
- [39] Nakata, Kazuya, and Akira Fujishima. "TiO₂ photocatalysis: design and applications." *Journal of Photochemistry and Photobiology C: Photochemistry Reviews* 13.3 (2012): 169-189.
- [40] Mor, G. K., et al. "A self-cleaning, room-temperature titania-nanotube hydrogen gas sensor." *Sensor Letters* 1.1 (2003): 42-46.
- [41] Mor, Gopal K., et al. "A room-temperature TiO₂-nanotube hydrogen sensor able to self-clean photoactively from environmental contamination." *Journal of Materials Research* 19.02 (2004): 628-634.

References

- [42] Choi, Sung Yeun, et al. "Electrochromic performance of viologen-modified periodic mesoporous nanocrystalline anatase electrodes." *Nano letters* 4.7 (2004): 1231-1235.
- [43] Cummins, David, et al. "Ultrafast electrochromic windows based on redox-chromophore modified nanostructured semiconducting and conducting films." *The Journal of Physical Chemistry B* 104.48 (2000): 11449-11459.
- [44] Bach, Udo, et al. "Nanomaterials-Based Electrochromics for Paper-Quality Displays." *Advanced Materials* 14.11 (2002): 845-848.
- [45] Choi Sung Yeun, et al. "Electrochromic performance of viologen-modified periodic mesoporous nanocrystalline anatase electrodes." *Nano letters* 4.7 (2004): 1231-1235.
- [46] Pichot, François, et al. "Flexible Solid-State Photoelectrochromic Windows." *Journal of the Electrochemical Society* 146.11 (1999): 4324-4326.
- [47] Cahen, David, et al. "Nature of photovoltaic action in dye-sensitized solar cells." *The Journal of Physical Chemistry B* 104.9 (2000): 2053-2059.
- [48] Grätzel, Michael. "Perspectives for dye-sensitized nanocrystalline solar cells." *Progress in photovoltaics: research and applications* 8.1 (2000): 171-185.
- [49] Pichot, François, and Brian A. Gregg. "The photovoltage-determining mechanism in dye-sensitized solar cells." *The Journal of Physical Chemistry B* 104.1 (2000): 6-10.
- [50] Cahen, David, et al. "Nature of photovoltaic action in dye-sensitized solar cells." *The Journal of Physical Chemistry B* 104.9 (2000): 2053-2059.
- [51] Mor, Gopal K., et al. "Enhanced photocleavage of water using titania nanotube arrays." *Nano letters* 5.1 (2005): 191-195.
- [52] Hameed, A., and M. A. Gondal. "Laser induced photocatalytic generation of hydrogen and oxygen over NiO and TiO₂." *Journal of Molecular Catalysis A: Chemical* 219.1 (2004): 109-119.
- [53] Bosc, Florence, et al. "Mesoporous TiO₂-based photocatalysts for UV and visible light gas-phase toluene degradation." *Thin Solid Films* 495.1 (2006): 272-279.
- [54] Nguyen, Vi Nu Hoai, DoniaBeydoun, and Rose Amal. "Photocatalytic reduction of selenite and selenate using TiO₂ photocatalyst." *Journal of Photochemistry and Photobiology A: Chemistry* 171.2 (2005): 113-120.

References

- [55] Yang, Juan, et al. "Mechanism of TiO₂-assisted photocatalytic degradation of dyes under visible irradiation: photoelectrocatalytic study by TiO₂-film electrodes." *The Journal of Physical Chemistry B* 109.46 (2005): 21900-21907.
- [56] Kikuchi, Yoshihiko, et al. "Photocatalytic bactericidal effect of TiO₂ thin films: dynamic view of the active oxygen species responsible for the effect." *Journal of Photochemistry and Photobiology A: chemistry* 106.1 (1997): 51-56.
- [57] Cai, Ruxiong, et al. "Increment of Photocatalytic Killing of Cancer Cells Using TiO₂ with the Aid of Superoxide Dismutase." *Chemistry Letters* 3 (1992): 427-430.
- [58] Gu, Zhong-Ze, Akira Fujishima, and Osamu Sato. "Patterning of a colloidal crystal film on a modified hydrophilic and hydrophobic surface." *Angewandte Chemie* 114.12 (2002): 2171-2174.
- [59] Feng, Xinjian, JinZhai, and Lei Jiang. "The fabrication and switchable superhydrophobicity of TiO₂nanorod films." *Angewandte Chemie International Edition* 44.32 (2005): 5115-5118.
- [60] Gao, Lichao, and Thomas J. McCarthy. "The "lotus effect" explained: two reasons why two length scales of topography are important." *Langmuir* 22.7 (2006): 2966-2967.
- [61] Yaminsky, V. V. "Molecular mechanisms of hydrophobic transitions." *Journal of adhesion science and technology* 14.2 (2000): 187-233.
- [62] Gao, Lichao, and Thomas J. McCarthy. "How Wenzel and Cassie were wrong." *Langmuir* 23.7 (2007): 3762-3765.
- [63] Cassie, A. B. D. "Contact angles." *Discussions of the Faraday Society* 3 (1948): 11-16.
- [64] Wenzel, Robert N. "Resistance of solid surfaces to wetting by water." *Industrial & Engineering Chemistry* 28.8 (1936): 988-994.
- [65] Marmur, Abraham. "Wetting on hydrophobic rough surfaces: to be heterogeneous or not to be?" *Langmuir* 19.20 (2003): 8343-8348.
- [66] Bico, José, Uwe Thiele, and David Quéré. "Wetting of textured surfaces." *Colloids and Surfaces A: Physicochemical and Engineering Aspects* 206.1 (2002): 41-46.
- [67] Chu, Paul K., et al. "Plasma-surface modification of biomaterials." *Materials Science and Engineering: R: Reports* 36.5 (2002): 143-206.
- [68] Ratner, Buddy D. "Surface modification of polymers: chemical, biological and surface analytical challenges." *Biosensors and Bioelectronics* 10.9 (1995): 797-804.

References

- [69] Kim, Soonhyun, Seong-Ju Hwang, and Wonyong Choi. "Visible light active platinum-ion-doped TiO₂ photocatalyst." *The Journal of Physical Chemistry B* 109.51 (2005): 24260-24267.
- [70] Liu, Rui, et al. "UV- and visible-light photocatalytic activity of simultaneously deposited and doped Ag/Ag (I)-TiO₂ photocatalyst." *The Journal of Physical Chemistry C* 116.33 (2012): 17721-17728.
- [71] Yogi, Chihiro, et al. "Size effect of Au nanoparticles on TiO₂ crystalline phase of nanocomposite thin films and their photocatalytic properties." *The Journal of Physical Chemistry C* 115.14 (2011): 6554-6560.
- [72]. Zhu, Hong, Jie Tao, and Xiang Dong. "Preparation and photoelectrochemical activity of Cr-doped TiO₂ nanorods with nanocavities." *The Journal of Physical Chemistry C* 114.7 (2010): 2873-2879.
- [73] Zhang, Jinzhong, et al. "Synthesis, surface morphology, and photoluminescence properties of anatase iron-doped titanium dioxide nano-crystalline films." *Physical Chemistry Chemical Physics* 13.28 (2011): 13096-13105.
- [74] Zhang, Hongye, et al. "Preparation and characterization of room temperature ferromagnetic Co-doped anatase TiO₂ nanobelts." *The Journal of Physical Chemistry C* 112.23 (2008): 8604-8608.
- [75] Sathasivam, Sanjayan, et al. "Tungsten Doped TiO₂ with Enhanced Photocatalytic and Optoelectrical Properties via Aerosol Assisted Chemical Vapor Deposition." *Scientific reports* 5 (2015).
- [76] Zuas, Oman, and Harry Budiman. "Synthesis of nanostructured copper-doped titania and its properties." *Nano-Micro Letters* 5.1 (2013): 26-33.
- [77]. Sene, Jeosadaque J., Walter A. Zeltner, and Marc A. Anderson. "Fundamental photoelectrocatalytic and electrophoretic mobility studies of TiO₂ and V-doped TiO₂ thin-film electrode materials." *The Journal of Physical Chemistry B* 107.7 (2003): 1597-1603.
- [78] Mills, Andrew, et al. "Photocatalytic oxidation of deposited sulfur and gaseous sulfur dioxide by TiO₂ films." *The Journal of Physical Chemistry C* 111.14 (2007): 5520-5525.
- [79] Sotelo-Vazquez, Carlos, et al. "Multifunctional P-doped TiO₂ films: a new approach to self-cleaning, transparent conducting oxide materials." *Chemistry of Materials* 27.9 (2015): 3234-3242.

References

- [80] Yu, Jimmy C., et al. "Effects of F-doping on the photocatalytic activity and microstructures of nanocrystalline TiO₂ powders." *Chemistry of Materials* 14.9 (2002): 3808-3816.
- [81] Sathish, M., et al. "Synthesis, characterization, electronic structure, and photocatalytic activity of nitrogen-doped TiO₂ nanocatalyst." *Chemistry of materials* 17.25 (2005): 6349-6353.
- [82] Ren, Wenjie, et al. "Low temperature preparation and visible light photocatalytic activity of mesoporous carbon-doped crystalline TiO₂." *Applied Catalysis B: Environmental* 69.3 (2007): 138-144.
- [83] Hoffmann, Michael R., et al. "Environmental applications of semiconductor photocatalysis." *Chemical reviews* 95.1 (1995): 69-96.
- [84] Choi, Wonyong, Andreas Termin, and Michael R. Hoffmann. "The role of metal ion dopants in quantum-sized TiO₂: correlation between photoreactivity and charge carrier recombination dynamics." *The Journal of Physical Chemistry* 98.51 (1994): 13669-13679.
- [85] Wu, Jeffrey C-S., and Chih-Hsien Chen. "A visible-light response vanadium-doped titaniananocatalyst by sol-gel method." *Journal of Photochemistry and Photobiology A: Chemistry* 163.3 (2004): 509-515.
- [86] Ali, A., et al. "Interplay of Vanadium States and Oxygen Vacancies in the Structural and Optical Properties of TiO₂: V Thin Films." *The Journal of Physical Chemistry C* 117.38 (2013): 19517-19524.
- [87].Sathasivam, Sanjayan, et al. "Tungsten Doped TiO₂ with Enhanced Photocatalytic and Optoelectrical Properties via Aerosol Assisted Chemical Vapor Deposition." *Scientific reports* 5 (2015).
- [88] Xin, Baifu, et al. "Effect of surface species on Cu-TiO₂ photocatalytic activity." *Applied surface science* 254.9 (2008): 2569-2574.
- [89] Tian, Jianjun, et al. "Effects of Co doping on structure and optical properties of TiO₂ thin films prepared by sol-gel method." *Thin Solid Films* 520.16 (2012): 5179-5183.
- [90] Peng, Yan-Hua, Gui-Fang Huang, and Wei-Qing Huang. "Visible-light absorption and photocatalytic activity of Cr-doped TiO₂ nanocrystal films." *Advanced Powder Technology* 23.1 (2012): 8-12.
- [91] Kato, Hideki, and Akihiko Kudo. "Visible-light-response and photocatalytic activities of TiO₂ and SrTiO₃ photocatalysts codoped with antimony and chromium." *The Journal of Physical Chemistry B* 106.19 (2002): 5029-5034.

References

- [92] Herrmann, Jean-Marie, Jean Disdier, and Pierre Pichat. "Effect of chromium doping on the electrical and catalytic properties of powder titania under UV and visible illumination." *Chemical Physics Letters* 108.6 (1984): 618-622.
- [93] Diwald, Oliver, et al. "Photochemical activity of nitrogen-doped rutile TiO₂ (110) in visible light." *The journal of physical chemistry B* 108.19 (2004): 6004-6008.
- [94] Sato, Shinri. "Photocatalytic activity of NO_x-doped TiO₂ in the visible light region." *Chemical Physics Letters* 123.1 (1986): 126-128.
- [95] Asahi, R. Y. O. J. I., et al. "Visible-light photocatalysis in nitrogen-doped titanium oxides." *science* 293.5528 (2001): 269-271.
- [96] Hattori, Akihiko, et al. "Photoreactivity of sol-gel TiO₂ films formed on soda-lime glass substrates: effect of SiO₂ underlayer containing fluorine." *Langmuir* 15.16 (1999): 5422-5425.
- [97] Sotelo-Vazquez, Carlos, et al. "Multifunctional P-doped TiO₂ films: a new approach to self-cleaning, transparent conducting oxide materials." *Chemistry of Materials* 27.9 (2015): 3234-3242.
- [98] Ren, Wenjie, et al. "Low temperature preparation and visible light photocatalytic activity of mesoporous carbon-doped crystalline TiO₂." *Applied Catalysis B: Environmental* 69.3 (2007): 138-144.
- [99] Park, Chang-Sun, Uzma KH Bangi, and Hyung-Ho Park. "Effect of sulfur dopants on the porous structure and electrical properties of mesoporous TiO₂ thin films." *Materials Letters* 106 (2013): 401-404.
- [100] Chen, Xiaobo, et al. "Properties of disorder-engineered black titanium dioxide nanoparticles through hydrogenation." *Scientific reports* 3 (2013).
- [101] Lu, Haiqiang, et al. "Safe and facile hydrogenation of commercial Degussa P25 at room temperature with enhanced photocatalytic activity." *RSC Advances* 4.3 (2014): 1128-1132.
- [102] Sasinska, Alexander, et al. "Enhanced photocatalytic performance in atomic layer deposition grown TiO₂ thin films via hydrogen plasma treatment." *Journal of Vacuum Science & Technology A* 33.1 (2015): 01A152.
- [103] Chae, Y. K., S. Mori, and M. Suzuki. "Visible-light photocatalytic activity of anatase TiO₂ treated with argon plasma." *Thin Solid Films* 517.14 (2009): 4260-4263.

References

- [104] Huang, Chao-Ming, et al. "Effect of nitrogen-plasma surface treatment to the enhancement of TiO₂ photocatalytic activity under visible light irradiation." *Journal of Molecular Catalysis A: Chemical* 261.2 (2007): 218-224.
- [105] Kim, HyungJin, Jumi Kim, and Byungyou Hong. "Effect of hydrogen plasma treatment on nano-structured TiO₂ films for the enhanced performance of dye-sensitized solar cell." *Applied Surface Science* 274 (2013): 171-175.
- [106] Han, Jun-Bo, et al. "Effect of plasma treatment on hydrophilic properties of TiO₂ thin films." *Surface and coatings technology* 200.16 (2006): 4876-4878.
- [107] Mirshekari, M., R. Azimirad, and A. Z. Moshfegh. "Superhydrophilic stability enhancement of RF co-sputtered Ti_xSi_{1-x}O₂ thin films in dark." *Applied Surface Science* 256.8 (2010): 2500-2506.
- [108] Jung, Chung-Kyung, et al. "Plasma surface modification of TiO₂ photocatalysts for improvement of catalytic efficiency." *Surface and coatings Technology* 200.5 (2005): 1320-1324.
- [109] Han, Jun-Bo, et al. "Effect of plasma treatment on hydrophilic properties of TiO₂ thin films." *Surface and coatings technology* 200.16 (2006): 4876-4878.
- [110] Yang, Wenli, and Colin A. Wolden. "Plasma-enhanced chemical vapor deposition of TiO₂ thin films for dielectric applications." *Thin Solid Films* 515.4 (2006): 1708-1713.
- [111] Kolouch, Aleš, et al. "Photocatalytic TiO₂ thin Film Prepared by PE CVD at low Temperature." *Plasma Processes and Polymers* 4.S1 (2007): S350-S355.
- [112] Iancu, Andrei T., et al. "Atomic Layer Deposition of Undoped TiO₂ Exhibiting p-Type Conductivity." *ACS applied materials & interfaces* 7.9 (2015): 5134-5140.
- [113] Nam, Sang Hun, Jae-Sung Hyun, and Jin-Hyo Boo. "Synthesis of TiO₂ thin films using single molecular precursors by MOCVD method for dye-sensitized solar cells application and study on film growth mechanism." *Materials Research Bulletin* 47.10 (2012): 2717-2721.
- [114] Dongale, T. D., et al. "Nanostructured TiO₂ thin film memristor using hydrothermal process." *Journal of Alloys and Compounds* 593 (2014): 267-270.
- [115] György, E., et al. "Anatase phase TiO₂ thin films obtained by pulsed laser deposition for gas sensing applications." *Applied Surface Science* 247.1 (2005): 429-433.
- [116] Karki, Kishor, K. I. Gnanasekar, and B. Rambabu. "NANOSTRUCTURED SEMICONDUCTOR OXIDE POWDERS AND THIN FILMS FOR GAS SENSORS." 195.

References

- [117] Zhao, Lei, Qing Jiang, and JiansheLian. "Visible-light photocatalytic activity of nitrogen-doped TiO₂ thin film prepared by pulsed laser deposition." *Applied Surface Science* 254.15 (2008): 4620-4625.
- [118] Calloni, A., et al. "Growth of stoichiometric TiO₂ thin films on Au (100) substrates by molecular beam epitaxy." *Thin Solid Films* 520.11 (2012): 3922-3926.
- [119] Lyandres, Olga, et al. "Preferred orientation in sputtered TiO₂ thin films and its effect on the photo-oxidation of acetaldehyde." *Chemistry of Materials* 24.17 (2012): 3355-3362.
- [120] Wang, Yang, et al. "Influence of Solution Chemistry on the Dielectric Properties of TiO₂ Thin-Film Porous Electrodes." *The Journal of Physical Chemistry C* 120.38 (2016): 21543-21551.
- [121] Hashizume, Mineo, and ToyokiKunitake. "Preparation of self-supporting ultrathin films of titania by spin coating." *Langmuir* 19.24 (2003): 10172-10178.
- [122] Jumali, Mohammad Hafizuddin Haji, et al. "Comparative studies on microstructural and gas sensing performance of TiO₂ and TiO₂-PANi nanocomposite thin films." *Sol SciTechnol* 17 (2009): 126-131.
- [123] Verma, Amita, M. Kar, and D. P. Singh. "Aging effect of diethanolamine derived precursor sol on TiO₂ films deposited at different annealing temperatures." *Journal of sol-gel science and technology* 54.2 (2010): 129-138.
- [124] Shahini, Sharif, MasoudAskari, and S. K. Sadrnezhaad. "Gel-sol synthesis and aging effect on highly crystalline anatase nanopowder." *Bulletin of Materials Science* 34.6 (2011): 1189-1195.
- [125] Bharti, Bandna, Santosh Kumar, and Rajesh Kumar. "Superhydrophilic TiO₂ thin film by nanometer scale surface roughness and dangling bonds." *Applied Surface Science* 364 (2016): 51-60.
- [126] Siow, Kim Shyong, et al. "Plasma Methods for the Generation of Chemically Reactive Surfaces for Biomolecule Immobilization and Cell Colonization-A Review." *Plasma processes and polymers* 3.6-7 (2006): 392-418.
- [127] Liston, E. M., L. Martinu, and M. R. Wertheimer. "Plasma surface modification of polymers for improved adhesion: a critical review." *Journal of adhesion science and technology* 7.10 (1993): 1091-1127.

References

- [128] Burkstrand, James M. "Electron spectroscopic study of oxygen-plasma-treated polymer surfaces." *Journal of Vacuum Science and Technology* 15.2 (1978): 223-226.
- [129] Yasuda H, Marsh H C, Brandt S and Reilley C N, *J PolymSciPolymChemedn*, 15 (1977) 991.
- [130] Hsieh, You Lo, and Elizabeth Y. Chen. "Improvement of hydrophilicity of poly (ethylene terephthalate) by non-polymer-forming gaseous glow discharge." *Industrial & Engineering Chemistry Product Research and Development* 24.2 (1985): 246-252.
- [131] Pandiyaraj, K. Navaneetha, et al. "Modification of surface properties of polypropylene (PP) film using DC glow discharge air plasma." *Applied Surface Science* 255.7 (2009): 3965-3971.
- [132] Deshmukh, Rajendra R., and Narendra V. Bhat. "The mechanism of adhesion and printability of plasma processed PET films." *Materials Research Innovations* 7.5 (2003): 283-290.
- [133] Standard CPDS X-ray diffraction spectra database.
- [134] Magonov, S. N. "M.-H, Whangbo, Surface Analysis with STM and AFM." (1996).
- [135] Microscopy, Noncontact Atomic Force. "S. Morita, R. Wiesendanger, and E. Meyer." (2002).
- [136] Masuda, Yoshitake, and Kazumi Kato. "Anatase TiO₂ films crystallized on SnO₂: F substrates in an aqueous solution." *Thin Solid Films* 516.9 (2008): 2547-2552.
- [137] Chiba, Yasuo, et al. "Dye-sensitized solar cells with conversion efficiency of 11.1%." *Japanese Journal of Applied Physics* 45.7L (2006): L638.
- [138] Liu, Bin, and Eray S. Aydil. "Growth of oriented single-crystalline rutile TiO₂ nanorods on transparent conducting substrates for dye-sensitized solar cells." *Journal of the American Chemical Society* 131.11 (2009): 3985-3990.
- [139] Hanaor, Dorian AH, and Charles C. Sorrell. "Review of the anatase to rutile phase transformation." *Journal of Materials science* 46.4 (2011): 855-874.
- [140] Wan, Lin, et al. "Phase selection and visible light photo-catalytic activity of Fe-doped TiO₂ prepared by the hydrothermal method." *Materials Research Bulletin* 46.3 (2011): 442-446.
- [141] Savage, Nancy, et al. "Composite n-p semiconducting titanium oxides as gas sensors." *Sensors and Actuators B: Chemical* 79.1 (2001): 17-27.

References

- [142] Seo, Min-Hyun, et al. "Gas sensing characteristics and porosity control of nanostructured films composed of TiO₂ nanotubes." *Sensors and Actuators B: Chemical* 137.2 (2009): 513-520.
- [143] Gan, Wee Yong, et al. "Novel TiO₂ thin film with non-UV activated superwetting and antifogging behaviours." *Journal of Materials Chemistry* 17.10 (2007): 952-954.
- [144] Le, Duy Dam, et al. "The fabrication of visible light responsive Ag-SiO₂ co-doped TiO₂ thin films by the sol-gel method." *Advances in natural sciences: nanoscience and nanotechnology* 1.1 (2010): 015007.
- [145] Huang, Weixin, et al. "Effect of polyethylene glycol on hydrophilic TiO₂ films: porosity-driven superhydrophilicity." *Surface and Coatings Technology* 204.24 (2010): 3954-3961.
- [146] Wang, S., et al. "Superhydrophilic Cu-doped TiO₂ thin film for solar-driven photocatalysis." *Ceramics International* 40.4 (2014): 5107-5110.
- [147] Feng, Xinjian, et al. "Reversible super-hydrophobicity to super-hydrophilicity transition of aligned ZnO nanorod films." *Journal of the American Chemical Society* 126.1 (2004): 62-63.
- [148] Wang, Rong, et al. "Studies of surface wettability conversion on TiO₂ single-crystal surfaces." *The Journal of Physical Chemistry B* 103.12 (1999): 2188-2194.
- [149] Nakamura, Masatoshi, et al. "Study on hydrophilic property of hydro-oxygenated amorphous TiO_x: OH thin films." *Surface science* 507 (2002): 778-782.
- [150] Hugenschmidt, Markus B., Lara Gamble, and Charles T. Campbell. "The interaction of H₂O with a TiO₂ (110) surface." *Surface Science* 302.3 (1994): 329-340.
- [151] Bormashenko, Edward Yu. *Wetting of real surfaces*. Vol. 19. Walter de Gruyter, 2013.
- [152] Chan, C-M., T-M. Ko, and H. Hiraoka. "Polymer surface modification by plasmas and photons." *Surface science reports* 24.1 (1996): 1-54.
- [153] Ozdemir, Murat, Caner U. Yurteri, and Hasan Sadikoglu. "Physical polymer surface modification methods and applications in food packaging polymers." *Critical reviews in food science and nutrition* 39.5 (1999): 457-477.
- [154] Siow, Kim Shyong, et al. "Plasma Methods for the Generation of Chemically Reactive Surfaces for Biomolecule Immobilization and Cell Colonization-A Review." *Plasma processes and polymers* 3.6-7 (2006): 392-418.
- [155] Liston, E. M., L. Martinu, and M. R. Wertheimer. "Plasma surface modification of polymers for improved adhesion: a critical review." *Journal of adhesion science and technology* 7.10 (1993): 1091-1127.

References

- [156] Kim, Y. S., et al. "Surface modification of porous nanocrystalline TiO₂ films for dye-sensitized solar cell application by various gas plasmas." *J. Vac. Sci. Technol. A* 25.4 (2007).
- [157] Szabová, Renáta, et al. "Coating of TiO₂ nanoparticles on the plasma activated polypropylene fibers." *Acta Chimica Slovaca* 2.1 (2009): 70-76.
- [158] Verma, Amita, M. Kar, and D. P. Singh. "Aging effect of diethanolamine derived precursor sol on TiO₂ films deposited at different annealing temperatures." *Journal of sol-gel science and technology* 54.2 (2010): 129-138.
- [159] Shahini, Sharif, Masoud Askari, and S. K. Sadrnezhad. "Gel-sol synthesis and aging effect on highly crystalline anatase nanopowder." *Bulletin of Materials Science* 34.6 (2011): 1189-1195.
- [160] Kumar, Rajesh, et al. "Effect of DC glow discharge treatment on the surface energy and surface resistivity of thin film of polypropylene." *Journal of applied polymer science* 104.2 (2007): 767-772.
- [161] Pandiyaraj, K. Navaneetha, et al. "Modification of surface properties of polypropylene (PP) film using DC glow discharge air plasma." *Applied Surface Science* 255.7 (2009): 3965-3971.
- [162] Deshmukh, Rajendra R., and Narendra V. Bhat. "The mechanism of adhesion and printability of plasma processed PET films." *Materials Research Innovations* 7.5 (2003): 283-290.
- [163] Dhayal, Marshal, et al. "Surface chemistry and optical property of TiO₂ thin films treated by low-pressure plasma." *Journal of Solid State Chemistry* 180.10 (2007): 2696-2701.
- [164] Gongadze, Ekaterina, et al. "Adhesion of osteoblasts to a vertically aligned TiO₂ nanotube surface." *Mini reviews in medicinal chemistry* 13.2 (2013): 194-200.
- [165] Podhorodecki, A., et al. "Influence of annealing on europium photoexcitation doped into nanocrystalline titania film prepared by magnetron sputtering." *Journal of the Electrochemical Society* 156.3 (2009): H214-H219.
- [166] Fridman, Alexander. *Plasma chemistry*. Cambridge university press, 2008.
- [167] Konstantakou, Maria, et al. "Influence of fluorine plasma treatment of TiO₂ films on the behavior of dye solar cells employing the Co (II)/(III) redox couple." *The Journal of Physical Chemistry C* 118.30 (2014): 16760-16775.

References

- [168] Oktem, T., et al. "Improvement in surface-related properties of poly (ethylene terephthalate)/cotton fabrics by glow-discharge treatment." *Indian Journal of Fibre and Textile Research* 27.2 (2002): 161-165.
- [169] Bhat, N. V., and D. J. Upadhyay. "Plasma-induced surface modification and adhesion enhancement of polypropylene surface." *Journal of Applied Polymer Science* 86.4 (2002): 925-936.
- [170] Yamasaki, Satoshi, Ujjwal K. Das, and Kenji Ishikawa. "Direct observation of surface dangling bonds during plasma process: chemical reactions during H₂ and Ar plasma treatments." *Thin solid films* 407.1 (2002): 139-143.
- [171] Sanchis, M. R., et al. "Surface modification of low density polyethylene (LDPE) film by low pressure O₂ plasma treatment." *European polymer journal* 42.7 (2006): 1558-1568.
- [172] Goldstein, A. N., C. M. Echer, and A. P. Alivisatos. "Melting in semiconductor nanocrystals." *Science* 256.5062 (1992): 1425-1427.
- [173] Borrás, Ana, and Agustín R. González-Elipe. "Wetting properties of polycrystalline TiO₂ surfaces: A scaling approach to the roughness factors." *Langmuir* 26.20 (2010): 15875-15882.
- [174] Wang, Rong, et al. "Light-induced amphiphilic surfaces." *Nature* 388 (1997): 431-432.
- [175] Galuska, A. A., et al. "Ion mixing of Ti and TiO_y films on SiO_x." *Journal of Vacuum Science & Technology A* 6.4 (1988): 2403-2409.
- [176] Xu, Nuo, et al. "Characteristics and mechanism of conduction/set process in TiN/ZnO/Pt resistance switching random-access memories." *Applied Physics Letters* 92.23 (2008): 232112.
- [177] Hsieh, P-T., et al. "Luminescence mechanism of ZnO thin film investigated by XPS measurement." *Applied Physics A* 90.2 (2008): 317-321.
- [178] Massaro, C., et al. "Comparative investigation of the surface properties of commercial titanium dental implants. Part I: chemical composition." *Journal of Materials Science: Materials in Medicine* 13.6 (2002): 535-548.
- [179] Miyauchi, Masahiro, et al. "Photocatalysis and photoinduced hydrophilicity of various metal oxide thin films." *Chemistry of Materials* 14.6 (2002): 2812-2816.
- [180] Cebeci, Fevzi Ç., et al. "Nanoporosity-driven superhydrophilicity: a means to create multifunctional antifogging coatings." *Langmuir* 22.6 (2006): 2856-2862.
- [181] Hamal, Dambar B., et al. "A multifunctional biocide/sporicide and photocatalyst based on titanium dioxide (TiO₂) codoped with silver, carbon, and sulfur." *Langmuir* 26.4 (2009): 2805-2810.

References

- [182]O'regan, Brian, and M. Grfitzeli. "A low-cost, high-efficiency solar cell based on dye-sensitized." *nature* 353.6346 (1991): 737-740.
- [183]Zhou, Minghua, Jiaguo Yu, and Bei Cheng. "Effects of Fe-doping on the photocatalytic activity of mesoporous TiO₂ powders prepared by an ultrasonic method." *Journal of Hazardous Materials* 137.3 (2006): 1838-1847.
- [184]Lin, Yongjing, et al. "TiO₂/TiSi₂ heterostructures for high-efficiency photoelectrochemical H₂O splitting." *Journal of the American Chemical Society* 131.8 (2009): 2772-2773.
- [185]Sauvage, Frédéric, et al. "Dye-sensitized solar cells employing a single film of mesoporous TiO₂ beads achieve power conversion efficiencies over 10%." *Acs Nano* 4.8 (2010): 4420-4425.
- [186]Zhang, Yanyan, et al. "Synthesis and characterization of TiO₂ nanotubes for humidity sensing." *Applied Surface Science* 254.17 (2008): 5545-5547.
- [187]Lee, Kyu-Sung, et al. "Transparent conductive electrodes of mixed TiO_{2-x}-indium tin oxide for organic photovoltaics." *Applied Physics Letters* 100.21 (2012): 213302.
- [188]Rabaste, S., et al. "Sol-gel fabrication of thick multilayers applied to Bragg reflectors and microcavities." *Thin Solid Films* 416.1 (2002): 242-247.
- [189]Liao, Yulong, et al. "New Mechanistic Insight of Low Temperature Crystallization of Anodic TiO₂ Nanotube Array in Water." *Crystal Growth & Design* 16.4 (2016): 1786-1791.
- [190]Gültekin, Aytaç. "Effect of Au Nanoparticles Doping on The Properties of TiO₂ Thin Films." *Materials Science* 20.1 (2014): 10-14.
- [191]Shin, Ji-Yong, et al. "Oxygen-deficient TiO_{2-δ} nanoparticles via hydrogen reduction for high rate capability lithium batteries." *Chemistry of Materials* 24.3 (2012): 543-551.
- [192]Peng, Bo, et al. "General synthesis and optical properties of monodisperse multifunctional metal-ion-doped TiO₂ hollow particles." *The Journal of Physical Chemistry C* 113.47 (2009): 20240-20245.
- [193]Asahi, R. Y. O. J. I., et al. "Visible-light photocatalysis in nitrogen-doped titanium oxides." *science* 293.5528 (2001): 269-271.
- [194]Kurtoglu, Murat E., et al. "Strong coupling of Cr and N in Cr-N-doped TiO₂ and its effect on photocatalytic activity." *The Journal of Physical Chemistry C* 115.35 (2011): 17392-17399.
- [195] Amano, Fumiaki, et al. "Effect of Ti³⁺ Ions and Conduction Band Electrons on Photocatalytic and Photoelectrochemical Activity of Rutile Titania for Water Oxidation." *The Journal of Physical Chemistry C* 120.12 (2016): 6467-6474.

References

- [196] Chen, C. S. *et al.* Effect of Ti^{3+} on TiO_2 -supported Cu catalysts used for CO oxidation. *Langmuir* **28**, 9996–10006 (2012).
- [197] Liu, Hong, et al. "The enhancement of TiO_2 photocatalytic activity by hydrogen thermal treatment." *Chemosphere* 50.1 (2003): 39-46.
- [198] Nakamura, Isao, Shinichi Sugihara, and Koji Takeuchi. "Mechanism for NO Photooxidation over the Oxygen-Deficient TiO_2 Powder under Visible Light Irradiation." *Chemistry Letters* 11 (2000): 1276-1277.
- [199] Zhang, Zhi-Kun, et al. "Plasma-electrolysis synthesis of TiO_2 nano/microspheres with optical absorption extended into the infra-red region." *Chemical Communications* 47.29 (2011): 8439-8441.
- [200] Jing, Dengwei, Yaojun Zhang, and Liejin Guo. "Study on the synthesis of Ni doped mesoporous TiO_2 and its photocatalytic activity for hydrogen evolution in aqueous methanol solution." *Chemical Physics Letters* 415.1 (2005): 74-78.
- [201] Gracia, F., et al. "Structural, Optical, and Photoelectrochemical Properties of M^{n+} - TiO_2 Model Thin Film Photocatalysts." *The Journal of Physical Chemistry B* 108.45 (2004): 17466-17476.
- [202] Zhu, Jiefang, et al. "Hydrothermal doping method for preparation of Cr^{3+} - TiO_2 photocatalysts with concentration gradient distribution of Cr^{3+} ." *Applied Catalysis B: Environmental* 62.3 (2006): 329-335.
- [203] Colon, G., et al. "Cu-doped TiO_2 systems with improved photocatalytic activity." *Applied Catalysis B: Environmental* 67.1 (2006): 41-51.
- [204] Yang, Kesong, Ying Dai, and Baibiao Huang. "Understanding photocatalytic activity of S- and P-doped TiO_2 under visible light from first-principles." *The Journal of Physical Chemistry C* 111.51 (2007): 18985-18994.
- [205] Ren, Wenjie, et al. "Low temperature preparation and visible light photocatalytic activity of mesoporous carbon-doped crystalline TiO_2 ." *Applied Catalysis B: Environmental* 69.3 (2007): 138-144.
- [206] Yu, Jimmy C., et al. "Effects of F-doping on the photocatalytic activity and microstructures of nanocrystalline TiO_2 powders." *Chemistry of Materials* 14.9 (2002): 3808-3816.
- [207] Sato, Shinri, Ryuhei Nakamura, and Shinji Abe. "Visible-light sensitization of TiO_2 photocatalysts by wet-method N doping." *Applied Catalysis A: General* 284.1 (2005): 131-137.

References

- [208]Xing, Mingyang, et al. "An economic method to prepare vacuum activated photocatalysts with high photo-activities and photosensitivities." *Chemical Communications* 47.17 (2011): 4947-4949.
- [209]Pan, Xiaoyang, et al. "Defective TiO₂ with oxygen vacancies: synthesis, properties and photocatalytic applications." *Nanoscale* 5.9 (2013): 3601-3614.
- [210]Pan, Xiaoyang, Min-Quan Yang, and Yi-Jun Xu. "Morphology control, defect engineering and photoactivity tuning of ZnO crystals by graphene oxide—a unique 2D macromolecular surfactant." *Physical Chemistry Chemical Physics* 16.12 (2014): 5589-5599.
- [211]Zhang, Nan, et al. "Waltzing with the versatile platform of graphene to synthesize composite photocatalysts." *Chemical reviews* 115.18 (2015): 10307-10377.
- [212] Liu, Yumeng, et al. "Self-modification of TiO₂ one-dimensional nano-materials by Ti³⁺ and oxygen vacancy using Ti₂O₃ as precursor." *RSC Advances* 5.76 (2015): 61657-61663.
- [213] Lu, Xihong, et al. "Hydrogenated TiO₂ nanotube arrays for supercapacitors." *Nano letters* 12.3 (2012): 1690-1696.
- [214]Konstantakou, Maria, et al. "Influence of fluorine plasma treatment of TiO₂ films on the behavior of dye solar cells employing the Co (II)/(III) redox couple." *The Journal of Physical Chemistry C* 118.30 (2014): 16760-16775.
- [215] Lu, Haiqiang, et al. "Safe and facile hydrogenation of commercial Degussa P25 at room temperature with enhanced photocatalytic activity." *RSC Advances* 4.3 (2014): 1128-1132.
- [216] Zheng, Zhaoke, et al. "Hydrogenated titania: synergy of surface modification and morphology improvement for enhanced photocatalytic activity." *Chemical Communications* 48.46 (2012): 5733-5735.
- [217]Heo, Cheol Ho, Soon-Bo Lee, and Jin-Hyo Boo. "Deposition of TiO₂ thin films using RF magnetron sputtering method and study of their surface characteristics." *Thin Solid Films* 475.1 (2005): 183-188.
- [218]Li, Yanan, and Ben W-L. Jang. "Investigation of calcination and O₂ plasma treatment effects on TiO₂-supported palladium catalysts." *Industrial & Engineering Chemistry Research* 49.18 (2010): 8433-8438.
- [219]Yamada, Kenji, et al. "Photocatalytic activity of TiO₂ thin films doped with nitrogen using a cathodic magnetron plasma treatment." *Thin Solid Films* 516.21 (2008): 7560-7564.

References

- [220] Cong, Ye, et al. "Preparation, photocatalytic activity, and mechanism of nano-TiO₂ co-doped with nitrogen and iron (III)." *The Journal of Physical Chemistry C* 111.28 (2007): 10618-10623.
- [221] Li, Shuang, et al. "Comparison of amorphous, pseudo-hexagonal and orthorhombic Nb₂O₅ for high-rate lithium ion insertion." *CrystEngComm* 18.14 (2016): 2532-2540.
- [222] Bhachu, Davinder S., et al. "Solution Processing Route to Multifunctional Titania Thin Films: Highly Conductive and Photocatalytically Active Nb: TiO₂." *Advanced Functional Materials* 24.32 (2014): 5075-5085.
- [223] White, C. W., et al. "Ion Implantation and Annealing of Crystalline Oxides." *MRS Proceedings*. Vol. 60. Cambridge University Press, 1985.
- [224] Sathish, M., et al. "Synthesis, characterization, electronic structure, and photocatalytic activity of nitrogen-doped TiO₂ nanocatalyst." *Chemistry of materials* 17.25 (2005): 6349-6353.
- [225] George, Saji, et al. "Role of Fe doping in tuning the band gap of TiO₂ for the photo-oxidation-induced cytotoxicity paradigm." *Journal of the American Chemical Society* 133.29 (2011): 11270-11278.
- [226] Shwetharani, R., C. A. N. Fernando, and Geetha R. Balakrishna. "Excellent hydrogen evolution by a multi approach via structure–property tailoring of titania." *RSC Advances* 5.49 (2015): 39122-39130.
- [227] Moser, Jacques, Michael Grätzel, and Roland Gally. "Inhibition of Electron-Hole Recombination in Substitutionally Doped Colloidal Semiconductor Crystallites." *Helvetica chimica acta* 70.6 (1987): 1596-1604.
- [228] Umebayashi, Tsutomu, et al. "Analysis of electronic structures of 3d transition metal-doped TiO₂ based on band calculations." *Journal of Physics and Chemistry of Solids* 63.10 (2002): 1909-1920.
- [229] Yang, J. Y., et al. "Grain size dependence of electrical and optical properties in Nb-doped anatase TiO₂." *applied physics letters* 95.21 (2009): 3105.
- [230] Sanjines, R., et al. "Electronic structure of anatase TiO₂ oxide." *Journal of Applied Physics* 75.6 (1994): 2945-2951.
- [231] Bertoti, I., et al. "Surface characterisation of plasma-nitrided titanium: an XPS study." *Applied surface science* 84.4 (1995): 357-371.

References

- [232] Wang, Enjun, Wensheng Yang, and Yaan Cao. "Unique surface chemical species on indium doped TiO₂ and their effect on the visible light photocatalytic activity." *The Journal of Physical Chemistry C* 113.49 (2009): 20912-20917.
- [233] Xu, Nuo, et al. "Characteristics and mechanism of conduction/set process in TiN/ ZnO/ Pt resistance switching random-access memories." *Applied Physics Letters* 92.23 (2008): 232112.
- [234] Hsieh, P-T., et al. "Luminescence mechanism of ZnO thin film investigated by XPS measurement." *Applied Physics A* 90.2 (2008): 317-321.
- [235] Mekki, A., et al. "An XPS study of iron sodium silicate glass surfaces." *Journal of non-crystalline solids* 208.3 (1996): 267-276.
- [236] Kim, Hyung Jin, Jumi Kim, and Byungyou Hong. "Effect of hydrogen plasma treatment on nano-structured TiO₂ films for the enhanced performance of dye-sensitized solar cell." *Applied Surface Science* 274 (2013): 171-175.
- [237] Fu, Lei, et al. "Beaded cobalt oxide nanoparticles along carbon nanotubes: towards more highly integrated electronic devices." *Advanced Materials* 17.2 (2005): 217-221.
- [238] Tan, Beng Jit, Kenneth J. Klabunde, and Peter MA Sherwood. "XPS studies of solvated metal atom dispersed (SMAD) catalysts. Evidence for layered cobalt-manganese particles on alumina and silica." *Journal of the American Chemical Society* 113.3 (1991): 855-861.
- [239] Brik, Younes, et al. "Titania-supported cobalt and cobalt-phosphorus catalysts: characterization and performances in ethane oxidative dehydrogenation." *Journal of catalysis* 202.1 (2001): 118-128.
- [240] Radecka, M., M. Rekas, and K. Zakrzewska. "Electrical and optical properties of undoped and Fe-doped TiO₂ single crystals." *Solid State Phenomena*. Vol. 39. Trans Tech Publications, 1994.
- [241] Zhang, Jinzhong, et al. "Synthesis, surface morphology, and photoluminescence properties of anatase iron-doped titanium dioxide nano-crystalline films." *Physical Chemistry Chemical Physics* 13.28 (2011): 13096-13105.
- [242] Simpson, J. R., et al. "Optical band-edge shift of anatase Ti_{1-x}Co_x O_{2-δ}." *Physical Review B* 69.19 (2004): 193205.
- [243] Kong, L. G., et al. "Oxygen-vacancies-related room-temperature ferromagnetism in polycrystalline bulk co-doped TiO₂." *Electrochemical and solid-state letters* 9.1 (2006): G1-G3.

References

- [244] Anisimov, V. I., et al. "The role of transition metal impurities and oxygen vacancies in the formation of ferromagnetism in Co-doped TiO₂." *Journal of Physics: Condensed Matter* 18.5 (2006): 1695.
- [245] Kafizas, Andreas, and Ivan P. Parkin. "Inorganic thin-film combinatorial studies for rapidly optimising functional properties." *Chemical Society Reviews* 41.2 (2012): 738-781.
- [246] Walter, Michael G., et al. "Solar water splitting cells." *Chemical reviews* 110.11 (2010): 6446-6473.
- [247] Morterra, Claudio, et al. "Surface characterization of some TiO₂-based pigments. Part 3.— Coating of the pigments." *Journal of Materials Chemistry* 2.3 (1992): 341-355.
- [248] Hu, Chao, et al. "Large-scale, ultrathin and (001) facet exposed TiO₂ nanosheet superstructures and their applications in photocatalysis." *Journal of Materials Chemistry A* 2.7 (2014): 2040-2043.
- [249] Yun, Ho-Gyeong, et al. "Dye-sensitized solar cells with TiO₂ nano-particles on TiO₂ nano-tube-grown Ti substrates." *Journal of Materials Chemistry* 21.11 (2011): 3558-3561.
- [250] Rossmeisl, Jan, et al. "Electrolysis of water on oxide surfaces." *Journal of Electroanalytical Chemistry* 607.1 (2007): 83-89.
- [251] Yang et al. "Iodide management in formamidium-lead-halide-based perovskite layers for efficient solar cell" *Science* 356 (2017): 1376-1379.
- [252] Feng, Ningdong, et al. "Understanding the high photocatalytic activity of (B, Ag)-codoped TiO₂ under solar-light irradiation with XPS, solid-state NMR, and DFT calculations." *Journal of the American Chemical Society* 135.4 (2013): 1607-1616.
- [253] He, Wei, et al. "Continuous synthesis of a co-doped TiO₂ photocatalyst and its enhanced visible light catalytic activity using a photocatalysis microreactor." *RSC Advances* 5.68 (2015): 54853-54860.
- [254] Ismail, Adel A., and Detlef W. Bahnemann. "Mesoporous titania photocatalysts: preparation, characterization and reaction mechanisms." *Journal of Materials Chemistry* 21.32 (2011): 11686-11707.
- [255] Boxi, Siddhartha Sankar, and Santanu Paria. "Visible light induced enhanced photocatalytic degradation of organic pollutants in aqueous media using Ag doped hollow TiO₂ nanospheres." *RSC Advances* 5.47 (2015): 37657-37668.

References

- [256] Lu, Jibao, et al. "Chemical and optical properties of carbon-doped TiO₂: A density-functional study." *Applied Physics Letters* 100.10 (2012): 102114.
- [257] Li, Min, Junying Zhang, and Yue Zhang. "First-principles calculation of compensated (2N, W) codoping impacts on band gap engineering in anatase TiO₂." *Chemical Physics Letters* 527 (2012): 63-66.
- [258] Su, Chunyan, et al. "Fabrication of Ag/TiO₂ nanoheterostructures with visible light photocatalytic function via a solvothermal approach." *CrystEngComm* 14.11 (2012): 3989-3999.
- [259] Zhang, Yanhui, et al. "TiO₂- graphene nanocomposites for gas-phase photocatalytic degradation of volatile aromatic pollutant: is TiO₂- graphene truly different from other TiO₂-carbon composite materials?" *ACS nano* 4.12 (2010): 7303-7314.
- [260] Choi, Jina, Hyunwoong Park, and Michael R. Hoffmann. "Effects of single metal-ion doping on the visible-light photoreactivity of TiO₂." *The Journal of Physical Chemistry C* 114.2 (2009): 783-792.
- [261] Foo, Wei Jian, Chun Zhang, and Ghim Wei Ho. "Non-noble metal Cu-loaded TiO₂ for enhanced photocatalytic H₂ production." *Nanoscale* 5.2 (2013): 759-764.
- [262] Ajmal, Anila, et al. "Principles and mechanisms of photocatalytic dye degradation on TiO₂ based photocatalysts: a comparative overview." *Rsc Advances* 4.70 (2014): 37003-37026.
- [263] Benjwal, Poonam, and Kamal K. Kar. "One-step synthesis of Zn doped titania nanotubes and investigation of their visible photocatalytic activity." *Materials Chemistry and Physics* 160 (2015): 279-288.
- [264] Deng, Q. R., et al. "Mn-doped TiO₂ nanopowders with remarkable visible light photocatalytic activity." *Materials Letters* 65.13 (2011): 2051-2054.
- [265] Yang, Sitao, et al. "Synthesis of titanium dioxide with oxygen vacancy and its visible-light sensitive photocatalytic activity." *Materials Research Bulletin* 46.4 (2011): 531-537.
- [266] Khan, Matiullah, et al. "Effect of oxygen vacancy on the improved photocatalytic activity of Cr-doped TiO₂." *International Journal of Modern Physics B* 28.25 (2014): 1450170.
- [267] Khan, Hayat, and Imran Khan Swati. "Fe³⁺-doped Anatase TiO₂ with d-d Transition, Oxygen Vacancies and Ti³⁺ Centers: Synthesis, Characterization, UV-vis Photocatalytic and Mechanistic Studies." *Industrial & Engineering Chemistry Research* 55.23 (2016): 6619-6633.
- [268] Gao, Yanfeng, et al. "Room temperature deposition of a TiO₂ thin film from aqueous peroxotitanate solution." *Journal of materials chemistry* 13.3 (2003): 608-613.

References

- [269] Molea, Andreia, et al. "Correlation of Physicochemical Properties with the Catalytic Performance of Fe-Doped Titanium Dioxide Powders." *Industrial & Engineering Chemistry Research* 54.30 (2015): 7346-7351.
- [270] T Tachikawa, Takashi, Mamoru Fujitsuka, and Tetsuro Majima. "Mechanistic insight into the TiO₂ photocatalytic reactions: design of new photocatalysts." *The Journal of Physical Chemistry C* 111.14 (2007): 5259-5275.
- [271] Cozzoli, P. D., et al. "Photocatalytic activity of organic-capped anatase TiO₂ nanocrystals in homogeneous organic solutions." *Materials Science and Engineering: C* 23.6 (2003): 707-713.
- [272] Hoffman, Amy J., Elizabeth R. Carraway, and Michael R. Hoffmann. "Photocatalytic production of H₂O₂ and organic peroxides on quantum-sized semiconductor colloids." *Environmental science & technology* 28.5 (1994): 776-785.
- [273] Wu, Ren-Jang, et al. "Phorate degradation by TiO₂ photocatalysis: Parameter and reaction pathway investigations." *Desalination* 250.3 (2010): 869-875.
- [274] Vasilopoulou, Maria, et al. "The influence of hydrogenation and oxygen vacancies on molybdenum oxides work function and gap states for application in organic optoelectronics." *Journal of the American Chemical Society* 134.39 (2012): 16178-16187.
- [275] Thiruvengkatachari, Ramesh, Saravanamuthu Vigneswaran, and Il Shik Moon. "A review on UV/TiO₂ photocatalytic oxidation process (Journal Review)." *Korean Journal of Chemical Engineering* 25.1 (2008): 64-72.
- [276] Pera-Titus, Marc, et al. "Degradation of chlorophenols by means of advanced oxidation processes: a general review." *Applied Catalysis B: Environmental* 47.4 (2004): 219-256.

LIST OF PUBLICATIONS

PAPERS IN INTERNATIONAL REFEREED JOURNALS:

1. **Bandna Bharti**, Santosh Kumar, Heung-No Lee & Rajesh Kumar “Formation of oxygen vacancies and Ti^{3+} state in TiO_2 thin film and enhanced optical properties by air plasma treatment” **Scientific Reports** 6:32355 (**I.F 4.8**).
2. **Bandna Bharti**, Santosh Kumar & Rajesh Kumar “Superhydrophilic TiO_2 thin film by nanometer scale surface roughness and dangling bonds” **Applied Surface Science** (Vol 364, Pages 51–60, 2016) (**I.F. 3.15**).

Other Publication:

3. Richa khokhra, **Bandna Bharti**, Heung-No Lee & Rajesh Kumar “Visible and photodetector in ZnO nanostructured thin films via simple tuning of solution method” **Scientific reports** 7 (2017) (**I.F 4.8**).

4.

PUBLICATIONS IN PROCEEDINGS:

1. **Bandna Bharti** and Rajesh Kumar (2016). Formation of surface groups to enhance the wettability of titanium dioxide (TiO_2) thin films, International Conference on Advances in Nanomaterials and Nanotechnology (ICANN-2016) from 4-5 November 2016, organized by center for Nanoscience and Nanotechnology, JamiaMilliaIslamia, New Delhi, India.
2. **Bandna Bharti**, ParthaBir Barman, Rajesh Kumar (2015). XRD analysis of Titanium Dioxide (TiO_2) and Fe doped TiO_2 nanoparticles by Williamson Hall Method, 4th National conference on advanced materials and radiation physics. *AIP Proceedings of the AMRP2015* [Sangrur, Punjab, India: March 13-14, 2015].

MANUSCRIPT COMMUNICATED:

1. Cobalt doped TiO_2 Nano thin films: Plasma treatment, Phase Structure, Surface, and Magnetic Properties”
2. Photocatalytic activity of Fe and Co doped TiO_2 thin films-Effect of plasma treatment.

PRESENTATIONS IN NATIONAL AND INTERNATIONAL

CONFERENCES:

1. International Conference on Advances in Nanomaterials and Nanotechnology (ICANN-2016) from 4-5 November 2016, organized by center for Nanoscience and Nanotechnology, Jamia Millia Islamia, New Delhi, India.
2. International Conference on Science: Emerging Scenario & Future Challenges (SESFC 2016) 11 - 12 June 2016, Dharamshala (H.P.) (**Best Poster Presentation**).
3. International conference Nano SciTech 2014 held in Punjab University, Chandigarh from 18-20 March 2016.
4. National Conference on Advanced Materials and Radiation Physics (AMRP-2015) (March 13-14, 2015)[SLIET, Longowal (Punjab) India].
5. National Conference on Multifunctional Advanced Materials, at Shoolini University, Solan, India, June 11-12, 2014.
6. National Seminar on “Recent Trends in Materials, Energy and Environment” (NSRTMEE-2014) held in Sri Sai University Palampur, (H.P) 18th January 2014.
7. One-week Workshop on “Nanotechnology (Fabrication and Characterization)” December 11, 2013 at JUIT Wagnaghat.